First-Order Hyperbolic-Relaxation Turbulence Modelling for Moment-Closures

by

Chao Yan

Thesis submitted to the
University of Ottawa
In partial fulfillment of the requirements
For the Ph.D. degree in
Mechanical Engineering

Department of Mechanical Engineering
Faculty of Engineering
University of Ottawa

Abstract

This dissertation presents a study of hyperbolic turbulence modelling for the Gaussian ten-moment equations. In gaskinetic theory, moment closures offer the possibility of deriving a series of gas-dynamic governing equations from the Boltzmann equation. One typical example, the Gaussian ten-moment model, which takes the form of hyperbolic-relaxation equations, is considered as a competitive model for viscous gas flow when heat transfer effects are negligible. The hyperbolic nature of this model gives it several numerical advantages, compared to the Navier-Stokes equations. However, until this study, the application of the ten-moment equations has been limited to laminar flows, due to the lack of appropriate turbulence models. In this work, the ten-moment equations are, for the first time, Reynolds-averaged. The resulting equations inherit the hyperbolic balance-law form from the original equations with new unknowns, which require approximation by turbulence models. Most of the traditional turbulence models for the Reynolds-averaged Navier-Stokes equations are not perfectly well-suited for the Reynolds-averaged ten-moment equations, because the second-order derivatives presented in these models can break the pure hyperbolic nature of the original model. The relaxation methods are therefore proposed in this project to reform the existing turbulence models. Two relaxation methods, the Chen-Levermore-Liu p-system and Cattaneo-Vernotte models, are used to hyperbolize the Prandtl's one-equation model, standard k-ϵ model and Wilcox k-ω model. The hyperbolic versions of these turbulence models are first shown to be equivalent to their original forms. They are then coupled to the Reynolds-averaged ten-moment equations to build the overall hyperbolic governing equations for turbulence flows. An axisymmetric version of Reynolds-averaged ten-moment equations is also derived. A dispersion analysis is conducted for the resulting governing equations, which shows the corresponding dispersive behaviour and stability. The effect of the relaxation parameters is investigated through several numerical tests. All derived turbulence models are applied to solve canonical validation test problems, including two-dimensional planar mixing-layer, free-jet and circular free-jet. The numerical evaluations are analysed and compared against existing experimental measurements.

Acknowledgements

First and foremost, I would like to thank my supervisor, Professor James Gerald McDonald, who constantly supported me with his vast knowledge and experience throughout my Ph.D. studies. Learning and working with him was a challenge but also an enjoyable experience. His unending passion in research and optimism encouraged and motivated me through the low points of my research. I am honored to be his first doctoral student.

I would also like to thank Professor Catherine Mavriplis, who provided me an opportunity to be a member of Génie Par la Simulation. It allows me to participate a graduate training program and many workshops for numerical simulation in my last two years of study. Thanks to the committee of my research proposal, Professor Matei Radulescu and Professor Joana Rocha, who provided many helpful questions, comments, and suggestions during my research proposal review. I am also thankful to Dr.Osamu Terashima, from Toyama Prefectural University, who supported me by providing careful collection of all requested experimental data.

My family have supported me unconditionally over the years. I must first thank my wife, Min, who is always willing to help me in any way she could. I would also like to thank my parents for their unending encouragement and support. They respect my decision and always be there for backing. In addition, I thank my daughter, Zi-Chu, whose shining smile is the resource of my power.

I also feel lucky that I have been studied and worked in a wonderful research group. Thanks to my colleagues François Forgues, Andre Fecteau, Alireza Miri, Fabien Giroux, William Morin, Andrée-Anne Dion-Dallaire for helping me in the graduate courses. Special thanks go to Willem Kaufmann, who have helped me on programming and learning the group code.

Finally, I would like to acknowledge the Natural Science and Engineering Research Council of Canada for their funding of my research through research assistantship and Simulation Based Engineering Science scholarship. I am also thankful to Professor Natalie Baddour, who have released my financial stress by assigning me additional teaching assistantship in every summer throughout my Ph.D. study.

Table of Contents

List of Tables

List of Figures

Nomenclature

Abbreviations

BGK	Bhatnagar-Gross-Krook
CFD	Computational Fluid Dynamics
DNS	Direct Numerical Simulation
GKS	Gas-Kinetic Scheme
HPC	High Performance Computing
LES	Large Eddy Simulation
PDE	Partial Differential Equation
RANS	Reynolds-Averaged Navier-Stokes
RSM	Reynolds-Stress Model

Scalar Quantities

α	General diffusivity or constant
A	Area of cell
a	Particle acceleration or fastest acoustic-like speed
c	Random velocity of particle
Δl	Length of cell face
Δt	Time step

δ_{ij}	Kronecker delta
ϵ	Dissipation rate
e	Exponential constant
$\mathcal{F}$	General distribution function
f	Probability density function
$\mathcal{G}$	Gaussian distribution function
H	Total entropy of gas
i	Imaginary number
J	Function of maximization problem
κ	Boltzmann's constant
Kn	Knudsen number
k	Turbulence kinetic energy
λ	Wave speed
L	Characteristic length scale
l	Length scale of turbulence
$\mathcal{M}$	Equilibrium Maxwell-Boltzmann distribution function
Ma	Ratio of bulk velocity to fastest acoustic-like speed
μ	Dynamic viscosity
μ_T	Dynamic Eddy viscosity
M	Velocity-dependent weight
m	Particle mass
ν	Kinematic viscosity
ν_T	Kinematic eddy viscosity

N	Total number of particles over all phase-space volume
n	Local number density of particles
$N_{\hat{x}_i,\hat{v}_i}$	Number of particles within a particular phase-space volume
ω	General angular frequency
ω_{I}	Imaginary part of angular frequency
ω_{R}	Real part of angular frequency
$\bar{\phi}$,ϕ'	Mean and fluctuating component of instantaneous flow variable
Φ	Source of entropy
ϕ	Arbitrary property or flux components in hyperbolic-relaxation two-equation models
ψ	Flux in p-system or flux component in Cattaneo-Vernotte model
ψ_1	Flux deviation
$\tilde{\phi}$,ϕ''	Mass-averaged and fluctuating component of instantaneous flow variable
p	Thermodynamic pressure
ρ	Local mass density of gas
r,θ,z	Cylindrical coordinates
σ_k,C_D,C_μ,β^*	Closure coefficients for turbulence kinetic energy equation
σ_ϵ,$C_{\epsilon 1}$,$C_{\epsilon 2}$	Closure coefficients for dissipation rate equation
σ_ω,γ,β	Closure coefficients for specific dissipation rate equation
S	Source or entropy density of gas
s	Source
τ	Relaxation time
T	Local temperature or time interval

t	Time
u	Bulk velocity
$\hat{V}$	Phase-space volume
V	Arbitrary spacial domain
v	Particle velocity
ξ	Wave number
x,y,z	Cartesian coordinates

Vector Quantities

$\boldsymbol{\alpha}$	Closure coefficients vector
$\hat{\boldsymbol{\alpha}}$	Lagrange multipliers vector
$\mathbf{A}$	General first-order tensor
$\mathbf{C}$	Random-velocity weights vector
$\mathbf{F}$	Flux vector
$\mathbf{l}$	Left eigenvectors for flux Jacobian
$\mathbf{M}$	Velocity-dependent weights vector
$\mathbf{n}$	Normal unit vector of cell face
$\boldsymbol{\Psi}$	Flux of entropy
$\mathbf{r}$	Right eigenvectors for flux Jacobian
$\mathbf{S}$	Source vector
$\mathbf{U}$	Conserved variables vector
$\mathbf{V}$	Solution ansatz or velocity-dependent weights vector for ten-moment equations
$\mathbf{W}$	Primitive moments or variables vector

Matrix Quantities

$\mathbf{A}$	Flux Jacobian matrix
$\mathbf{B}$	General second-order tensor
$\mathbf{C}$	General third-order tensor
C_{ijk}	Triple fluctuating velocity correlation and fluctuating pressure-velocity correlation tensor
ϵ_{ij}	Dissipation tensor
Γ^i_{jk}	Christoffel symbols
$\mathbf{I}$	Identity matrix
$\mathbf{L}$	Inverse of transition matrix
$\mathbf{N}$	Nilpotent matrix
$\mathbf{\Omega}$	Diagonal matrix of angular frequencies
$\bar{\Psi}_{ij}$	Summation of averaged generalized pressure and Reynolds-stress tensors
Π_{ij}	Pressure-strain correlation tensor
P_{ij}	Generalized pressure tensor
$\mathbf{Q}$	Source Jacobian matrix
$\mathbf{R}$	Transition matrix
S_{ij}	Strain-rate tensor
τ_{ij}	Reynolds-stress tensor
Θ_{ij}	Anisotropic temperature tensor
t_{ij}	Deviatoric pressure tensor

Subscripts

0	Quiescent equilibrium state or initial condition

a	Axisymmetric form
c	Conserved form
d	Perturbed state
ϵ	Dissipation rate
e	Local equilibrium state
E	Ensemble averaging
$\mathcal{G}$	Gaussian
i,j,k,l	Dimension and cell indices
k	Turbulence kinetic energy
MB	Maxwell-Boltzmann
ω	Specific dissipation rate
p	Primitive form
T	Time averaging
V	Spatial averaging

Superscripts

k	Dimension index
n	Time level
*	Non-dimensional form
T	Transpose

Chapter 1

Introduction

The rapid growth of computational power enables the possibility of applying high-performance computing (HPC) to computational fluid dynamics (CFD). Accurate solutions of various fluid models can be efficiently evaluated, even when the computational grid is massive. One of the most popular fluid-dynamics models, the Navier-Stokes equations, has been widely used to simulate the behaviour of compressible and incompressible fluid flows. This model provides reliable solution for flows that are considered as continuum. The Knudsen number, Kn, is defined as the ratio of molecular mean free path length to a representative physical length scale. The value of this dimensionless number defines different flow regimes. For example, in the continuum regime $\mathrm{Kn} < 0.01$, while for the transition regime $0.01 < \mathrm{Kn} < 1$, and for the free-molecular regime $\mathrm{Kn} > 1$. The validity of the Navier-Stokes equations is generally assumed so long as $\mathrm{Kn} < 0.01$. In the Navier-Stokes model, second-order derivatives of the velocity field are used to model viscous stresses. One clue that this technique cannot be a completely true description of a fluid's behaviour is that such diffusive models for momentum transfer introduce infinite speed of information propagation, which is non-physical [37]. Alternative hyperbolic models that take the form of systems of first-order balance laws are offered by moment methods, which follow from the kinetic theory of gases [19, 26, 37, 42]. The moment methods introduce finite speeds of information propagation, which seems more physical. Moreover, it has been shown that these models can provide reliable solutions for higher Knudsen number [32].

Currently, there exist a wide range of moment methods that are applicable to viscous gases [47]. The most classical are the original closures of Grad [20]. Unfortunately, though these closures provide first-order balance laws, the hyperbolicity of the resulting system is limited by the possibility of the flux Jacobian developing eigenvalues with imaginary com-

ponents [8]. Regularization of these Grad methods have been proposed by Torrilhon and Struchtrup and proven to be quite successful [43]. However, the regularization technique reintroduces second-order derivatives, which is not desirable for the current study. Alternatively, a rich theory of moment methods based on an entropy maximization principle has been proposed [18, 29, 37]. More recently, other closures, based on a modified entropy, have also been developed [1]. These maximum-entropy closures appear to produce more robustly hyperbolic first-order models in balance-law form and appear very attractive from a computational perspective.

One successful maximum-entropy moment model, the Gaussian ten-moment model, provides a first-order hyperbolic model for compressible, viscous, adiabatic gas flows. This first-order model has been shown to provide accurate solutions, not only in the continuum regime, but also in the transition regime [5, 9, 10, 30, 32, 35, 45]. Unlike the Navier-Stokes equations, viscous effects are modelled by a hyperbolic system with a local relaxation source. The wave speeds in this model are known to remain real and finite. Moreover, this first-order model offers several numerical advantages. For example, the solution of first-order models can often achieve one order higher spacial accuracy for a given stencil as compared to Navier-Stokes equations. Also, the accuracy of numerical solution is less dependent on the computational mesh quality [32, 35]. This is very beneficial for practical calculations when complex geometries make the generation of high-quality meshes difficult, or when adaptive mesh refinement is used to automatically cluster cells in regions of interest.

Currently, the practical application of the ten-moment model is restricted to laminar flows. This is because no turbulence model has yet been developed that is tailored for such moment methods. In traditional computational fluid-dynamics of turbulent flows, the flow quantities can be decomposed into mean and fluctuating components, where the fluctuating components represent the flow's turbulent behaviour. To derive governing equations that predict the averaged effect of turbulent quantities, the concept of Reynolds-averaging is introduced. This averaging procedure is traditionally applied to the governing Navier-Stokes equations [50]. The averaged equations are traditionally called the Reynolds-averaged Navier-Stokes equations (RANS). In the past century, many RANS turbulence models have been developed and further refined for different types of engineering applications. In this work, the Reynolds-averaging technique is, for the first time, applied to the Gaussian ten-moment model. The resulting governing equations inherit first-order balance law form, while introducing some new unclosed terms. Turbulence models are, therefore, required

to close the system. Although the traditional RANS models could be adapted to close the Reynolds-averaged ten-moment equations, they contain second-order derivatives. If traditional RANS models are directly coupled to the Reynolds-averaged ten-moment equations, their diffusive nature would destroy the attractive first-order hyperbolic form of the moment equations. Therefore, the challenge of turbulence modelling using the moment-closure approach is to design a first-order hyperbolic turbulence model that maintains the numerical advantages from the original equations. This is the goal of the present study.

The relaxation method is a well-known mathematical technique that transforms linear and non-linear convection-diffusion equations into an equivalent hyperbolic system with relaxation source terms [13, 31, 48], which is further referred to as a hyperbolic-relaxation system of equations. In this thesis, the term "equivalent" is used to mean two models, not necessarily describing the same physics, that predict the same solutions. Reviewing many popular RANS models, one notices that they are expressed in terms of equations with a very similar form, which consists of an unsteady and convection term on the left-hand side as well as a production, dissipation, and diffusion term on the right-hand side. The production term and dissipation term are usually treated as local source terms or related to the mean velocity gradient, while the diffusion terms are conventionally approximated by second-order derivatives. Therefore, all extra equations take the form of convection-diffusion equations. In this project, different types of relaxation methods are utilized to re-express traditional turbulence models in hyperbolic-relaxation form. The resultant hyperbolic forms can then be coupled with the Reynolds-averaged ten-moment equations to provide a fully hyperbolic model for turbulent gas flows.

In this thesis, as a first step, two types of relaxation methods, the Chen-Levermore-Liu p-system and the Cattaneo-Vernotte approach, are used to derive equivalent hyperbolic-relaxation forms of the incompressible Prandtl's one-equation model [50]. The derived hyperbolic-relaxation versions produce a set of equations, including one convection equation describing the translation of turbulence kinetic energy and one equation per dimension describing the fluxes or diffusive flux components in different spacial direction. Even though the equivalent systems contain more equations, the global first-order hyperbolic balance-law form can be maintained. The eigenstructure of the Reynolds-averaged ten-moment equations with p-system type hyperbolic-relaxation Prandtl's one-equation model is studied. Similarly, the Cattaneo-Vernotte approach is further applied to the traditional k-ϵ [27] and k-ω two-equation models [50], which results in the number of the corresponding hyperbolic-relaxation equations being doubled, since the number of the original equations

is doubled. The dispersive behaviour of all derived models are investigated. Several sets of one- and two-dimensional tests are built for the derived models, which aim to show the equivalence between the original RANS models and their hyperbolic-relaxation versions. The selection of relaxation parameters for the hyperbolic turbulence models are discussed. These models are further validated by solving a canonical two-dimensional turbulent plane mixing-layer and several free-jet problems. In this project, governing equations for low-speed flow are targeted, which implies the compressibility effect can be neglected for now.

It is also worth to mention another interesting turbulence research in the field of kinetic theory of gases has been conducted by Xu [53]. Xu has established the framework of the gas-kinetic scheme (GKS) based on the Bhatnagar-Gross-Krook (BGK) model, and developed associated higher-order accurate numerical treatments [54]. The high-order GKS has recently been used to solve turbulent flow problems [12]. In this model, the turbulence influence is taken into account by enlarging particle collision time. The enlarged portion is referred to as the turbulent relaxation time, which is calculated based on a turbulent eddy viscosity provided by traditional turbulence models. This technique is somewhat similar to one aspect of the current research. In principle, any existing turbulence models that approximate turbulent eddy viscosity can be coupled with GKS-BGK model, which offers a new possibility of turbulence approximation using the existing turbulence models. In fact, it might be possible to adapt the new first-order hyperbolic turbulence models developed in this work for use with the GKS, though that is not within the scope of this work.

1.1 Structure of Thesis

This thesis consists of the introduction of the relevant background theory, the details of mathematical derivation and analysis, as well as the discussion of numerical observation and the data analysis. The outline of the thesis is as follows:

- In Chapter 2, the theory of relaxation methods is reviewed. The different types of equivalent hyperbolic-relaxation forms of a typical convection-diffusion equation are derived as an example.
- In Chapter 3, the background of the moment-closure method is briefly reviewed and the Gaussian ten-moment model is introduced.

- In Chapter 4, the Reynolds-averaging technique is applied to the Gaussian ten-moment equations and the resulting closure problem is discussed.

- In Chapter 5, two equivalent hyperbolic-relaxation forms of Prandtl's one-equation model are derived. The derived models are then used to close the Reynolds-averaged ten-moment equations. The eigenstructure of the Reynolds-averaged ten-moment equations with p-system type hyperbolic-relaxation one-equation model is studied. The dispersive behaviour of the resulting hyperbolic-relaxation system is investigated.

- In Chapter 6, the equivalent Cattaneo-Vernotte type hyperbolic-relaxation form of the standard k-ϵ and Wilcox (1988) k-ω model are derived. The dispersive relations of these new models are studied.

- In Chapter 7, the axisymmetric version of the Reynolds-averaged ten-moment equations coupled with hyperbolic-relaxation one- and two-equation turbulence models are derived.

- In Chapter 8, several one- and two-dimensional numerical tests are built to show the equivalence between the derived hyperbolic-relaxation versions and the original turbulence models. The effects of relaxation time are investigated and an appropriate value is selected. The Reynolds-averaged ten-moment equations coupled with all derived hyperbolic-relaxation turbulence models are subsequently applied to solve a two-dimensional turbulent mixing-layer and two free-jet problems. Comparisons are made to existing experimental data.

- In Chapter 9, a strategy of compressible turbulence modelling for the moment-closure is discussed.

- In Chapter 10, conclusions are drawn and avenues for future work are discussed.

Chapter 2

Hyperbolic Balance-Laws with Local Relaxation

Relaxation phenomena play an important role in many physical situations. For example, in gaskinetic theory, a perturbed gas relaxes to the equilibrium state described by a Maxwellian velocity distribution, and in reacting flows, chemical reactions are modelled by stiff local source terms. In the field of applied mathematics, many existing hyperbolic-relaxation models can be used to approximate the relaxation phenomena. According to the stiffness of the local source term, hyperbolic-relaxation systems exhibit different asymptotic behaviours. In one asymptotic limit, the behaviour of hyperbolic-relaxation systems approaches that of a diffusion system [14, 31]. In this study, this diffusion limit is of interest, in which relaxation source terms are always stiff.

2.1 Conversions from Convection-Diffusion to Equivalent Hyperbolic-Relaxation System

The techniques used to derive the hyperbolic-relaxation models are referred to as the relaxation method, which is typically applied to transform linear or non-linear convection-diffusion equations into an equivalent hyperbolic-relaxation system [41]. Convection-diffusion equations are widely used to describe macro-scale flow transport and heat transfer. The equivalent hyperbolic-relaxation form of a convection-diffusion equation is defined to be a first-order system which produces the same solution as the original equation in an appro-

priate limit. One typical example is the hyperbolic form of the heat diffusion equation, which is also referred to as the generalized hyperbolic heat equation [4, 22, 44].

In this chapter, two types of relaxation methods, the Chen-Levermore-Liu p-system and the Cattaneo-Vernotte approach, are introduced. The equivalent hyperbolic-relaxation forms of a one-dimensional linear and non-linear convection-diffusion equation are derived as examples.

2.1.1 The Relaxation Methods

In this section, the details of Chen-Levermore-Liu p-system and the Cattaneo-Vernotte approach are shown. In general, both methods can reform convection-diffusion type equations into a system of first-order hyperbolic equations, which produce the same diffusion behaviour in an appropriate limit. These reformulations avoid the instantaneous propagation of information that is predicted by the original equation. They contain more partial differential equations (PDEs) describing the time evolution of the new variables. The extra variables introduced by different methods have different physical interpretations. The corresponding asymptotic form of the hyperbolic equations are distinct as well. It is found that, the p-system is only applicable for convection-diffusion equations with simple formulated diffusion coefficients. To derive the equivalent hyperbolic-relaxation form of convection-diffusion type equations using the p-system can be very difficult when the diffusion coefficient is dependent on multiple variables. However, the application of the Cattaneo-Vernotte approach, in such situation, remains much simpler. Moreover, to achieve the equivalent diffusion performance as the original equations, a smaller relaxation time is required for the p-system form in higher spacial dimensions. But, for the Cattaneo-Vernotte form, larger relaxation times can be used to maintain the same diffusion limit as the original equations in any higher spacial dimensions. This means that the stiffness effect from the fluxes and source terms introduced by the relaxation time can be less.

2.1.2 The Characteristics of Hyperbolic and Parabolic Partial Differential Equations

Partial differential equations are widely used to describe physical phenomena, which can be classified as hyperbolic, parabolic or elliptic type by the sign of the corresponding discriminant [38]. This terminology reflects an analogy between the PDEs and polynomial

functions. For example, if the general single second-order PDE is written as

$$a\frac{\partial^2\phi}{\partial x^2}+b\frac{\partial^2\phi}{\partial x\partial y}+c\frac{\partial^2\phi}{\partial y^2}+d\frac{\partial\phi}{\partial x}+e\frac{\partial\phi}{\partial y}+f\phi=g\,, \tag{2.1}$$

where the described property, $\phi\,(x,y)$, is a function of independent variables x and y, the corresponding discriminant is expressed as b^2-4ac. The PDE can then be classified as hyperbolic, parabolic or elliptic type if its discriminant is positive, zero or negative respectively. One notes that, the general single first-order PDE,

$$d\frac{\partial\phi}{\partial x}+e\frac{\partial\phi}{\partial y}+f\phi=g\,, \tag{2.2}$$

can be considered as a special case of the general single second-order PDE, which is always hyperbolic as long as e/d is real. The characteristics of a PDE are defined as the paths, in the solution domain, along which the described information propagates. Applying the chain rule to the first-order derivatives of ϕ, the total derivatives of $\frac{\partial\phi}{\partial x}$ and $\frac{\partial\phi}{\partial y}$ can be determined as

$$\mathrm{d}\left(\frac{\partial\phi}{\partial x}\right)=\frac{\partial^2\phi}{\partial x^2}\mathrm{d}x+\frac{\partial^2\phi}{\partial x\partial y}\mathrm{d}y\,, \tag{2.3}$$

$$\mathrm{d}\left(\frac{\partial\phi}{\partial y}\right)=\frac{\partial^2\phi}{\partial y\partial x}\mathrm{d}x+\frac{\partial^2\phi}{\partial y^2}\mathrm{d}y\,. \tag{2.4}$$

Equations (2.1)–(2.4), describing the full differential relationship of function, $\phi\,(x,y)$, can be written in a matrix form of equations system as

$$\begin{bmatrix} a & b & c \\ \mathrm{d}x & \mathrm{d}y & 0 \\ 0 & \mathrm{d}x & \mathrm{d}y \end{bmatrix}\begin{bmatrix} \frac{\partial^2\phi}{\partial x^2} \\ \frac{\partial^2\phi}{\partial x\partial y} \\ \frac{\partial^2\phi}{\partial y^2} \end{bmatrix}=\begin{bmatrix} -d\frac{\partial\phi}{\partial x}-e\frac{\partial\phi}{\partial y}-f\phi-g \\ \mathrm{d}\left(\frac{\partial\phi}{\partial x}\right) \\ \mathrm{d}\left(\frac{\partial\phi}{\partial y}\right) \end{bmatrix}. \tag{2.5}$$

A unique solution of Eq. (2.5) exists unless the determinant of the coefficient matrix is zero, where the second-order derivatives of function, $\frac{\partial^2\phi}{\partial x^2}$, $\frac{\partial^2\phi}{\partial x\partial y}$ and $\frac{\partial^2\phi}{\partial y^2}$, may be multivalued or discontinuous. Setting the determinant of the coefficient matrix equal to zero, the corresponding characteristic equation can be obtained

$$a\,(\mathrm{d}y)^2-b\,(\mathrm{d}x)\,(\mathrm{d}y)-c\,(\mathrm{d}x)^2=0\,, \tag{2.6}$$

which is equivalent to solve the differential equation,

$$\frac{\mathrm{d}y}{\mathrm{d}x}=\frac{b\pm\sqrt{b^2-4ac}}{2a}\,. \tag{2.7}$$

In general, this differential equation defines two families of curves, in the xy plane. As mentioned, along these curves, if they exist, the second-order derivatives of the described property are multivalued or discontinuous, which allow the propagation of discontinuous slope in the property distribution. These curves are defined as the characteristic paths of the PDE, Eq. (2.1). In many engineering models, the independent variables, x and y, are replaced by t and x, as time and spatial variable. In such a case, the slope of characteristic paths are interpreted as the propagation speed of the described information.

For example, the one-dimensional linear convection equation is a first-order hyperbolic PDE, which can be used to describe the translation of physical quantity, $\phi(x,t)$, within a fluid flow. It can be written as

$$\frac{\partial \phi}{\partial t} + u\frac{\partial \phi}{\partial x} = 0\,, \tag{2.8}$$

where the variable u represents the velocity of background flow. The total derivative of $\phi(x,t)$ can be expressed as

$$\mathrm{d}\phi = \frac{\partial \phi}{\partial t}\mathrm{d}t + \frac{\partial \phi}{\partial x}\mathrm{d}x\,. \tag{2.9}$$

Combining Eq. (2.8) and Eq. (2.9) in a matrix form

$$\begin{bmatrix} 1 & u \\ \mathrm{d}t & \mathrm{d}x \end{bmatrix} \begin{bmatrix} \frac{\partial \phi}{\partial t} \\ \frac{\partial \phi}{\partial x} \end{bmatrix} = \begin{bmatrix} 0 \\ \mathrm{d}\phi \end{bmatrix}\,. \tag{2.10}$$

Setting the determinant of the coefficient matrix as zero, the slope of characteristic path can be found as $\mathrm{d}x/\mathrm{d}t = u$. This means the information of the variable, ϕ, propagates along the characteristic path with the speed of background flow. A similar characteristic analysis can also be done for the second-order parabolic PDE. The typical example is the one-dimensional diffusion equation, which has the form as

$$\frac{\partial \phi}{\partial t} + \alpha\frac{\partial^2 \phi}{\partial x^2} = 0\,, \tag{2.11}$$

where the variable α is the diffusivity. It is commonly used to describe the diffusion of $\phi(x,t)$ within a stationary medium. The total derivative of $\frac{\partial \phi}{\partial x}$ and $\frac{\partial \phi}{\partial t}$ is expressed as

$$\mathrm{d}\left(\frac{\partial \phi}{\partial x}\right) = \frac{\partial^2 \phi}{\partial x^2}\mathrm{d}x + \frac{\partial^2 \phi}{\partial x \partial t}\mathrm{d}t\,, \tag{2.12}$$

$$\mathrm{d}\left(\frac{\partial \phi}{\partial t}\right) = \frac{\partial^2 \phi}{\partial t \partial x}\mathrm{d}x + \frac{\partial^2 \phi}{\partial t^2}\mathrm{d}t\,. \tag{2.13}$$

The matrix form can be written as

$$\begin{bmatrix} -\alpha & 0 & 0 \\ \mathrm{d}x & \mathrm{d}t & 0 \\ 0 & \mathrm{d}x & \mathrm{d}t \end{bmatrix} \begin{bmatrix} \frac{\partial^2 \phi}{\partial x^2} \\ \frac{\partial^2 \phi}{\partial x \partial t} \\ \frac{\partial^2 \phi}{\partial t^2} \end{bmatrix} = \begin{bmatrix} \frac{\partial \phi}{\partial t} \\ \mathrm{d}\left(\frac{\partial \phi}{\partial x}\right) \\ \mathrm{d}\left(\frac{\partial \phi}{\partial t}\right) \end{bmatrix}\,. \tag{2.14}$$

By solving the corresponding characteristic equation, one simply obtains $\mathrm{d}t = 0$, which leads to

$$\frac{\mathrm{d}x}{\mathrm{d}t} = \frac{\mathrm{d}x}{\pm 0} = \pm\infty\,. \tag{2.15}$$

This implies that the described information has infinite propagation speed in parabolic-type PDEs.

The second-order derivative is commonly used in traditional fluid models to approximate the diffusive behaviour of flow quantities. It provides good approximations under many fluid conditions, while it also introduces non-physical propagation speeds of information. In contrast, the finite propagation speeds of information introduced by hyperbolic PDEs seem more physical for the fluid models.

2.1.3 Hyperbolization by the Chen-Levermore-Liu P-System

In this section, the details of a hyperbolization procedure using the Chen-Levermore-Liu p-system are presented. As an example, the classic convection-diffusion equation with linear constant and variable background velocity are reformulated into the equivalent p-system type hyperbolic-relaxation form.

Linear convection with constant velocity

The one-dimensional convection-diffusion equation with constant velocity, u, and constant diffusivity, μ, can be written as

$$\frac{\partial \phi}{\partial t} + u\frac{\partial \phi}{\partial x} - \mu\frac{\partial^2 \phi}{\partial x^2} = 0\,. \tag{2.16}$$

Here, ϕ is some arbitrary physical quantity. The goal is to recast this equation in an equivalent hyperbolic-relaxation form,

$$\frac{\partial \phi}{\partial t} + \frac{\partial \psi}{\partial x} = 0\,, \tag{2.17}$$

$$\frac{\partial \psi}{\partial t} + \frac{\partial f(\phi)}{\partial x} = -\frac{1}{\tau}\left(\psi - g(\phi)\right)\,, \tag{2.18}$$

where ψ is defined as the flux of ϕ. This type of hyperbolic-relaxation equations are also called the Chen-Levermore-Liu p-system [15].

The flux, ψ, is assumed to consist of an equilibrium part, $g(\phi)$, towards which it is relaxing and a deviation, ψ_1. The total flux can, therefore, be written as $\psi = g(\phi) + \psi_1$.

Here, the deviation, ψ_1, is assumed to be small and its time and space derivatives are negligible [4, 16, 31]. The derivatives of ψ in time and space can then be approximated as

$$\frac{\partial \psi}{\partial t} = \frac{\partial g(\phi)}{\partial t} + \underbrace{\frac{\partial \psi_1}{\partial t}}_{\text{negligible}} \approx \frac{\partial g(\phi)}{\partial \phi}\frac{\partial \phi}{\partial t}, \tag{2.19}$$

$$\frac{\partial \psi}{\partial x} = \frac{\partial g(\phi)}{\partial x} + \underbrace{\frac{\partial \psi_1}{\partial x}}_{\text{negligible}} \approx \frac{\partial g(\phi)}{\partial \phi}\frac{\partial \phi}{\partial x}. \tag{2.20}$$

By substituting $\psi = g(\phi) + \psi_1$ into Eq. (2.18), an expression of ψ_1 is obtained as

$$\psi_1 = -\tau\left(\frac{\partial \psi}{\partial t} + \frac{\partial f(\phi)}{\partial x}\right). \tag{2.21}$$

Bringing Eq. (2.20) into Eq. (2.17) gives the time derivative of ϕ as

$$\frac{\partial \phi}{\partial t} = -\frac{\partial \psi}{\partial x} = -\frac{\partial g(\phi)}{\partial \phi}\frac{\partial \phi}{\partial x}. \tag{2.22}$$

Similarly, substituting Eq. (2.22) into Eq. (2.19) gives the time derivative of ψ,

$$\frac{\partial \psi}{\partial t} = \frac{\partial g(\phi)}{\partial \phi}\frac{\partial \phi}{\partial t} = -\left(\frac{\partial g(\phi)}{\partial \phi}\right)^2\frac{\partial \phi}{\partial x}, \tag{2.23}$$

which is further substituted into Eq. (2.21) to get the expression for ψ_1,

$$\psi_1 = -\tau\left[-\left(\frac{\partial g(\phi)}{\partial \phi}\right)^2\frac{\partial \phi}{\partial x} + \frac{\partial f(\phi)}{\partial \phi}\frac{\partial \phi}{\partial x}\right] = \tau\left[\left(\frac{\partial g(\phi)}{\partial \phi}\right)^2 - \frac{\partial f(\phi)}{\partial \phi}\right]\frac{\partial \phi}{\partial x}. \tag{2.24}$$

Eventually, the expression of ψ can be rewritten as

$$\psi = g(\phi) + \psi_1 = g(\phi) + \tau\left[\left(\frac{\partial g(\phi)}{\partial \phi}\right)^2 - \frac{\partial f(\phi)}{\partial \phi}\right]\frac{\partial \phi}{\partial x}, \tag{2.25}$$

which is then substituted into Eq. (2.17), giving

$$\frac{\partial \phi}{\partial t} + \frac{\partial g(\phi)}{\partial x} + \tau\frac{\partial}{\partial x}\left\{\left[\left(\frac{\partial g(\phi)}{\partial \phi}\right)^2 - \frac{\partial f(\phi)}{\partial \phi}\right]\frac{\partial \phi}{\partial x}\right\} = 0. \tag{2.26}$$

This is the asymptotic form of the Eqs. (2.17)–(2.18), which governs the behaviour of the p-system. The asymptotic behaviour of the p-system type hyperbolic-relaxation model changes depending on the size of the relaxation time, τ. If τ is much smaller than the time of interest, one can consider that the relaxation process happens in a very short time. In this situation, the system stays in the diffusion limit, and its asymptotic form approaches

a convection-diffusion equation, where the diffusivity is a function of τ [24, 31, 44]. If τ is much larger than the time of interest, one can consider that the relaxation process is so long that it is no longer important. In this case, the asymptotic form approaches a pure wave equation. In the limit of τ approaching zero, the terms multiplying τ approach zero. The asymptotic form then approaches another pure convection equation. In this project, a turbulence model is developed for the diffusion limit, where the relaxation time scales are very small, but non-zero, comparing to the time scale of interest.

To match the convection-diffusion equation, Eq. (2.16), the functions $f(\phi)$ and $g(\phi)$ are chosen to be

$$f(\phi) = u^2\phi + \frac{\mu}{\tau}\phi\,, \tag{2.27}$$

$$g(\phi) = u\phi\,. \tag{2.28}$$

In the limit of small relaxation time, τ, these first-order hyperbolic equations predict same diffusion behaviour as the original equation. In other words, the p-system provides the same solution as the convection-diffusion equation when a small relaxation time is chosen. This method can be easily extended to higher spacial dimensions by adding more equations, where the number of extra equations equals the number of space dimensions. For example, the multi-dimensional convection-diffusion equation with constant velocity, u_i, and constant isotropic diffusivity, μ, can be written as

$$\frac{\partial\phi}{\partial t} + u_i\frac{\partial\phi}{\partial x_i} - \mu\frac{\partial^2\phi}{\partial x_i^2} = 0\,. \tag{2.29}$$

Its equivalent p-system type hyperbolic-relaxation form is

$$\frac{\partial\phi}{\partial t} + \frac{\partial\psi_j}{\partial x_j} = 0\,, \tag{2.30}$$

$$\frac{\partial\psi_i}{\partial t} + \frac{\partial f_i(\phi)}{\partial x_i} = -\frac{1}{\tau}\left(\psi_i - g_i(\phi)\right)\,, \tag{2.31}$$

where functions $f_i(\phi)$ and $g_i(\phi)$ are defined as

$$f_i(\phi) = u_i^2\phi + \frac{\mu}{\tau}\phi\,, \quad g_i(\phi) = u_i\phi\,. \tag{2.32}$$

The equivalence of the high-dimensional systems can be easily verified in the same manner as was done for the one-dimensional system.

If the p-system, Eqs. (2.30)–(2.31), is written in balance-law form,

$$\frac{\partial\mathbf{U}}{\partial t} + \frac{\partial\mathbf{F}_i(\mathbf{U})}{\partial x_i} = \mathbf{S}(\mathbf{U})\,, \tag{2.33}$$

the flux Jacobian matrices are defined as $\mathbf{A}_i = \frac{\partial \mathbf{F}_i(\mathbf{U})}{\partial \mathbf{U}}$. The corresponding eigenvalues that represent the wave speeds of fundamental solutions can be found as

$$\lambda_{1-4} = \left(-\sqrt{f_i'(\phi)}, 0, 0, \sqrt{f_i'(\phi)} \right) .$$

If Cartesian coordinates are considered here, this means there are two waves with the same finite speed moving along the positive and negative axial direction in each axis.

Linear convection with variable velocity

In general, the velocity, $u_i(x_i, t)$, can be a complicated time- and space-dependent function. For example, the typical one-dimensional convection-diffusion equation with variable velocity can be written in a general form as

$$\frac{\partial \phi}{\partial t} + \frac{\partial u\phi}{\partial x} - \mu \frac{\partial^2 \phi}{\partial x^2} = 0 . \tag{2.34}$$

Its equivalent p-system type hyperbolic version maintains the same form as Eqs. (2.17)–(2.18), however, the temporal and spacial dependencies introduced by a varying velocity, $u(x, t)$, change the final asymptotic form. Following the same derivation as introduced, but using $f(u, \phi)$ and $g(u, \phi)$, the corresponding asymptotic form can be expressed as

$$\begin{aligned} \frac{\partial \phi}{\partial t} + \frac{\partial g(u,\phi)}{\partial x} + \tau \frac{\partial}{\partial x} \left\{ \left[\left(\frac{\partial g(u,\phi)}{\partial \phi} \right)^2 - \frac{\partial f(u,\phi)}{\partial \phi} \right] \frac{\partial \phi}{\partial x} \right\} \\ + \tau \left(\frac{\partial g(u,\phi)}{\partial \phi} \frac{\partial g(u,\phi)}{\partial u} \frac{\partial u}{\partial x} - \frac{\partial g(u,\phi)}{\partial u} \frac{\partial u}{\partial t} - \frac{\partial f(u,\phi)}{\partial u} \frac{\partial u}{\partial x} \right) = 0 . \end{aligned} \tag{2.35}$$

The last term on the left hand side of Eq. (2.35) contributes an extra deviation due to the variable velocity. This deviation is also suppressed by the relaxation time, τ. In other words, in the limit of small relaxation time, the effect of this term is negligible. This means a p-system type hyperbolization of a convection-diffusion equation with varying velocity is possible. However, smaller relaxation times may be needed to maintain equivalence of solutions.

Many numerical tests have been carried out to verify that the p-system is, indeed, equivalent to the corresponding linear and non-linear convection-diffusion equations in the diffusive limit [41]. Similarly, the p-system can also remain valid for variable diffusivity, $\mu(\phi)$, with the appropriately chosen function, f_i.

2.1.4 Hyperbolization by the Cattaneo-Vernotte Relaxation Approach

The original idea of the relaxation approach was first introduced by Cattaneo [13, 14] and Vernotte [48], which provides a more general hyperbolization reformulation. The general one-dimensional convection-diffusion equation with non-linear convective term, variable diffusion coefficient and local source term can be written as

$$\frac{\partial \phi}{\partial t} + \frac{\partial f(u,\phi)}{\partial x} = \frac{\partial}{\partial x}\left(\mu(\phi)\frac{\partial \phi}{\partial x}\right) + s(\phi)\ , \tag{2.36}$$

where the diffusion coefficient, $\mu(\phi)$, and source term, $s(\phi)$, are functions of ϕ, in general. The velocity, $u(x,t)$, is a function of time and space. Cattaneo and Vernotte proposed the equivalent hyperbolic-relaxation form as

$$\frac{\partial \phi}{\partial t} + \frac{\partial}{\partial x}\left(f(u,\phi) - \mu(\phi)\psi\right) = s(\phi)\ , \tag{2.37}$$

$$\frac{\partial \psi}{\partial t} + \frac{\partial}{\partial x}\left(-\frac{\phi}{\tau}\right) = -\frac{\psi}{\tau}\,, \tag{2.38}$$

where, if τ is a constant, Eq. (2.38) can be reformed as

$$\tau\frac{\partial \psi}{\partial t} = \frac{\partial \phi}{\partial x} - \psi\,. \tag{2.39}$$

It is obvious that, in the limit of small relaxation time, the left-hand side of Eq. (2.39) approaches zero. Consequently, ψ approaches $\frac{\partial \phi}{\partial x}$, which means Eq. (2.37) approaches Eq. (2.36). Akin to the p-system, this model can also be extended to higher dimensions by adding extra equations. The general form can be written as

$$\frac{\partial \phi}{\partial t} + \frac{\partial}{\partial x_j}\left(f_j(u_j,\phi) - \mu_j(\phi)\psi_j\right) = s(\phi)\ , \tag{2.40}$$

$$\frac{\partial \psi_i}{\partial t} + \frac{\partial}{\partial x_i}\left(-\frac{\phi}{\tau}\right) = -\frac{\psi_i}{\tau}\,. \tag{2.41}$$

If the above system of equations is written in the same conservative form as Eq. (2.33), the corresponding eigenvalues of each flux Jacobian matrix are more complex than those of the p-system, but can nevertheless be found as

$$\lambda_{1-4} = \left(\frac{f_i'(u_j,\phi)}{2} - \sqrt{\left(\frac{f_i'(u_i,\phi)}{2}\right)^2 + \frac{\mu_i(\phi)}{\tau}}, 0,\right.$$
$$\left. 0, \frac{f_i'(u_j,\phi)}{2} + \sqrt{\left(\frac{f_i'(u_i,\phi)}{2}\right)^2 + \frac{\mu_i(\phi)}{\tau}}\right)\ .$$

Even though both the Cattaneo-Vernotte and the p-system model can reproduce the behaviour of the same convection-diffusion equation, the structure of the equivalent hyperbolic-relaxation equations are different, as is the corresponding eigenstructure. Unlike the p-system, the relaxation source introduced by the Cattaneo-Vernotte method does not consist of a convective term, and the formulation of the first equation in the Cattaneo-Vernotte form is very similar to the original convection-diffusion equation. Moreover, according to the observation of the eigenvalues of the flux Jacobian matrix, it is obvious that neither p-system nor Cattaneo-Vernotte model is Galilean invariant, since their wavespeeds do not follow the form of $u_i \pm c$.

One notes that the difference between the asymptotic form of first-order hyperbolic-relaxation versions and the original equation is often referred to as formulation error, the magnitude of which is only controlled by the selection of an appropriate relaxation time. This formulation error is independent of the numerics chosen to solve problems. Based on numerical investigation, the smaller the relaxation time chosen, the smaller the formulation error, and therefore the better equivalence is gained. A detailed study of this effect is presented in Chapter 8.

To conclude, in the Cattaneo-Vernotte model, the formulation change of convection term does not form additional formulation errors, as in the p-system. There is another attractive feature carried by the Cattaneo-Vernotte model. In this model, the diffusion coefficient can be a function of multiple variables, $\mu(\phi, \varphi)$, where all variables can be time and space dependent. This feature is important when the desired diffusion coefficients are complicated and, in such a case, to build the equivalent p-system type hyperbolic-relaxation form is very difficult. The details of this are discussed in Chapter 6.

2.2 Dispersion Analysis

The solution of hyperbolic-relaxation equations exhibits dispersive wave behaviour, which is an important feature of this type of model. This means that the apparent propagation speed and damping rate of a perturbed solution are dependent on the frequency, ω, or wave number of the disturbance, ξ. This relation between the wave number and propagation speed or damping rate is often referred to as the dispersion relation. This dispersion relation provides important information about how a small disturbance evolves in the system for a range of wave numbers, which also determines the stability of the model [9, 10, 22]. In

this section, the technique used to determine the dispersion relation of a one-dimensional hyperbolic-relaxation model is reviewed in general.

The general one-dimensional hyperbolic-relaxation model can be written as

$$\frac{\partial \mathbf{U}}{\partial t} + \frac{\partial \mathbf{F}}{\partial x} = \mathbf{S}\,. \tag{2.42}$$

For a local equilibrium, $\mathbf{U}_e$, assuming $\mathbf{S}\left(\mathbf{U}_e\right) = 0$, the Eq. (2.42) satisfies

$$\frac{\partial \mathbf{U}_e}{\partial t} + \frac{\partial \mathbf{F}\left(\mathbf{U}_e\right)}{\partial x} = 0\,. \tag{2.43}$$

Therefore, the system of equations for small perturbations from a local equilibrium, $\mathbf{U}_d$, can be written in a form as

$$\frac{\partial \mathbf{U}_d}{\partial t} + \mathbf{A}\frac{\partial \mathbf{U}_d}{\partial x} = \mathbf{Q}\mathbf{U}_d\,. \tag{2.44}$$

where the flux Jacobian, $\mathbf{A} = \frac{\partial \mathbf{F}}{\partial \mathbf{U}}$, and source Jacobian, $\mathbf{Q} = \frac{\partial \mathbf{S}}{\partial \mathbf{U}}$, are evaluated at $\mathbf{U}_e$. To study the evolutions of the small perturbations described by the hyperbolic-relaxation system, the system of equations, Eq. (2.44), can be written as a linear operator acting on a solution vector [22],

$$\left(\mathbf{I}\frac{\partial}{\partial t} + \mathbf{A}\frac{\partial}{\partial x} - \mathbf{Q}\right)\mathbf{U}_d = \mathbf{0}\,. \tag{2.45}$$

In an initial-value problem, dispersion analysis aims to identify how this linear operator acts on a Fourier mode with wave number, $\xi \in \mathbb{R}$. For example, if the initial condition has the form

$$\mathbf{U}_d\left(x, 0\right) = \mathbf{U}_0 e^{-i\xi x}\,, \tag{2.46}$$

the solution ansatz can be expressed as

$$\mathbf{U}_d\left(x, t\right) = \mathbf{V}_d\left(t\right) e^{-i\xi x}\,. \tag{2.47}$$

Substituting Eq. (2.47) into Eq. (2.45), the problem is transformed into a system of ordinary differential equations,

$$\frac{\mathrm{d}\mathbf{V}_d}{\mathrm{d}t} = \left(i\xi\mathbf{A} + \mathbf{Q}\right)\mathbf{V}_d\,, \tag{2.48}$$

for which the solution, $\mathbf{V}_d\left(t\right)$, has form

$$\mathbf{V}_d\left(t\right) = e^{it\left(\xi\mathbf{A} - i\mathbf{Q}\right)}\mathbf{U}_0\,. \tag{2.49}$$

The Jordan canonical form of matrix, $\xi\mathbf{A} - i\mathbf{Q}$, can be determined as

$$\xi\mathbf{A} - i\mathbf{Q} = \mathbf{R}\left(\mathbf{\Omega} + \mathbf{N}\right)\mathbf{L}\,, \tag{2.50}$$

where $\mathbf{\Omega}$ is the diagonal matrix of eigenvalues,

$$\mathbf{\Omega} = \begin{pmatrix} \omega_1 & \cdots & 0 \\ \vdots & \ddots & \vdots \\ 0 & \cdots & \omega_n \end{pmatrix} , \tag{2.51}$$

$\mathbf{R}$ is the transition matrix, $\mathbf{L} = \mathbf{R}^{-1}$, and $\mathbf{N}$ is a nilpotent matrix which is zero if the matrix $\xi\mathbf{A} - i\mathbf{Q}$ is diagonalizible. The eigenvalues of $\xi\mathbf{A} - i\mathbf{Q}$ represent the frequency which are given the symbol ω_i. Therefore, the solution Eq. (2.49) can be rewritten as

$$\begin{aligned} \mathbf{V}_d(t) &= e^{it\mathbf{R}(\mathbf{\Omega}+\mathbf{N})\mathbf{L}}\mathbf{U}_0 \\ &= \mathbf{R}e^{it(\mathbf{\Omega}+\mathbf{N})}\mathbf{L}\mathbf{U}_0 \\ &= \mathbf{R}e^{it\mathbf{\Omega}}(\mathbf{I} + it\mathbf{N})\mathbf{L}\mathbf{U}_0 , \end{aligned} \tag{2.52}$$

and the solution of the original system Eq. (2.42) can then be expressed as [22]

$$\mathbf{U}_d(x,t) = \mathbf{R}e^{i(t\mathbf{\Omega}-\xi x\mathbf{I})}(\mathbf{I} + it\mathbf{N})\mathbf{L}\mathbf{U}_0 . \tag{2.53}$$

To investigate the wave speed and damping rate of the disturbed solution, the eigenvalue matrix, $\mathbf{\Omega}$, must be found. The eigenvalues of the matrix $\xi\mathbf{A} - i\mathbf{Q}$ can be determined by solving the characteristic equation

$$\det(\xi\mathbf{A} - i\mathbf{Q} - \omega\mathbf{I}) = 0 . \tag{2.54}$$

In general, these eigenvalues are complex

$$\omega = \omega_{\mathrm{R}} + i\omega_{\mathrm{I}} . \tag{2.55}$$

According to Eq. (2.53), the wave speed of the disturbed solution is defined as $v = \omega_{\mathrm{R}}(\xi)/\xi$, which is a function of wave number, ξ. For the system to be linearly stable, the attenuation rate, which is defined as $e^{-\omega_{\mathrm{I}}}$, must stay in the range $[0\ ,\ 1]$ for all wave numbers, ξ, or in other words, $\omega_{\mathrm{I}} > 0$.

For example, the general one-dimensional convection-diffusion equation, Eq. (2.34), has equivalent p-system type hyperbolic-relaxation form as

$$\frac{\partial\phi}{\partial t} + \frac{\partial\psi}{\partial x} = 0 , \tag{2.56}$$

$$\frac{\partial\psi}{\partial t} + \frac{\partial}{\partial x}\left(u^2\phi + \frac{\mu}{\tau}\phi\right) = -\frac{1}{\tau}(\psi - u\phi) , \tag{2.57}$$

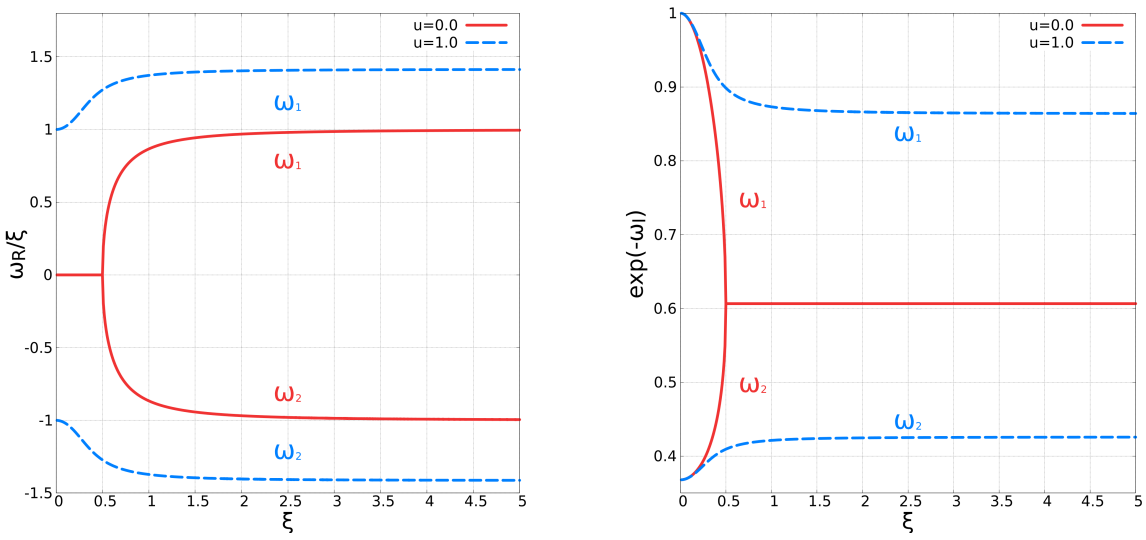

(a) phase speed (b) attenuation rate

Figure 2.1: Variation with wave number of the phase speed and attenuation rate for the p-system type hyperbolic heat equation for zero and non-zero background velocity

and Cattaneo-Vernotte type hyperbolic-relaxation form as

$$\frac{\partial \phi}{\partial t} + \frac{\partial}{\partial x}\left(u\phi - \mu\psi\right) = 0\,, \tag{2.58}$$

$$\frac{\partial \psi}{\partial t} + \frac{\partial}{\partial x}\left(-\frac{\phi}{\tau}\right) = -\frac{\psi}{\tau}\,, \tag{2.59}$$

which can be written in a general form as Eq. (2.42). Following the procedure as introduced, the flux Jacobian matrix, $\mathbf{A}$, and matrix $\mathbf{Q}$ can be derived, and the corresponding dispersion relations can be easily found. In this analysis, the diffusivity, μ, and relaxation time, τ, are chosen as 1. Two velocities, $u = 0$ and $u = 1$, are selected for study. One notes that, in the case of $u = 0$, the hyperbolic-relaxation equations are in fact equivalent to the heat diffusion equation in the diffusion limit. The phase speeds, ω_{R}/ξ, and the attenuation rates, $e^{-\omega_{\mathrm{I}}}$, over the wave number, ξ, of these two models are plotted in the Figs. (2.1) and (2.2).

As shown, the p-system and Cattaneo-Vernotte type hyperbolic-relaxation models are dispersive due to the fact that their phase speeds and attenuation rates are dependent on the wave number. In the short and long wave length limit, both phase speeds and attenuation rates approach different values. Interestingly, these two models have exactly the same dispersive behaviour when the background velocity is zero. In the limit of small wave number, where the considered time scale is much larger than the relaxation time, the

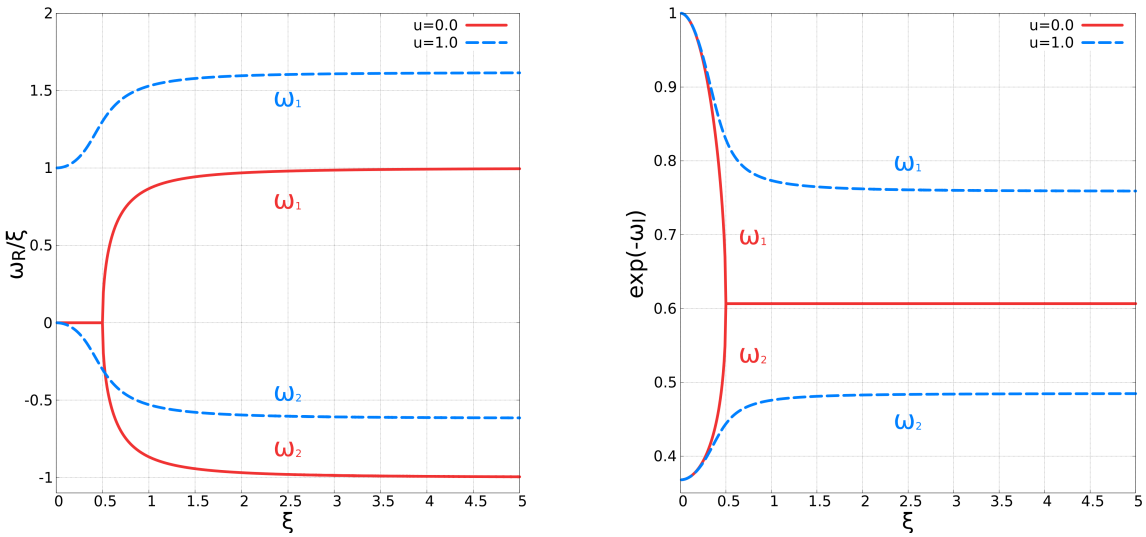

(a) phase speed (b) attenuation rate

Figure 2.2: Variation with wave number of the phase speed and attenuation rate for the Cattaneo-Vernotte type hyperbolic heat equation for zero and non-zero background velocity

phase speeds are identical. In the limit of large wave number, where the considered time scale is much smaller than the relaxation time, the phase speeds are distinct. The opposite feature can be observed in the attenuation rates. When the background velocity is non-zero, the phase speeds and damping rates of these models are always distinct over the wave number. It is important to note that the attenuation rates always stay in the range, [0 , 1], for all wave numbers, which illustrates that either the p-system or Cattaneo-Vernotte type hyperbolic-relaxation system are linearly stable for the perturbed solution.

2.3 The Relaxation Limits of Hyperbolic-Relaxation Equations

As discussed, the size of the relaxation time, τ, determines the relative impact of relaxation process over the time of interest. It affects the asymptotic form of the hyperbolic-relaxation equations, which can approach either a convection equation or a convection-diffusion equation. These two limits of hyperbolic-relaxation equations can be clearly illustrated by the solutions of a simple one-dimensional initial-value problem. In this section, the p-system model, Eq. (2.57), and Cattaneo-Vernotte model, Eq. (2.59), are used to numerically solve the same initial-value problem. Their solutions are further compared to the analytical

solution of the convection and convection-diffusion equation.

The initial condition is defined as a step function,

$$\phi(x) = \begin{cases} 1 & x \leq 1 \\ 0 & x > 1 \end{cases}, \tag{2.60}$$

which introduces a discontinuity at location, $x = 1$. This discontinuity is expected to only convect in the convection equation, or convect and diffuse in the convection-diffusion equation. A constant non-dimensional velocity and diffusivity, $u = 1.0$ and $\mu = 0.01$, are chosen. Three values of the relaxation time, $\tau = 1 \times 10^{-3}$, 1×10^{-1} and 1×10^{3}, are selected to study the limits of the hyperbolic-relaxation models. The initial condition and the solutions of the convection equation, convection-diffusion equation and hyperbolic-relaxation equations at $t = 1.0$ are plotted in Fig. (2.3). The solutions clearly illustrate different limits of hyperbolic-relaxation equations with different relaxation times. For a small relaxation time, $\tau = 1 \times 10^{-3}$, the relaxation process is much shorter compared to the time considered, and the hyperbolic-relaxation models approach their diffusion limits. The initial discontinuity convects and diffuses. The solution of the hyperbolic-relaxation models agree with the solution of the convection-diffusion equation. For a relaxation time, $\tau = 1 \times 10^{-1}$, which is close to the time scale of interest, the solution of the hyperbolic-relaxation models neither agree with the solution of the convection-diffusion nor the convection equation. The initial discontinuity convects and partially diffuses. For a large relaxation time, $\tau = 1 \times 10^{3}$, the relaxation process is much longer compared to the time considered, and the hyperbolic-relaxation models approach their convection limits. The initial discontinuity only convects. The solution of the hyperbolic-relaxation models agree with the solution of convection equation. All these results also agree with the analysis for the asymptotic form of hyperbolic-relaxation models.

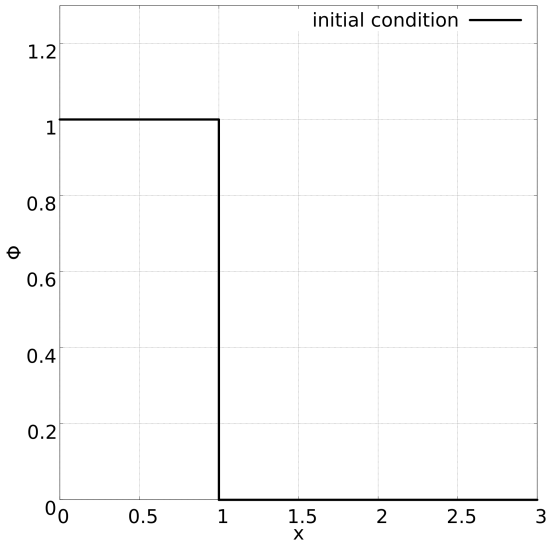

(a) $t = 0.0\,\mathrm{s}$

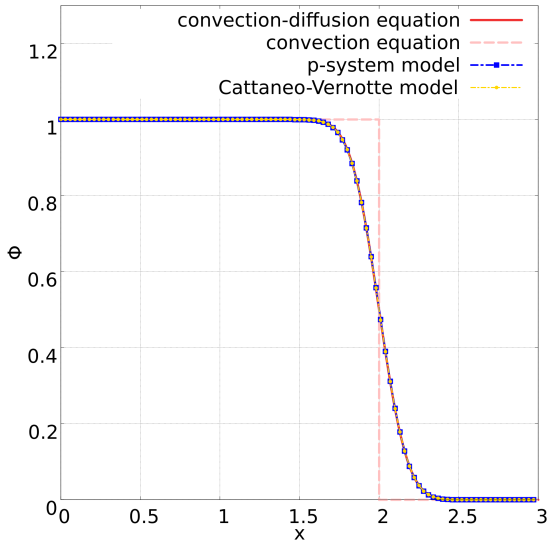

(b) $\tau = 1 \times 10^{-3}$

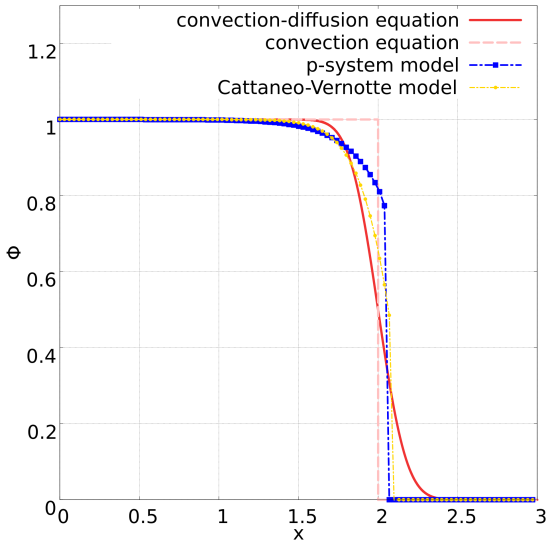

(c) $\tau = 1 \times 10^{-1}$

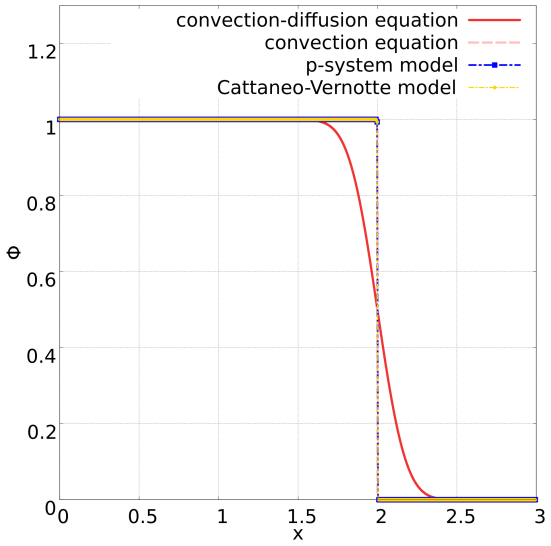

(d) $\tau = 1 \times 10^{3}$

Figure 2.3: The initial condition and solutions of the convection equation, convection-diffusion equation and hyperbolic-relaxation equations with multiple choices of τ_k at $t = 1.0$

Chapter 3

Elements of Kinetic Theory

3.1 Velocity Distribution Functions and Moments

In the kinetic theory of gases, it is assumed that all gases are comprised of many discrete particles. However, to describe the behaviour of a gas, the direct description of each individual gas particle is unnecessary. In this theory, a probability density function, $f(x_i, v_i, t)$, is used to describe the statistics of the distribution of particle velocities. This distribution function is defined in a six-dimensional phase space. For example, the well-known Maxwell-Boltzmann distribution function for a gas at rest is given by

$$f_{\mathrm{MB}}\left(x_i, v_i, t\right) = \left(\frac{m}{2\pi\kappa T\left(x_i, t\right)}\right)^{\frac{3}{2}} e^{-\frac{m v_j v_j}{2\kappa T(x_i, t)}}, \tag{3.1}$$

where m is the particle mass, v_i is the particle velocity, $T(x_i, t)$ is the local temperature and κ is Boltzmann's constant. This is also called the thermodynamics equilibrium distribution function, due to the fact that a gas in any arbitrary state will be eventually driven to this velocity distribution by the effect of particle collisions [19].

Taking the integral of a general distribution function in velocity space,

$$\int_{v_{x_1}}^{v_{x_2}} \int_{v_{y_1}}^{v_{y_2}} \int_{v_{z_1}}^{v_{z_2}} f\left(x_i, v_i, t\right) \, \mathrm{d}v_x \mathrm{d}v_y \mathrm{d}v_z \,, \tag{3.2}$$

gives the fraction of particles whose velocity lies within the velocity domain $v_x \in [v_{x_1}, v_{x_2}]$, $v_y \in [v_{y_1}, v_{y_2}]$ and $v_z \in [v_{z_1}, v_{z_2}]$ at position, x_i, and time, t. Multiplying f by the local number density of particles, $n\left(x_i, t\right)$, yields the distribution function, which is denoted by

capital calligraphic letters,

$$\mathcal{F}\left(x_i, v_i, t\right) = n\left(x_i, t\right) f\left(x_i, v_i, t\right) \, . \tag{3.3}$$

The integral of $\mathcal{F}(x_i, v_i, t)$ in velocity space gives the number density of particles whose velocity are within a specified velocity domain at a given location, x_i, and time, t. Conventionally, the notation $\mathcal{F}(x_i, v_i, t)$ is often used to denote general distribution function and $\mathcal{M}(x_i, v_i, t)$ is specifically used to denote the equilibrium Maxwell-Boltzmann distribution function.

The macroscopic properties of a gas can be determined by taking velocity moments of the distribution function, which refers to integrating the product of the distribution function, $\mathcal{F}$, and an appropriate velocity-dependent weight, $M(v_i)$, over all velocity space. For example, the local mass density of a gas is defined as

$$\rho = \iiint\limits_{\infty} m\mathcal{F} \, \mathrm{d}^3 v_i = \langle m\mathcal{F} \rangle \, , \tag{3.4}$$

where the molecular mass is taken as the velocity-dependent weight function. The compact notation, $\langle \cdot \rangle$, denotes integration over all velocity space. Similarly, the local momentum and total pressure of a gas can be determined as

$$\rho u_i = \langle m v_i \mathcal{F} \rangle \, , \tag{3.5}$$

$$\rho u_i u_j + P_{ij} = \langle m v_i v_j \mathcal{F} \rangle \, , \tag{3.6}$$

where P_{ij} is the generalized pressure tensor. The bulk velocity of fluid can, therefore, be obtained as

$$u_i = \frac{\langle m v_i \mathcal{F} \rangle}{\langle m \mathcal{F} \rangle} \, . \tag{3.7}$$

Once the bulk velocity, u_i, is known, the particle velocity, v_i, can be separated into two parts, $v_i = u_i + c_i$, where c_i is the random velocity of particle, which refers to the deviation between the velocity of a individual particle and local bulk velocity of the gas. One notes that the random or primitive moments can be defined by taking the velocity moment with random velocity-dependent weights. For example, the generalized pressure tensor, P_{ij}, can then also be defined by the moment associated with random velocity-dependent weight

$$P_{ij} = \langle m c_i c_j \mathcal{F} \rangle \, . \tag{3.8}$$

This pressure tensor can be related to the thermodynamic pressure, p, and deviatoric stress tensor, t_{ij}, as

$$P_{ij} = p\delta_{ij} - t_{ij} \, , \tag{3.9}$$

where $p = P_{kk}/3$ and $t_{kk} = 0$ for a monatomic gas.

Based on this method, the traditional macro-scale gas quantities are defined as appropriate moments of the velocity distribution function using appropriate velocity-dependent weights. To determine equations that govern the evolution of these macroscopic fluid properties, the governing equation of the distribution function must first be introduced.

3.2 The Boltzmann Equation

The Boltzmann equation describes the time evolution of the velocity distribution function [19, 42]. It can be written as

$$\frac{\partial \mathcal{F}}{\partial t} + v_i \frac{\partial \mathcal{F}}{\partial x_i} + \frac{\partial}{\partial v_i}\left(a_i \mathcal{F}\right) = \frac{\delta \mathcal{F}}{\delta t}\,, \tag{3.10}$$

where a_i is the particle acceleration due to external forces, which is taken as zero in this project, and $\frac{\delta \mathcal{F}}{\delta t}$ is the collision operator, which represents the effect of particle collisions on the velocity distribution function. In general, this collision operator is prohibitively complicated to evaluate, even for a simple engineering problem. Therefore, simplified collision models are usually adopted. For example, the BGK, or relaxation-time, model is one of the common approximation [6]. It has the form

$$\frac{\delta \mathcal{F}}{\delta t} = -\frac{\mathcal{F}\left(x_i, v_i, t\right) - \mathcal{M}\left(x_i, v_i, t\right)}{\tau\left(x_i, t\right)}\,. \tag{3.11}$$

It is obvious that the collision operator will vanish when the non-equilibrium distribution, $\mathcal{F}$, is everywhere equal to the equilibrium distribution, $\mathcal{M}$. This model can also be shown to respect the second law of thermodynamics and recover the correct gas behaviour as the continuum limit is approached.

3.3 Method of Moment and Moment-Closure

Multiplying the Boltzmann equation, Eq. (3.10), by a velocity-dependent weight, $M(v_i)$, and integrating the resulting equation over all velocity space gives

$$\iiint mM \frac{\partial \mathcal{F}}{\partial t}\,\mathrm{d}^3 v_i + \iiint mM v_i \frac{\partial \mathcal{F}}{\partial x_i}\,\mathrm{d}^3 v_i + \underbrace{\iiint mM \frac{\partial}{\partial v_i}\left(a_i \mathcal{F}\right)\,\mathrm{d}^3 v_i}_{=0} = \iiint mM \frac{\delta \mathcal{F}}{\delta t}\,\mathrm{d}^3 v_i\,, \tag{3.12}$$

As mentioned, since the particle acceleration, a_i, is taken as zero in this project, the third term on the left-hand side of Eq. (3.12) is zero. Applying the product rule, Eq. (3.12) can be reformed as

$$\frac{\partial}{\partial t}\iiint mM\mathcal{F}\,\mathrm{d}^3v_i + \frac{\partial}{\partial x_i}\iiint mMv_i\mathcal{F}\,\mathrm{d}^3v_i - \underbrace{\iiint\left(\frac{\partial mM}{\partial t} + v_i\frac{\partial mM}{\partial x_i}\right)\mathcal{F}\,\mathrm{d}^3v_i}_{=0} = \iiint mM\frac{\delta\mathcal{F}}{\delta t}\,\mathrm{d}^3v_i\,, \quad (3.13)$$

where the third integral on the left hand side of Eq. (3.13) is zero when the velocity-dependent weight is independent of space and time, which is usually the case. This leads to Maxwell's equation of change,

$$\frac{\partial}{\partial t}\left\langle mM\mathcal{F}\right\rangle + \frac{\partial}{\partial x_i}\left\langle mv_iM\mathcal{F}\right\rangle = \Delta\left[M\mathcal{F}\right]\,. \quad (3.14)$$

Here, the right-hand-side term, $\Delta\left[M\mathcal{F}\right] = \left\langle mM\frac{\delta\mathcal{F}}{\delta t}\right\rangle$, represents the effect of particle collisions on the moment of interest. If the individual weight, $M(v_i)$, is replaced by a vector of N velocity-dependent weights, $\mathbf{M}$, a set of N moment equations can be obtained as

$$\frac{\partial}{\partial t}\left\langle m\mathbf{M}\mathcal{F}\right\rangle + \frac{\partial}{\partial x_i}\left\langle mv_i\mathbf{M}\mathcal{F}\right\rangle = \Delta\left[\mathbf{M}\mathcal{F}\right]\,. \quad (3.15)$$

These equations describe the evolution of the corresponding moments. It is obvious that, to describe the time evolution of a lower-order moment, $\langle mM\mathcal{F}\rangle$, the divergence of a moment of one order higher, $\langle mv_iM\mathcal{F}\rangle$, is required. To fully describe the macroscopic fluid properties defined by lower-order moments, an infinite number of higher-order moment equations is required. An approach that closes the moment system with a finite number of equations is called a moment closure. This is usually done by restricting the distribution function to a prescribed form in terms of a chosen number of free parameters [19, 26, 42]. The values of the free parameters are chosen such that the distribution function is consistent with known moments, for example, Eqs. (3.4)–(3.8). Once the assumed distribution function is known, higher-order moments, that are present in the flux but not the solution vector, can simply be integrated. Moreover, the collision term can also be determined, if the collision model is selected, which closes the moment system.

3.3.1 Grad Moment Closures

One classic closure technique is Grad's moment method. It introduces a series of polynomial expansions about the equilibrium as the approximate form of the distribution function. It

can be expressed as

$$\mathcal{F} = \mathcal{M}\left[1 + \boldsymbol{\alpha}^{\mathrm{T}}\mathbf{C}\right] , \tag{3.16}$$

where $\boldsymbol{\alpha}$ and $\mathbf{C}$ are the column vectors with N closure coefficients associated with the desired lower-order moments and the corresponding random-velocity weights respectively. The N primitive moments of interest can be obtained by taking the velocity moment

$$\mathbf{W} = \langle m\mathbf{C}\mathcal{F}\rangle . \tag{3.17}$$

However, one deficiency of the Grad-type distribution function, Eq. (3.16), is that it can possibly predict negative probabilities, which is non-physical. Moreover, in the near equilibrium, the hyperbolicity of the resulting moment equations are not guaranteed for some moment values, which can lead the moment equations to become ill-posed for initial-value problems. These properties greatly limit the application of Grad-type polynomial series expansion.

3.3.2 Maximum-Entropy Moment Closures

Another well-known technique for choosing the form of the distribution function is to choose the function that maximizes the entropy, while satisfying the given velocity moments [18, 29, 37]. This is commonly referred as the maximum-entropy distribution function, which describes the most likely state that is consistent with prescribed velocity moments [36].

Boltzmann's H-theorem first described the relationship between macroscopic entropy and the velocity distribution of gas-particles. Inserting the velocity-dependent weight

$$M = -\frac{k}{m}\ln\frac{\mathcal{F}}{y} , \tag{3.18}$$

into Eq. (3.12), gives

$$\left\langle -k\ln\frac{\mathcal{F}}{y}\frac{\partial\mathcal{F}}{\partial t}\right\rangle + \left\langle -k\ln\frac{\mathcal{F}}{y}v_i\frac{\partial\mathcal{F}}{\partial x_i}\right\rangle = \Delta\left[-k\ln\frac{\mathcal{F}}{y}\mathcal{F}\right] , \tag{3.19}$$

where y is a constant. Following the same steps as previously introduced, Eq. (3.19) can be reformed as

$$\begin{aligned}\frac{\partial}{\partial t}\left\langle -k\ln\frac{\mathcal{F}}{y}\mathcal{F}\right\rangle + \frac{\partial}{\partial x_i}\left\langle -k\ln\frac{\mathcal{F}}{y}v_i\mathcal{F}\right\rangle \\ - \left[\left\langle \mathcal{F}\frac{\partial}{\partial t}\left(-k\ln\frac{\mathcal{F}}{y}\right)\right\rangle + \left\langle v_i\mathcal{F}\frac{\partial}{\partial x_i}\left(-k\ln\frac{\mathcal{F}}{y}\right)\right\rangle\right] = \Delta\left[-k\ln\frac{\mathcal{F}}{y}\mathcal{F}\right] .\end{aligned} \tag{3.20}$$

It is notable that, here the velocity-dependent weight, Eq. (3.18), is a function of the distribution function, which is dependent on time and space. Therefore, the last two integrals on the left-hand side of Eq. (3.20) can not be cancelled for the same reason as used in Eq. (3.13). However, these terms can be further reformed as

$$\begin{aligned}
&\left\langle \mathcal{F}\frac{\partial}{\partial t}\left(-k\ln\frac{\mathcal{F}}{y}\right)\right\rangle + \left\langle v_i\mathcal{F}\frac{\partial}{\partial x_i}\left(-k\ln\frac{\mathcal{F}}{y}\right)\right\rangle \\
=&\left\langle -ky\mathcal{F}\frac{1}{\mathcal{F}}\frac{\partial\mathcal{F}}{\partial t}\right\rangle + \left\langle -kyv_i\mathcal{F}\frac{1}{\mathcal{F}}\frac{\partial\mathcal{F}}{\partial x_i}\right\rangle \\
=&-ky\left(\left\langle\frac{\partial\mathcal{F}}{\partial t}\right\rangle + \left\langle v_i\frac{\partial\mathcal{F}}{\partial x_i}\right\rangle\right) \\
=&\,0\,,
\end{aligned} \tag{3.21}$$

which equals zero due to the expression in parentheses on the third line simply being the continuity equation. Thus, Eq. (3.19) can be written as

$$\frac{\partial}{\partial t}\left\langle -k\ln\frac{\mathcal{F}}{y}\mathcal{F}\right\rangle + \frac{\partial}{\partial x_i}\left\langle -k\ln\frac{\mathcal{F}}{y}v_i\mathcal{F}\right\rangle = \Delta\left[-k\ln\frac{\mathcal{F}}{y}\mathcal{F}\right]. \tag{3.22}$$

Defining the variable $S = \left\langle -k\ln\frac{\mathcal{F}}{y}\mathcal{F}\right\rangle$, the corresponding flux $\Psi_i = \left\langle -k\ln\frac{\mathcal{F}}{y}v_i\mathcal{F}\right\rangle$ and source $\Phi = \Delta\left[-k\ln\frac{\mathcal{F}}{y}\mathcal{F}\right]$, the Eq. (3.22) can be expressed as

$$\frac{\partial S}{\partial t} + \frac{\partial\Psi_i}{\partial x_i} = \Phi\,. \tag{3.23}$$

If Eq. (3.23) is integrated over an isolated system, where the flux terms are zero on the boundary, the rate of change of the variable, S, within the system is only affected by the source, Φ. It can be shown that Φ is always non-negative and only equal to zero if $\mathcal{F} = \mathcal{M}$. That is, entropy never decreases [7]. In fact, the variable S is an entropy density of the gas, by which the total entropy within an arbitrary spacial domain, V, can be obtained as

$$H = \iiint_V S\ \mathrm{d}^3x_i = \iiint_V\iiint_\infty -k\ln\frac{\mathcal{F}}{y}\mathcal{F}\ \mathrm{d}^3v_i\ \mathrm{d}^3x_i\,. \tag{3.24}$$

A probabilistic view of entropy

Based on the definition of distribution function, $\mathcal{F}$, the number of particles within a particular phase-space volume, $\mathrm{d}\hat{V}$, at location of x_i and v_i can be expressed as

$$N_{\hat{x}_i,\hat{v}_i} = \mathcal{F}\left(\hat{x}_i,\hat{v}_i\right)\ \mathrm{d}^3x_i\ \mathrm{d}^3v_i = \mathcal{F}\left(\hat{x}_i,\hat{v}_i\right)\mathrm{d}\hat{V}\,, \tag{3.25}$$

and the total number of particles can be calculated by summing over all phase-space volumes, $N = \sum_{\hat{x}_i,\hat{v}_i} N_{\hat{x}_i,\hat{v}_i}$. This allows the total entropy to be expressed as

$$\begin{aligned} H &= -k \sum_{\hat{x}_i,\hat{v}_i} N_{\hat{x}_i,\hat{v}_i} \ln \frac{N_{\hat{x}_i,\hat{v}_i}}{y\mathrm{d}\hat{V}} \\ &= -k \sum_{\hat{x}_i,\hat{v}_i} N_{\hat{x}_i,\hat{v}_i} \ln N_{\hat{x}_i,\hat{v}_i} + kN \ln \left(y\mathrm{d}\hat{V} \right) . \end{aligned} \tag{3.26}$$

Applying Sterling's approximation, $\ln N! \approx N \ln N - N$, and choosing the constant $y = \frac{N}{\mathrm{d}\hat{V}}$, the expression of total entropy can be further simplified as

$$\begin{aligned} H &= k \ln \left(\frac{N!}{\prod_{\hat{x}_i,\hat{v}_i} N_{\hat{x}_i,\hat{v}_i}!} \right) + kN \ln \left(\frac{y\mathrm{d}\hat{V}}{N} \right) \\ &= k \ln \left(\frac{N!}{\prod_{\hat{x}_i,\hat{v}_i} N_{\hat{x}_i,\hat{v}_i}!} \right) , \end{aligned} \tag{3.27}$$

where $\frac{N!}{\prod_{\hat{x}_i,\hat{v}_i} N_{\hat{x}_i,\hat{v}_i}!}$ represents the number of ways to distribute N particles such that $N_{\hat{x}_i,\hat{v}_i}$ particles are distributed at phase-space location x_i and v_i. In the other words, the entropy represents the number of possible arrangements of gaseous particles distribution described by the distribution function, and the velocity distribution function with the highest entropy describes the most likely state of particle distribution. This realization gives a strong argument for the maximum-entropy closure technique. In essence, the moment-closure technique requires one to assume a form for the distribution function based on incomplete moment information. As entropy simply measures the likelihood of a given distribution, choosing the distribution that maximizes the entropy while remaining consistent with the known moments is a highly justifiable choice.

Solving the entropy-maximization problem

The form of the entropy-maximizing distribution function can be determined by solving an optimization problem, in which the entropy is maximized while satisfying N specified moment, $\mathbf{U}$, corresponding to velocity weights, $\mathbf{M}$. By choosing the constant relationship, $y = ez$, in the velocity-dependent weight, Eq. (3.18), the maximization problem can be described as

$$\max_{\mathcal{F}} \left\langle -k \left(\mathcal{F} \ln \frac{\mathcal{F}}{z} - \mathcal{F} \right) \right\rangle \tag{3.28}$$

subject to

$$\mathbf{U} = \langle \mathbf{M}\mathcal{F} \rangle . \tag{3.29}$$

This constrained maximization problem can be solved by using the method of Lagrange multipliers. The method introduces a new function, J, which is defined as

$$J = \left\langle -k\left(\mathcal{F}\ln\frac{\mathcal{F}}{z} - \mathcal{F}\right)\right\rangle - \hat{\boldsymbol{\alpha}}^T\left(\mathbf{U} - \langle \mathbf{M}\mathcal{F}\rangle\right) , \tag{3.30}$$

where $\hat{\boldsymbol{\alpha}}$ indicates the vector of Lagrange multipliers. The original constrained maximization problem is then converted to a problem that searches the critical point, $\frac{\mathrm{d}J}{\mathrm{d}\mathcal{F}} = 0$, of the new function, J. It can be expressed as

$$\frac{\mathrm{d}J}{\mathrm{d}\mathcal{F}} = \left\langle -k\ln\frac{\mathcal{F}}{z}\right\rangle - \hat{\boldsymbol{\alpha}}^T\langle \mathbf{M}\rangle \tag{3.31}$$

$$= \left\langle \ln\mathcal{F} - \boldsymbol{\alpha}^T\mathbf{M}\right\rangle \tag{3.32}$$

$$= 0\,, \tag{3.33}$$

where the variables k and z are combined with the Lagrange multipliers. Due to the convexity of the entropy function, the unique solution for the distribution function takes the form of

$$\mathcal{F} = \exp\left(\boldsymbol{\alpha}^T\mathbf{M}\right) , \tag{3.34}$$

and the corresponding closure coefficients, $\boldsymbol{\alpha}$, are the Lagrange multipliers of the constrained maximization problem.

3.4 The Gaussian Ten-Moment Equations

The Gaussian distribution function is found by taking the form of the entropy-maximizing distribution function and $N = 10$ lower-order velocity moments [29]. The vector of velocity weights in this case is $\boldsymbol{V} = m\left[1, v_i, v_iv_j\right]^{\mathrm{T}}$. The resulting distribution function for the Gaussian ten-moment model is

$$\mathcal{F} = \mathcal{G} = \frac{\rho}{m\left(2\pi\right)^{3/2}\left(\det\Theta_{ij}\right)^{1/2}} e^{-\frac{1}{2}\Theta_{ij}^{-1}c_ic_j} , \tag{3.35}$$

where $\Theta_{ij} = P_{ij}/\rho$ is an anisotropic temperature tensor. Applying the Gaussian distribution function in Maxwell's equation of change results in a set of PDEs given as

$$\frac{\partial\rho}{\partial t} + \frac{\partial}{\partial x_k}\left(\rho u_k\right) = \Delta\left[\mathcal{G}\right] , \tag{3.36}$$

$$\frac{\partial}{\partial t}\left(\rho u_i\right) + \frac{\partial}{\partial x_k}\left(\rho u_iu_k + P_{ik}\right) = \Delta\left[v_i\mathcal{G}\right] , \tag{3.37}$$

$$\frac{\partial}{\partial t}\left(\rho u_iu_j + P_{ij}\right) + \frac{\partial}{\partial x_k}\left(\rho u_iu_ju_k + u_iP_{jk} + u_jP_{ik} + u_kP_{ij}\right) = \Delta\left[v_iv_j\mathcal{G}\right] . \tag{3.38}$$

One notable feature of Gaussian closure is that the corresponding third-order random-velocity moments, $\langle mc_ic_jc_k\mathcal{G}\rangle$, are zero, which leads to the zero vector of heat flux, $q_i = \frac{1}{2}\langle mc_ic_jc_j\mathcal{G}\rangle$. This feature limits the application of the Gaussian closure, since the effect of heat diffusion can not be predicted.

Using the BGK model to approximate the collision operator for the Gaussian closure gives

$$\frac{\delta\mathcal{G}}{\delta t} = -\frac{\mathcal{G}\left(x_i, v_i, t\right) - \mathcal{M}\left(x_i, v_i, t\right)}{\tau_{\mathcal{G}}\left(x_i, t\right)}\,, \tag{3.39}$$

by which the moments of this relaxation model can be obtained by taking the integral in velocity space as

$$\Delta\left[\mathcal{G}\right] = \left\langle m\frac{\delta\mathcal{G}}{\delta t}\right\rangle = -\iiint\limits_{\infty}\frac{m\left(\mathcal{G}-\mathcal{M}\right)}{\tau_{\mathcal{G}}}\,\mathrm{d}^3v_i = 0\,, \tag{3.40}$$

$$\Delta\left[v_i\mathcal{G}\right] = \left\langle mv_i\frac{\delta\mathcal{G}}{\delta t}\right\rangle = -\iiint\limits_{\infty}\frac{mv_i\left(\mathcal{G}-\mathcal{M}\right)}{\tau_{\mathcal{G}}}\,\mathrm{d}^3v_i = 0\,, \tag{3.41}$$

$$\Delta\left[v_iv_j\mathcal{G}\right] = \left\langle mv_iv_j\frac{\delta\mathcal{G}}{\delta t}\right\rangle = -\iiint\limits_{\infty}\frac{mv_iv_j\left(\mathcal{G}-\mathcal{M}\right)}{\tau_{\mathcal{G}}}\,\mathrm{d}^3v_i = -\frac{P_{ij}-\frac{1}{3}P_{kk}\delta_{ij}}{\tau_{\mathcal{G}}}\,. \tag{3.42}$$

Finally, the Gaussian ten-moment equations are derived, which have the form

$$\frac{\partial\rho}{\partial t} + \frac{\partial}{\partial x_k}\left(\rho u_k\right) = 0\,, \tag{3.43}$$

$$\frac{\partial}{\partial t}\left(\rho u_i\right) + \frac{\partial}{\partial x_k}\left(\rho u_iu_k + P_{ik}\right) = 0\,, \tag{3.44}$$

$$\frac{\partial}{\partial t}\left(\rho u_iu_j + P_{ij}\right) + \frac{\partial}{\partial x_k}\left(\rho u_iu_ju_k + u_iP_{jk} + u_jP_{ik} + u_kP_{ij}\right) = -\frac{3P_{ij}-P_{kk}\delta_{ij}}{3\tau_{\mathcal{G}}}\,. \tag{3.45}$$

The first equation is the continuity equation and describes the conservation of mass. The second sets of equations are the momentum equations which describe the conservation of momentum. The last sets of equations take a balance-law form and describe the balance of energy. In the equilibrium limit, $P_{ij} = p\delta_{ij}$, the Gaussian ten-moment equation recovers the Euler equations, as one half of the trace of Eq. (3.45) gives

$$\frac{\partial}{\partial t}\left(\frac{1}{2}\rho u_iu_i + \frac{3}{2}p\right) + \frac{\partial}{\partial x_k}\left[u_k\left(\frac{1}{2}\rho u_iu_i + \frac{5}{2}p\right)\right] = 0\,, \tag{3.46}$$

which describes the conservation of total energy density for a monatomic gas with $\gamma = \frac{5}{3}$. In the ten-moment equations, $\tau_{\mathcal{G}}$ is the relaxation time associated with collisional processes, which, for low-Knudsen numbers, is related to the gas viscosity through the relation $\tau_{\mathcal{G}} =$

μ/p. This illustrates another important feature of the ten-moment model: in the near-equilibrium limit, solutions of Eqs. (3.43)–(3.45) recover solutions of the Navier-Stokes equations.

From Eqs. (3.43)–(3.45), the governing equation of the generalized pressure tensor P_{ij} can be extracted

$$\frac{\partial P_{ij}}{\partial t} + \frac{\partial}{\partial x_k}\left(u_k P_{ij}\right) + P_{jk}\frac{\partial u_i}{\partial x_k} + P_{ik}\frac{\partial u_j}{\partial x_k} = -\frac{3P_{ij} - P_{kk}\delta_{ij}}{3\tau_{\mathcal{G}}}\,. \tag{3.47}$$

As mentioned, for a monotonic gas, the trace of the deviatoric stress tensor $t_{kk} = 0$, therefore, the thermodynamic pressure $p = \frac{1}{3}P_{kk}$ and the deviatoric stress tensor can be expressed as $t_{ij} = \frac{1}{3}P_{kk}\delta_{ij} - P_{ij}$. The source term in Eq. (3.47) can then be replaced using t_{ij},

$$\frac{\partial P_{ij}}{\partial t} + \frac{\partial}{\partial x_k}\left(u_k P_{ij}\right) + P_{jk}\frac{\partial u_i}{\partial x_k} + P_{ik}\frac{\partial u_j}{\partial x_k} = \frac{t_{ij}}{\tau_{\mathcal{G}}}\,. \tag{3.48}$$

Taking the trace of Eq. (3.48) gives

$$\frac{\partial P_{ll}}{\partial t} + \frac{\partial}{\partial x_k}\left(u_k P_{ll}\right) + 2P_{lk}\frac{\partial u_l}{\partial x_k} = \underbrace{\frac{t_{ll}}{\tau_{\mathcal{G}}}}_{=0}\,, \tag{3.49}$$

where the right-hand source term is zero for a monotonic gas. One can combine Eqs. (3.48) and (3.49) and obtain

$$\begin{aligned}\frac{\partial}{\partial t}\left(P_{ij} - \frac{1}{3}P_{kk}\delta_{ij}\right) + \frac{\partial}{\partial x_k}\left[u_k\left(P_{ij} - \frac{1}{3}P_{kk}\delta_{ij}\right)\right] + P_{jk}\frac{\partial u_i}{\partial x_k} + P_{ik}\frac{\partial u_j}{\partial x_k} \\ - \frac{2}{3}P_{lk}\frac{\partial u_l}{\partial x_k}\delta_{ij} = \frac{t_{ij}}{\tau_{\mathcal{G}}}\,,\end{aligned} \tag{3.50}$$

which can be rewritten as

$$\begin{aligned}\frac{\partial t_{ij}}{\partial t} + \frac{\partial}{\partial x_k}\left(u_k t_{ij}\right) + \left(-p\delta_{jk} + t_{jk}\right)\frac{\partial u_i}{\partial x_k} + \left(-p\delta_{ik} + t_{ik}\right)\frac{\partial u_j}{\partial x_k} \\ - \frac{2}{3}\left(-p\delta_{lk} + t_{lk}\right)\frac{\partial u_l}{\partial x_k}\delta_{ij} = -\frac{t_{ij}}{\tau_{\mathcal{G}}}\,.\end{aligned} \tag{3.51}$$

This equation can be reformed as

$$\begin{aligned}\tau_{\mathcal{G}}\left[\frac{\partial t_{ij}}{\partial t} + \frac{\partial}{\partial x_k}\left(u_k t_{ij}\right) + t_{jk}\frac{\partial u_i}{\partial x_k} + t_{ik}\frac{\partial u_j}{\partial x_k} - \frac{2}{3}t_{lk}\frac{\partial u_l}{\partial x_k}\delta_{ij}\right] \\ - \underbrace{\tau_{\mathcal{G}}\cdot p}_{=\mu}\left(\frac{\partial u_i}{\partial x_j} + \frac{\partial u_j}{\partial x_i} - \frac{2}{3}\frac{\partial u_k}{\partial x_k}\delta_{ij}\right) = -t_{ij}\,.\end{aligned} \tag{3.52}$$

Due to the fact that, in the near-equilibrium regime, the relaxation time, $\tau_{\mathcal{G}}$, is small, and the thermodynamic pressure, p, is much larger than t_{ij}, Eq (3.52) approaches

$$\mu\left(\frac{\partial u_i}{\partial x_j}+\frac{\partial u_j}{\partial x_i}-\frac{2}{3}\frac{\partial u_k}{\partial x_k}\delta_{ij}\right)=t_{ij}\,, \tag{3.53}$$

which is the traditional constitutive equation for an isotropic Newtonian fluid. This coincides with the approximation of viscous stress used within the Navier-Stokes equations. Therefore, in near-equilibrium limits, the Gaussian ten-moment model can be considered as equivalent to the Navier-Stokes equations in terms of predictions.

Following the theoretical development and analysis, the Gaussian ten-moment equations has been applied to solve a wide variety laminar gas flow problems and compared to traditional models. Brown [9, 10] and Levermore [30] presented numerical studies of one-dimensional shock structure using the ten-moment model. Groth presented the approximation of ten-moment model for planar Couette flow, in which the predicted shear stress agrees with the analytical solution of the gas from continuum up to the transition regime. Hittinger [22] and McDonald [32, 34] conducted numerical experiments of the diatomic ten-moment for a wide range of canonical problems. Suzuki [45] presented a comparison between the numerical results of Gaussian ten-moment equations, Navier-Stokes equations and direct-simulation Monte Carlo method.

3.4.1 Eigenstructure

The Gaussian ten-moment equations, Eqs. (3.43)–(3.45), can be expressed in a non-conservative, or primitive, form as

$$\frac{\partial \rho}{\partial t}+\rho\frac{\partial u_k}{\partial x_k}+u_k\frac{\partial \rho}{\partial x_k}=0\,, \tag{3.54}$$

$$\frac{\partial u_i}{\partial t}+u_k\frac{\partial u_i}{\partial x_k}+\frac{1}{\rho}\frac{\partial P_{ik}}{\partial x_k}=0\,, \tag{3.55}$$

$$\frac{\partial P_{ij}}{\partial t}+u_k\frac{\partial P_{ij}}{\partial x_k}+P_{ij}\frac{\partial u_k}{\partial x_k}+P_{jk}\frac{\partial u_i}{\partial x_k}+P_{ik}\frac{\partial u_j}{\partial x_k}=-\frac{3P_{ij}-P_{kk}\delta_{ij}}{3\tau_{\mathcal{G}}}\,. \tag{3.56}$$

This can be written in a more compact way as

$$\frac{\partial \mathbf{W}}{\partial t}+\mathbf{A}_k\left(\mathbf{W}\right)\frac{\partial \mathbf{W}}{\partial x_k}=\mathbf{S}\left(\mathbf{W}\right)\,, \tag{3.57}$$

where $\mathbf{W}$ is the primitive state vector defined as

$$\mathbf{W}=\begin{bmatrix}\rho & u_x & u_y & u_z & P_{xx} & P_{xy} & P_{xz} & P_{yy} & P_{yz} & P_{zz}\end{bmatrix}^{\mathrm{T}}\,. \tag{3.58}$$

Ten eigenvalues of the matrix $\mathbf{A}_k$, denoted as λ^k, can be found by solving the characteristic polynomial of the matrix, $\det\left(\mathbf{A}_k - \lambda^k \mathbf{I}\right)$. They include five distinct values as

$$\begin{aligned}
\lambda_1^k &= u_k - \sqrt{3\Theta_{kk}}\,, \\
\lambda_{2,3}^k &= u_x - \sqrt{\Theta_{kk}}\,, \\
\lambda_{4,5,6,7}^k &= u_k\,, \\
\lambda_{8,9}^k &= u_k + \sqrt{\Theta_{kk}}\,, \\
\lambda_{10}^k &= u_k + \sqrt{3\Theta_{kk}}\,,
\end{aligned}$$

which are the speeds of waves that carry the information of fundamental solutions as well as the perturbations. The corresponding right eigenvectors, $\mathbf{r}_i^k$, can be found and are given by

$$r_1^k = \begin{bmatrix}
1 \\
-\sqrt{\frac{3}{\Theta_{kk}}}\frac{\Theta_{xk}}{\rho} \\
-\sqrt{\frac{3}{\Theta_{kk}}}\frac{\Theta_{yk}}{\rho} \\
-\sqrt{\frac{3}{\Theta_{kk}}}\frac{\Theta_{zk}}{\rho} \\
\Theta_{xx} + 2\frac{\Theta_{xk}^2}{\Theta_{kk}} \\
\Theta_{xy} + 2\frac{\Theta_{xk}\Theta_{yk}}{\Theta_{kk}} \\
\Theta_{xz} + 2\frac{\Theta_{xk}\Theta_{zk}}{\Theta_{kk}} \\
\Theta_{yy} + 2\frac{\Theta_{yk}^2}{\Theta_{kk}} \\
\Theta_{yz} + 2\frac{\Theta_{yk}\Theta_{zk}}{\Theta_{kk}} \\
\Theta_{zz} + 2\frac{\Theta_{zk}^2}{\Theta_{kk}}
\end{bmatrix}, \; r_2^k = \begin{bmatrix}
0 \\
0 \\
-\frac{\sqrt{\Theta_{kk}}}{\rho}\left(\delta_{xk} + \delta_{zk}\right) \\
-\frac{\sqrt{\Theta_{yy}}}{\rho}\delta_{yk} \\
0 \\
\Theta_{xk}\left(\delta_{xk} + \delta_{yk}\right) \\
\Theta_{xy}\delta_{yk} \\
2\Theta_{yk}\left(\delta_{xk} + \delta_{zk}\right) \\
\Theta_{zk}\left(\delta_{xk} + \delta_{zk}\right) + \Theta_{yy}\delta_{yk} \\
2\Theta_{yz}\delta_{yk}
\end{bmatrix},$$

$$r_3^k = \begin{bmatrix}
0 \\
0 \\
-\frac{\sqrt{\Theta_{zz}}}{\rho}\delta_{zk} \\
-\frac{\sqrt{\Theta_{kk}}}{\rho}\left(\delta_{xk} + \delta_{yk}\right) \\
0 \\
\Theta_{xz}\delta_{zk} \\
\Theta_{xk}\delta_{yk}\left(\delta_{xk} + \delta_{yk}\right) \\
2\Theta_{yz}\delta_{zk} \\
\Theta_{yk}\left(\delta_{xk} + \delta_{yk}\right) + \Theta_{zz}\delta_{zk} \\
2\Theta_{zk}\left(\delta_{xk} + \delta_{yk}\right)
\end{bmatrix}, r_4^k = \begin{bmatrix}
1 \\
0 \\
0 \\
0 \\
0 \\
0 \\
0 \\
0 \\
0 \\
0
\end{bmatrix}, \; r_5^k = \begin{bmatrix}
0 \\
0 \\
0 \\
0 \\
\Theta_{kk}\left(\delta_{yk} + \delta_{zk}\right) \\
0 \\
0 \\
\Theta_{xx}\delta_{xk} \\
0 \\
0
\end{bmatrix},$$

$$r_6^k = \begin{bmatrix} 0 \\ 0 \\ 0 \\ 0 \\ 0 \\ \Theta_{zz}\delta_{zk} \\ \Theta_{yy}\delta_{yk} \\ 0 \\ \Theta_{xx}\delta_{xk} \\ 0 \end{bmatrix}, \; r_7^k = \begin{bmatrix} 0 \\ 0 \\ 0 \\ 0 \\ 0 \\ 0 \\ 0 \\ \Theta_{zz}\delta_{zk} \\ 0 \\ \Theta_{kk}\left(\delta_{xk}+\delta_{yk}\right) \end{bmatrix}, r_8^k = \begin{bmatrix} 0 \\ 0 \\ \frac{\sqrt{\Theta_{zz}}}{\rho}\delta_{zk} \\ \frac{\sqrt{\Theta_{kk}}}{\rho}\left(\delta_{xk}+\delta_{yk}\right) \\ 0 \\ \Theta_{xz}\delta_{zk} \\ \Theta_{xk}\delta_{yk}\left(\delta_{xk}+\delta_{yk}\right) \\ 2\Theta_{yz}\delta_{zk} \\ \Theta_{yk}\left(\delta_{xk}+\delta_{yk}\right)+\Theta_{zz}\delta_{zk} \\ 2\Theta_{zk}\left(\delta_{xk}+\delta_{yk}\right) \end{bmatrix},$$

$$r_9^k = \begin{bmatrix} 0 \\ 0 \\ \frac{\sqrt{\Theta_{kk}}}{\rho}\left(\delta_{xk}+\delta_{zk}\right) \\ \frac{\sqrt{\Theta_{yy}}}{\rho}\delta_{yk} \\ 0 \\ \Theta_{xk}\left(\delta_{xk}+\delta_{yk}\right) \\ \Theta_{xy}\delta_{yk} \\ 2\Theta_{yk}\left(\delta_{xk}+\delta_{zk}\right) \\ \Theta_{zk}\left(\delta_{xk}+\delta_{zk}\right)+\Theta_{yy}\delta_{yk} \\ 2\Theta_{yz}\delta_{yk} \end{bmatrix}, \; r_{10}^k = \begin{bmatrix} 1 \\ \sqrt{\frac{3}{\Theta_{kk}}}\frac{\Theta_{xk}}{\rho} \\ \sqrt{\frac{3}{\Theta_{kk}}}\frac{\Theta_{yk}}{\rho} \\ \sqrt{\frac{3}{\Theta_{kk}}}\frac{\Theta_{zk}}{\rho} \\ \Theta_{xx}+2\frac{\Theta_{xk}^2}{\Theta_{kk}} \\ \Theta_{xy}+2\frac{\Theta_{xk}\Theta_{yk}}{\Theta_{kk}} \\ \Theta_{xz}+2\frac{\Theta_{xk}\Theta_{zk}}{\Theta_{kk}} \\ \Theta_{yy}+2\frac{\Theta_{yk}^2}{\Theta_{kk}} \\ \Theta_{yz}+2\frac{\Theta_{yk}\Theta_{zk}}{\Theta_{kk}} \\ \Theta_{zz}+2\frac{\Theta_{zk}^2}{\Theta_{kk}} \end{bmatrix},$$

which provides the detail of each macroscopic quantities that is affected by each wave. The corresponding left eigenvectors, $\mathbf{l}_i^k$, are

$$l_1^k = \begin{bmatrix} 0 \\ -\frac{\rho}{6}\sqrt{\frac{3}{\Theta_{xx}}}\delta_{xk} \\ -\frac{\rho}{6}\sqrt{\frac{3}{\Theta_{yy}}}\delta_{yk} \\ -\frac{\rho}{6}\sqrt{\frac{3}{\Theta_{zz}}}\delta_{zk} \\ \frac{1}{6\Theta_{xx}}\delta_{xk} \\ 0 \\ 0 \\ \frac{1}{6\Theta_{yy}}\delta_{yk} \\ 0 \\ \frac{1}{6\Theta_{zz}}\delta_{zk} \end{bmatrix}^{\mathrm{T}}, \; l_2^k = \begin{bmatrix} 0 \\ \frac{\rho\left[\Theta_{yk}\left(\delta_{xk}-\delta_{yk}\right)-\Theta_{zz}\delta_{zk}\right]}{2\Theta_{kk}^{3/2}} \\ -\frac{\rho\Theta_{xk}\left(\delta_{xk}-\delta_{yk}\right)}{2\Theta_{kk}^{3/2}} \\ \frac{\rho\Theta_{xz}\delta_{zk}}{2\Theta_{zz}^{3/2}} \\ -\frac{\Theta_{xy}\delta_{xk}}{2\Theta_{xx}^2} \\ \frac{\delta_{xk}+\delta_{yk}}{2\Theta_{kk}} \\ \frac{\delta_{zk}}{2\Theta_{zz}} \\ -\frac{\Theta_{xy}\delta_{yk}}{2\Theta_{yy}^2} \\ 0 \\ -\frac{\Theta_{xz}\delta_{zk}}{2\Theta_{zz}^2} \end{bmatrix}^{\mathrm{T}}, \; l_3^k = \begin{bmatrix} 0 \\ \frac{\rho\Theta_{xz}\delta_{xk}}{2\Theta_{xx}^{3/2}} \\ -\frac{\rho\Theta_{zk}\left(\delta_{zk}-\delta_{yk}\right)}{2\Theta_{kk}^{3/2}} \\ \frac{\rho\left[\Theta_{yk}\left(\delta_{zk}-\delta_{yk}\right)-\Theta_{xx}\delta_{xk}\right]}{2\Theta_{kk}^{3/2}} \\ -\frac{\Theta_{xz}\delta_{xk}}{2\Theta_{xx}^2} \\ 0 \\ \frac{\delta_{xk}}{2\Theta_{xx}} \\ -\frac{\Theta_{yz}\delta_{yk}}{2\Theta_{yy}^2} \\ \frac{\delta_{yk}+\delta_{zk}}{2\Theta_{kk}} \\ -\frac{\Theta_{yz}\delta_{zk}}{2\Theta_{zz}^2} \end{bmatrix}^{\mathrm{T}},$$

$$l_4^k = \begin{bmatrix} 1 \\ 0 \\ 0 \\ 0 \\ -\frac{1}{3\Theta_{xx}}\delta_{xk} \\ 0 \\ 0 \\ -\frac{1}{3\Theta_{yy}}\delta_{yk} \\ 0 \\ -\frac{1}{3\Theta_{zz}}\delta_{zk} \end{bmatrix}^{\mathrm{T}}, \; l_5^k = \begin{bmatrix} 0 \\ 0 \\ 0 \\ 0 \\ \frac{4\Theta_{yk}^2-\Theta_{yy}\Theta_{kk}}{3\Theta_{kk}^3}\left(\delta_{xk}+\delta_{yk}\right)+\frac{\delta_{zk}}{\Theta_{zz}} \\ -2\frac{\Theta_{xy}}{\Theta_{kk}^2}\left(\delta_{xk}+\delta_{yk}\right) \\ -2\frac{\Theta_{xz}}{\Theta_{zz}^2}\delta_{zk} \\ \frac{4\Theta_{xk}^2-\Theta_{xx}\Theta_{kk}}{3\Theta_{kk}^3}\left(\delta_{xk}+\delta_{yk}\right) \\ 0 \\ \frac{4\Theta_{xz}^2-\Theta_{xx}\Theta_{zz}}{3\Theta_{zz}^3}\delta_{zk} \end{bmatrix},$$

$$l_6^k = \begin{bmatrix} 0 \\ 0 \\ 0 \\ 0 \\ \frac{4\Theta_{xy}\Theta_{xz}-\Theta_{xx}\Theta_{yz}}{3\Theta_{xx}^3}\delta_{xk} \\ \frac{2\delta_{zk}}{\Theta_{zz}^2}-\frac{\Theta_{zk}}{\Theta_{kk}^2} \\ \frac{2\delta_{yk}}{\Theta_{yy}^2}-\frac{\Theta_{yk}}{\Theta_{kk}^2} \\ \frac{4\Theta_{xy}\Theta_{yz}-\Theta_{xz}\Theta_{yy}}{3\Theta_{yy}^3}\delta_{yk} \\ \frac{2\delta_{xk}}{\Theta_{xx}^2}-\frac{\Theta_{xk}}{\Theta_{kk}^2} \\ \frac{4\Theta_{xz}\Theta_{yz}-\Theta_{xy}\Theta_{zz}}{3\Theta_{zz}^3}\delta_{zk} \end{bmatrix}^{\mathrm{T}}, \; l_7^k = \begin{bmatrix} 0 \\ 0 \\ 0 \\ 0 \\ \frac{4\Theta_{xz}^2-\Theta_{xx}\Theta_{zz}}{3\Theta_{xx}^3}\delta_{xk} \\ 0 \\ -2\frac{\Theta_{xz}\delta_{xk}}{\Theta_{xx}^2} \\ \frac{4\Theta_{zk}^2-\Theta_{zz}\Theta_{kk}}{3\Theta_{kk}^3}\left(\delta_{yk}+\delta_{zk}\right) \\ -2\frac{\Theta_{yz}}{\Theta_{kk}^2}\left(\delta_{yk}+\delta_{zk}\right) \\ \frac{4\Theta_{yk}^2-\Theta_{yy}\Theta_{kk}}{3\Theta_{kk}^3}\left(\delta_{yk}+\delta_{zk}\right)+\frac{\delta_{xk}}{\Theta_{xx}} \end{bmatrix}^{\mathrm{T}},$$

$$l_8^k = \begin{bmatrix} 0 \\ -\frac{\rho\Theta_{xz}\delta_{xk}}{2\Theta_{xx}^{3/2}} \\ \frac{\rho\Theta_{zk}\left(\delta_{zk}-\delta_{yk}\right)}{2\Theta_{kk}^{3/2}} \\ -\frac{\rho\left[\Theta_{yk}\left(\delta_{zk}-\delta_{yk}\right)-\Theta_{xx}\delta_{xk}\right]}{2\Theta_{kk}^{3/2}} \\ -\frac{\Theta_{xz}\delta_{xk}}{2\Theta_{xx}^2} \\ 0 \\ \frac{\delta_{xk}}{2\Theta_{xx}} \\ -\frac{\Theta_{yz}\delta_{yk}}{2\Theta_{yy}^2} \\ \frac{\delta_{yk}+\delta_{zk}}{2\Theta_{kk}} \\ -\frac{\Theta_{yz}\delta_{zk}}{2\Theta_{zz}^2} \end{bmatrix}^{\mathrm{T}}, \; l_9^k = \begin{bmatrix} 0 \\ -\frac{\rho\left[\Theta_{yk}\left(\delta_{xk}-\delta_{yk}\right)-\Theta_{zz}\delta_{zk}\right]}{2\Theta_{kk}^{3/2}} \\ \frac{\rho\Theta_{xk}\left(\delta_{xk}-\delta_{yk}\right)}{2\Theta_{kk}^{3/2}} \\ -\frac{\rho\Theta_{xz}\delta_{zk}}{2\Theta_{zz}^{3/2}} \\ -\frac{\Theta_{xy}\delta_{xk}}{2\Theta_{xx}^2} \\ \frac{\delta_{xk}+\delta_{yk}}{2\Theta_{kk}} \\ \frac{\delta_{zk}}{2\Theta_{zz}} \\ -\frac{\Theta_{xy}\delta_{yk}}{2\Theta_{yy}^2} \\ 0 \\ -\frac{\Theta_{xz}\delta_{zk}}{2\Theta_{zz}^2} \end{bmatrix}^{\mathrm{T}}, \; l_{10}^k = \begin{bmatrix} 0 \\ \frac{\rho}{6}\sqrt{\frac{3}{\Theta_{xx}}}\delta_{xk} \\ \frac{\rho}{6}\sqrt{\frac{3}{\Theta_{yy}}}\delta_{yk} \\ \frac{\rho}{6}\sqrt{\frac{3}{\Theta_{zz}}}\delta_{zk} \\ \frac{1}{6\Theta_{xx}}\delta_{xk} \\ 0 \\ 0 \\ \frac{1}{6\Theta_{yy}}\delta_{yk} \\ 0 \\ \frac{1}{6\Theta_{zz}}\delta_{zk} \end{bmatrix}^{\mathrm{T}},$$

which are associated with the wave strengths.

The nature of the waves associated with the ten-moment equations has been analysed by Brown [9, 10] as well as by Hittinger [22]. The wave speeds $\lambda^k_{1,10}$ are associated with the acoustic waves of the system, which, as shown in the right eigenvectors $r^k_{1,10}$, affects all state variables. It is found in [9, 10], that these two waves are genuinely non-linear and convex, which can generate discontinuous solutions from smooth initial conditions. The wave speeds $\lambda^k_{2,3,8,9}$ correspond to the shear waves that affect the transverse velocities and shear stresses. These four waves are linearly degenerate, which means discontinuous solutions can not be generated from smooth initial data. The remaining five waves associated with $\lambda^k_{4,5,6,7}$ share the same wave speed as the flow velocity. They are linearly degenerate as well. The λ^k_4 wave corresponds to the entropy wave, through which the change of entropy is convected. The $\lambda^k_{5,6,7}$ correspond to the pressure waves that translate the variance of all pressure components unrelated to the k direction [22].

As mentioned earlier, due to its first-order hyperbolic form, the Gaussian ten-moment model has many numerical advantages that traditional models do not. These include gaining an extra order of accuracy in space for a given reconstruction stencil and lower sensitivity to grid irregularity [33]. However, until this current project, the usage of the ten-moment model has been limited to laminar flows. This is due to the lack of well-suited turbulence models. In the following chapter, turbulence modelling techniques are reviewed and applied to the Gaussian ten-moment model for the first time, which results in a set of governing equations that is appropriate for turbulent flow.

Chapter 4

Elements of Turbulence Modelling

Turbulence is a common physical phenomenon of fluids, gaseous or liquid, which can be easily observed from nature and daily life, for example, in river currents, the motion of clouds, the smoke of a cigarette and the mixing of cream and coffee on the breakfast table. Although numerous studies have been conducted by physicists and mathematicians, the mysteries of turbulence have not been completely discovered. Based on the existing definitions of turbulence, some features of turbulence can be deduded. For example, the motion of turbulence is seemingly random, highly irregular and sensitive to initial conditions. It consists of a wide and continuous spectrum of scales in time and space. The large-scale eddies of turbulence enhance the transfer and diffusion of mass, momentum and energy, which are further transfered into small scale eddies and eventually dissipate into heat through viscous interaction. Including all observed turbulent features into a mathematical model is a complicated procedure, which is an important aspect to understand the physics and mathematics underneath, but it is not within the scope of this thesis. As mentioned, the goal of this thesis is to develop the appropriate form of turbulence models for moment closure methods with several desired features. Therefore, fundamental study of the physics underlying each turbulence model is not fully discussed in this work.

Since no existing turbulence model is currently available for the Gaussian ten-moment equations, their application has been, up to now, restricted to laminar flows. However, most real-world industrial problems are turbulent. This has severely limited the practical problems for which the ten-moment model, and moment models in general, can be used. The introduction of turbulence models to the ten-moment model will greatly increase its practical applicability.

There are several means to simulate turbulence, which can be classified into three main families including Direct Numerical Simulation (DNS), Large Eddy Simulation (LES) and Reynolds-Averaged Navier-Stokes (RANS) models. In DNS, the governing equations of fluid flow are directly solved for all possible temporal and spatial scales of turbulence. The large requirement on the mesh resolution and time steps implies extremely high computational cost, even for a simple problem. This limits the practical application of this approach. In LES, only large scale turbulence is resolved directly, while the small scale turbulence contributions are approximated through modelling. The computational cost of LES is therefore less expensive compared to DNS, which makes this approach applicable to some practical engineering problems. In RANS, only the averaged effects of turbulence are of interest and approximated through models. Even though this approach does not directly resolve any turbulent structure, the evaluation of RANS models can provide good approximations of averaged turbulent influence, which is sufficient for many different engineering problems. Due to the economic cost of computational resources, RANS modelling is still the most common approach in industrial applications. All above mentioned techniques can be adapted for use with the ten-moment equations. The current project only focuses on Reynolds-averaged turbulence modelling.

4.1 Reynolds Averaging

In turbulence modelling, the "mean" term denotes the outcome of some averaging process, which can possibly indicate the time average, the spatial average, or the ensemble average, depending on the context.

Time averaging is commonly used for the turbulent flow whose averaged turbulence effect does not change over time. The time average of an arbitrary instantaneous flow variable, $\phi(x_i, t)$, is defined as

$$\phi_T(x_i) = \lim_{T\to\infty} \frac{1}{T} \int_t^{t+T} \phi(x_i, t)\, \mathrm{d}t\,. \tag{4.1}$$

Spatial averaging is usually used for the turbulence flow whose averaged turbulent effect is isotropic. It is defined as

$$\phi_V(t) = \lim_{V\to\infty} \frac{1}{V} \iiint_V \phi(x_i, t)\, \mathrm{d}V\,. \tag{4.2}$$

Different from time and spatial averaging, which takes the average of turbulence effects from one experiment, ensemble averaging considers the average of measurements from N

identical experiments. For $\phi_n(x_i,t)$ representing an arbitrary flow variable measured in the n^{th} experiment from a series, the corresponding average over N identical experiments is defined as

$$\phi_E(x_i,t) = \lim_{N\to\infty} \frac{1}{N} \sum_{n=1}^{N} \phi_n(x_i,t) \; . \tag{4.3}$$

In this work, only time averaging is considered, which is also referred to as Reynolds-averaging. As the result of the averaging procedure, the averaged or mean component of the flow variable is obtained. The instantaneous flow variables can then be decomposed into mean and fluctuation parts, where the fluctuating component is deemed to represent the turbulent effect. This can be expressed as

$$\phi(x_i,t) = \bar{\phi}(x_i) + \phi'(x_i,t) \; , \tag{4.4}$$

where $\bar{\phi}(x_i)$ and $\phi'(x_i,t)$ denote the mean and fluctuating components respectively. One notes that any time-averaged mean component gives the same mean value and the time-averaged fluctuation gives zero. This is because, based on the definition of time averaging in Eq. (4.1), the time-averaged mean component is given as

$$\overline{\bar{\phi}(x_i)} = \lim_{T\to\infty} \frac{1}{T} \int_t^{t+T} \bar{\phi}(x_i)\, \mathrm{d}t = \bar{\phi}(x_i) \; . \tag{4.5}$$

The time-averaged fluctuating part is given as

$$\overline{\phi'(x_i)} = \lim_{T\to\infty} \frac{1}{T} \int_t^{t+T} \left(\phi(x_i,t) - \bar{\phi}(x_i)\right) \mathrm{d}t = \bar{\phi}(x_i) - \overline{\bar{\phi}(x_i)} = 0 \, . \tag{4.6}$$

Therefore, the average of any quantity gives

$$\overline{\phi(x_i,t)} = \overline{\bar{\phi}(x_i) + \phi'(x_i,t)} = \bar{\phi}(x_i) + \underbrace{\overline{\phi'(x_i,t)}}_{=0} \, . \tag{4.7}$$

Based on the same concept, the averaged product of multiple properties can be found. For example, the averaged product of any two properties follows

$$\overline{\phi\psi} = \overline{\left(\bar{\phi}+\phi'\right)\left(\bar{\psi}+\psi'\right)} = \overline{\bar{\phi}\bar{\psi} + \bar{\phi}\psi' + \bar{\psi}\phi' + \phi'\psi'} = \bar{\phi}\bar{\psi} + \overline{\phi'\psi'} \, , \tag{4.8}$$

and, similarly, the average of a triple product can be found as

$$\overline{\phi\psi\xi} = \bar{\phi}\bar{\psi}\bar{\xi} + \overline{\phi'\psi'}\bar{\xi} + \overline{\phi'\xi'}\bar{\psi} + \overline{\psi'\xi'}\bar{\phi} + \overline{\phi'\psi'\xi'} \, . \tag{4.9}$$

In this procedure, the time averaging and spatial differentiation are assumed to be commutable, which means

$$\overline{\frac{\partial\phi}{\partial x_i}} = \frac{\partial\bar{\phi}}{\partial x_i} \tag{4.10}$$

stands for any quantity. Moreover, the average unsteady term for nonstationary turbulence is assumed to be

$$\overline{\frac{\partial \phi}{\partial t}} = \frac{\partial \bar{\phi}}{\partial t} \,. \tag{4.11}$$

Traditionally, to obtain the governing equations for turbulent flow, the Reynolds-averaging process is applied to the Navier-Stokes equations. This results in a decomposition of flow properties into their mean and fluctuation components. For example, the flow velocities and pressure can be expressed as

$$u_i = \bar{u}_i + u_i' \,, \tag{4.12}$$

$$p = \bar{p} + p' \,. \tag{4.13}$$

Averaging the governing equations produces equations for the mean values of the entries of the solution vector [50]. The resulting equations are referred to as the Reynolds-averaged Navier-Stokes equations (RANS), which are considered as the governing equations for turbulent flow problems. For incompressible flow, the RANS momentum equation has the form

$$\rho \frac{\partial \bar{u}_i}{\partial t} + \rho \bar{u}_j \frac{\partial \bar{u}_i}{\partial x_j} = -\frac{\partial \bar{p}}{\partial x_i} + \frac{\partial}{\partial x_j} \left(2\mu \overline{S}_{ij} - \rho \overline{u_i' u_j'} \right) \,, \tag{4.14}$$

where the averaged strain-rate tensor is defined as $\overline{S}_{ij} = \frac{1}{2}\left(\frac{\partial \bar{u}_i}{\partial x_j} + \frac{\partial \bar{u}_j}{\partial x_i}\right)$. The quantity $-\overline{u_i' u_j'}$ is known as the Reynolds-stress tensor, which is henceforth denoted by τ_{ij}. It is obvious that the Reynolds-stress tensor must be computed in advance of solving the RANS equations, and additional equations for the Reynolds-stress tensor are therefore required. The Reynolds-stress equation can be derived by taking moments of the Navier-Stokes equation, which includes multiplying the momentum equation by a fluctuating velocity and time averaging the product [50]. The equations can be written as

$$\frac{\partial \tau_{ij}}{\partial t} + \bar{u}_j \frac{\partial \tau_{ij}}{\partial x_k} = -\tau_{ik} \frac{\partial \bar{u}_j}{\partial x_k} - \tau_{jk} \frac{\partial \bar{u}_i}{\partial x_k} + \epsilon_{ij} - \Pi_{ij} + \frac{\partial}{\partial x_k} \left[\nu \frac{\partial \tau_{ij}}{\partial x_k} + C_{ijk} \right] \,, \tag{4.15}$$

in which many new unknowns are generated, including the dissipation tensor, ϵ_{ij}, the pressure-strain correlation tensor, Π_{ij}, and C_{ijk} contains the triple fluctuating velocity correlation and fluctuating pressure-velocity correlation. Taking higher moments, additional equations for the new unknowns can be derived, however, extra new unknowns are, once again, generated. This illustrates that this procedure can never balance the number of unknowns and equations to close the system. A model is therefore required to approximate the unknowns so that the system of equations can be closed.

Since the beginning of the last century, many turbulence models have been developed for the RANS equations. They can be separated into five main categories including algebraic (zero-equation) models, one-equation models, two-equation models, three-equation models, and full Reynolds-stress (seven-equation) models.

In many turbulence models, the turbulence kinetic energy, defined as $k = \frac{1}{2}\overline{u_i' u_i'}$, is of interest. It represents the energy stored in turbulent fluctuations. The evolution equation for turbulence kinetic energy is derived by taking the trace of the Reynolds-stress equations, Eq. (4.15), which leads to

$$\frac{\partial k}{\partial t} + \bar{u}_j \frac{\partial k}{\partial x_j} = \tau_{ij} \frac{\partial \bar{u}_i}{\partial x_j} - \epsilon + \frac{\partial}{\partial x_j} \left[(\nu + \nu_T/\sigma_k) \frac{\partial k}{\partial x_j} \right] . \tag{4.16}$$

Here ϵ is the dissipation rate, while ν and ν_T are the kinematic viscosity and kinematic eddy viscosity respectively. This equation is typically used in one-equation, two-equation and three-equation models. In this equation, the diffusion effect of turbulence kinetic energy is approximated by adding the kinematic eddy viscosity into the diffusion term, which requires the evaluation of second-order derivatives. One notes that the turbulence kinetic energy only provides information on the trace of the Reynolds-stress tensor, and due to the appearance of the Reynolds-stress tensor in the RANS momentum equations, the system still remains un-closed. Therefore, in these RANS models, the Boussinesq approximation is usually combined with the turbulence kinetic energy equation to predict the contribution of the Reynolds-stress tensor, which has the form

$$\tau_{ij} = -\overline{u_i' u_j'} = 2\nu_T \overline{S}_{ij} - \frac{2}{3} k \delta_{ij} . \tag{4.17}$$

In this formula, the Reynolds-stress tensor is related to the averaged strain-rate tensor, $\bar{S}_{ij}$, which is governed by gradients of the mean velocity. Based on the Boussinesq approximation, the momentum diffusion caused by the turbulence mixing is also taken into account by adding the eddy viscosity into the diffusion term of the RANS momentum equations. The formulation of eddy viscosity is one key point determining the performance of turbulence models in different flow situations. The downside of this approximation is that the time evolution of the Reynolds-stress is not governed directly by PDEs, thus many details can not be taken into account.

The full Reynolds-stress model (RSM) is designed to make up for the above mentioned problem, since it provides the full time evolution history of all Reynolds-stress components. This type of model is superior as the complete information of the Reynolds-stress

tensor in time and space is given. As mentioned, there are many new unknowns generated in Reynolds-stress equations, Eq. (4.15), which are modelled with different formulas in different RSMs. Aside from the Reynolds-stress equations, an additional equation describing the time evolution of dissipation rate or its equivalent is coupled to complete the Reynolds-stress model. Therefore, it is also referred to as the seven-equation model.

4.2 Reynolds-averaged Gaussian Ten-Moment Equations

To obtain the governing equations for turbulence flow, the same "recipe" is now applied to the Gaussian ten-moment equations, Eqs. (3.43)–(3.45). The decomposition of the flow variables must first be introduced, which includes the velocities as previously introduced, flow density and generalized pressure tensor

$$\rho = \bar{\rho} + \rho' \,, \tag{4.18}$$

$$P_{ij} = \overline{P}_{ij} + P'_{ij} \,. \tag{4.19}$$

After averaging the ten-moment equations with the decomposed flow variables the Reynolds-averaged ten-moment equations are obtained. For the current project, applications are restricted to low-speed flow, which implies the compressibility effect is negligible and $\rho' = 0$. The resulting governing equations have the form

$$\frac{\partial \bar{\rho}}{\partial t} + \frac{\partial}{\partial x_k}\left(\bar{\rho}\bar{u}_k\right) = 0 \,, \tag{4.20}$$

$$\frac{\partial}{\partial t}\left(\bar{\rho}\bar{u}_i\right) + \frac{\partial}{\partial x_k}\left(\bar{\rho}\bar{u}_i\bar{u}_k + \bar{\rho}\overline{u'_i u'_k} + \overline{P}_{ik}\right) = 0 \,, \tag{4.21}$$

$$\begin{aligned}\frac{\partial}{\partial t}\left(\bar{\rho}\bar{u}_i\bar{u}_j + \bar{\rho}\overline{u'_i u'_j} + \overline{P}_{ij}\right) + \frac{\partial}{\partial x_k}\Big(&\bar{\rho}\bar{u}_i\bar{u}_j\bar{u}_k + \bar{\rho}\overline{u'_j u'_k}\bar{u}_i + \bar{\rho}\overline{u'_i u'_k}\bar{u}_j + \bar{\rho}\overline{u'_i u'_j}\bar{u}_k + \bar{\rho}\overline{u'_i u'_j u'_k} \\ &+\bar{u}_i\overline{P}_{jk} + \bar{u}_j\overline{P}_{ik} + \bar{u}_k\overline{P}_{ij} + \overline{u'_i P'_{jk}} + \overline{u'_j P'_{ik}} + \overline{u'_k P'_{ij}}\Big) = -\frac{3\overline{P}_{ij} - \overline{P}_{kk}\delta_{ij}}{3\tau_{\mathcal{G}}} \,.\end{aligned} \tag{4.22}$$

Similar to the RANS equations, the Reynolds-averaged ten-moment equations contain many new unknowns generated by the averaging process that represent multiple-variable correlations. The Reynolds-stress tensor, $\overline{u'_i u'_j}$, and triple correlation of fluctuating velocity, $\overline{u'_i u'_j u'_k}$, are examples. Other new terms introduced, such as the pressure-velocity correlation $\overline{u'_i P'_{jk}}$, are uniquely generated by averaging the ten-moment equations. This is due to the presence of the generalized pressure tensor in the original model. At this point, the equation

system is not closed. To close the system, a model that provides the approximation of the above mentioned unknowns is needed.

To close the Reynolds-averaged ten-moment model, most of the traditional RANS models can be coupled relatively easily, but this is not an ideal solution. The first-order hyperbolic form makes the ten-moment equations an attractive alternative to the Navier-Stokes equations. This type of model carries several numerical advantages, as discussed earlier. However, unfortunately, most of the existing traditional RANS models take the form of hyperbolic-parabolic mixed-type PDEs, in which the second-order derivative is used to approximate diffusive behaviour. Moreover, due to the presence of the Reynolds-stress tensor in the Reynolds-averaged ten-moment equation, if the Boussinesq approximation is used with traditional models, it also introduces second-order derivatives into the momentum and energy equations. The Reynolds-stress models could be used to avoid the above mentioned situation, since each Reynolds-stress component has its own PDE. But, even though the Boussinesq approximation is not used, the production term, $\tau_{ij}\frac{\partial \bar{u}_i}{\partial x_j}$, in the traditional Reynolds-stress model contains the mean velocity gradient, which breaks the balance-law form. Furthermore, most of the RSMs relate the unknown tensors to the averaged velocity gradient. Thus, coupling this type of traditional turbulence model would damage the pure hyperbolic nature of the moment model, thereby sacrificing all previously mentioned numerical advantages. In order to maintain the first-order hyperbolic form, the coupled turbulence model must also be first-order. Thus, the development of first-order hyperbolic turbulence models is the major goal of this project.

In the following chapters, several hyperbolic-relaxation turbulence models are proposed for the Reynolds-averaged ten-moment equations, which contain the desired features. Furthermore, an eigenstructure and dispersion analysis of the resulting full system of governing equations is presented.

Chapter 5

Reynolds-Averaged Ten-Moment Model with Hyperbolic-Relaxation One-Equation Models

As discussed, the goal of this project is to develop first-order hyperbolic turbulence models that can be used with the Reynolds-averaged ten-moment equations. Due to the presence of diffusive second-order derivatives in traditional models, directly coupling the existing RANS model is not preferred. In this chapter, the previously introduced relaxation methods are used to derive hyperbolic-relaxation forms of Prandtl's one-equation model. A new form of the Reynolds-averaged ten-moment equation is derived, which avoids the second-order derivatives in the momentum and energy equations from the Boussinesq approximation [50]. The overall first-order hyperbolic governing equations for turbulent flow are obtained by coupling the hyperbolic-relaxation one-equation model to the Reynolds-averaged ten-moment equations. The corresponding eigenstructure and dispersion relation are studied and presented.

5.1 The Hyperbolic-Relaxation Form of Prandtl's One-Equation Model

A typical Prandtl one-equation model is targeted as a first step in turbulence modelling for the Gaussian closure. Prandtl's one-equation model provides an additional PDE to

describe the time evolution of the turbulence kinetic energy. The original model for the turbulent kinetic energy in an incompressible flow has the form

$$\frac{\partial k}{\partial t} + \bar{u}_j \frac{\partial k}{\partial x_j} = \tau_{ij} \frac{\partial \bar{u}_i}{\partial x_j} - \epsilon + \frac{\partial}{\partial x_j} \left[(\nu + \nu_T/\sigma_k) \frac{\partial k}{\partial x_j} \right] , \tag{5.1}$$

where the dissipation rate, ϵ, is modelled by $C_D \frac{k^{3/2}}{l}$, C_D and σ_k are closure coefficients with $\sigma_k = 1$ and C_D ranging between 0.07 and 0.09, and l is the length scale of the turbulence [50]. The prescription of length scale must be established empirically. Based on Prandtl's investigation, it is proportional to the mixing-length. Here, the kinematic eddy-viscosity model is proposed by Prandtl as

$$\nu_T = k^{1/2} l = C_D k^2 / \epsilon \, . \tag{5.2}$$

The Reynolds-stress tensor, τ_{ij}, in the production term is approximated by the Boussinesq approximation, Eq. (4.17). Thus, the production term can be fully expressed in three dimensions as

$$\begin{aligned} \tau_{ij} \frac{\partial \bar{u}_i}{\partial x_j} = \nu_T \Bigg\{ 2 \left[\left(\frac{\partial \bar{u}_x}{\partial x} \right)^2 + \left(\frac{\partial \bar{u}_y}{\partial y} \right)^2 + \left(\frac{\partial \bar{u}_z}{\partial z} \right)^2 \right] + \left(\frac{\partial \bar{u}_x}{\partial y} + \frac{\partial \bar{u}_y}{\partial x} \right)^2 \\ + \left(\frac{\partial \bar{u}_x}{\partial z} + \frac{\partial \bar{u}_z}{\partial x} \right)^2 + \left(\frac{\partial \bar{u}_y}{\partial z} + \frac{\partial \bar{u}_z}{\partial y} \right)^2 \Bigg\} - \frac{2}{3} k \underbrace{\left(\frac{\partial \bar{u}_x}{\partial x} + \frac{\partial \bar{u}_y}{\partial y} + \frac{\partial \bar{u}_z}{\partial z} \right)}_{=0} , \end{aligned} \tag{5.3}$$

where the last term is zero, as the velocity field is divergence free for incompressible flow.

To build a similar model for the moment equations, the velocity gradients in the production term can be replaced by a clever use of the generalized pressure tensor P_{ij}. As discussed, the equilibrium pressure, p, is related to the generalized pressure tensor by $P_{ij} = p\delta_{ij} - t_{ij}$, with $p = P_{kk}/3$. Thus, the average of P_{ij} can be expressed as

$$\overline{P}_{ij} = \bar{p}\delta_{ij} - \bar{t}_{ij} \, . \tag{5.4}$$

Since the deviatoric stress tensor, t_{ij}, is approximated by the viscous stress tensor in the Navier-Stokes equations, it allows the replacement of the averaged strain-rate tensor in the RANS equation by the averaged generalized pressure tensor, which gives

$$\bar{t}_{ij} = 2\mu \overline{S}_{ij} = \frac{1}{3} \overline{P}_{kk} \delta_{ij} - \overline{P}_{ij} \, . \tag{5.5}$$

According to this relation, the production term can be re-expressed algebraically as

$$\tau_{ij} \frac{\partial \bar{u}_i}{\partial x_j} = \frac{\nu_T}{2\mu^2} \bar{t}_{ij} \bar{t}_{ij} \, . \tag{5.6}$$

Rewriting the turbulence kinetic energy equation, Eq. (5.1), with this replacement gives

$$\frac{\partial k}{\partial t}+\bar{u}_j\frac{\partial k}{\partial x_j}=\frac{\nu_T}{2\mu^2}\bar{t}_{ij}\bar{t}_{ij}-C_D\frac{k^{3/2}}{l}+\frac{\partial}{\partial x_j}\left[(\nu+k^{1/2}l)\frac{\partial k}{\partial x_j}\right], \tag{5.7}$$

where both the production and dissipation terms are now algebraic. Equation (5.7) is designed for incompressible flow, where the velocity field is divergence free. To be more general, the averaged flow velocity, $\bar{u}_j$, can be brought into the derivative of the convection term, $\frac{\partial}{\partial x_j}(k\bar{u}_j)$, and Eq. (5.7) can be written in the form

$$\frac{\partial k}{\partial t}+\frac{\partial k\bar{u}_j}{\partial x_j}=s(k)+\frac{\partial}{\partial x_j}\left(d(k)\frac{\partial k}{\partial x_j}\right). \tag{5.8}$$

5.1.1 Chen-Levermore-Liu P-System Type Hyperbolic-Relaxation Prandtl's One-Equation Model

Equation (5.8) has the form of a convection-diffusion equation with an algebraic source term. In principle, its equivalent hyperbolic-relaxation system should exist. Based on the application of the p-system for a typical convection-diffusion equation, its hyperbolic-relaxation form in two-dimensions is assumed to be of the form

$$\frac{\partial k}{\partial t}+\frac{\partial \psi_x}{\partial x}+\frac{\partial \psi_y}{\partial y}=s(k), \tag{5.9}$$

$$\frac{\partial \psi_x}{\partial t}+\frac{\partial f_x(k)}{\partial x}=-\frac{1}{\tau_k}(\psi_x-g_x(k))+\frac{\partial g_x(k)}{\partial k}s(k), \tag{5.10}$$

$$\frac{\partial \psi_y}{\partial t}+\frac{\partial f_y(k)}{\partial y}=-\frac{1}{\tau_k}(\psi_y-g_y(k))+\frac{\partial g_y(k)}{\partial k}s(k). \tag{5.11}$$

Here, new fluxes, ψ_x and ψ_y, are introduced, τ_k is a constant relaxation time with which the solution of hyperbolic-relaxation equations approaches the convection-diffusion equation. The additional functions $f_i(k)$ and $g_i(k)$ can be determined by asymptotic analysis, as discussed earlier.

Based on the same assumption used in Section 2.1.3, ψ_x and ψ_y are decomposed into equilibrium fluxes and a small deviation,

$$\psi_x=g_x(k)+\psi_{x1}, \tag{5.12}$$

$$\psi_y=g_y(k)+\psi_{y1}, \tag{5.13}$$

where ψ_{x1} and ψ_{y1} are the small deviation components, whose time and space derivatives are negligible. Thus, the temporal and spacial derivative of ψ_x and ψ_y are taken as

$$\frac{\partial \psi_x}{\partial t} = \frac{\partial g_x(k)}{\partial t} + \frac{\partial \psi_{x1}}{\partial t} \approx \frac{\partial g_x(k)}{\partial k}\frac{\partial k}{\partial t}, \tag{5.14}$$

$$\frac{\partial \psi_x}{\partial x} = \frac{\partial g_x(k)}{\partial x} + \frac{\partial \psi_{x1}}{\partial x} \approx \frac{\partial g_x(k)}{\partial k}\frac{\partial k}{\partial x}, \tag{5.15}$$

$$\frac{\partial \psi_y}{\partial t} = \frac{\partial g_y(k)}{\partial t} + \frac{\partial \psi_{y1}}{\partial t} \approx \frac{\partial g_y(k)}{\partial k}\frac{\partial k}{\partial t}, \tag{5.16}$$

$$\frac{\partial \psi_y}{\partial y} = \frac{\partial g_y(k)}{\partial x} + \frac{\partial \psi_{y1}}{\partial y} \approx \frac{\partial g_y(k)}{\partial k}\frac{\partial k}{\partial y}. \tag{5.17}$$

Substituting Eq. (5.12) and Eq. (5.13) into Eq. (5.10) and Eq. (5.11) respectively, expressions for ψ_{x1} and ψ_{y1} are obtained

$$\psi_{x1} = -\tau_k \left(\frac{\partial \psi_x}{\partial t} + \frac{\partial f_x(k)}{\partial x} - \frac{\partial g_x(k)}{\partial k} s(k) \right), \tag{5.18}$$

$$\psi_{y1} = -\tau_k \left(\frac{\partial \psi_y}{\partial t} + \frac{\partial f_y(k)}{\partial y} - \frac{\partial g_y(k)}{\partial k} s(k) \right). \tag{5.19}$$

Substituting Eq. (5.15) and Eq. (5.17) into Eq. (5.9) leads to

$$\frac{\partial k}{\partial t} = s(k) - \left(\frac{\partial \psi_x}{\partial x} + \frac{\partial \psi_y}{\partial y} \right) = s(k) - \left(\frac{\partial g_x(k)}{\partial k}\frac{\partial k}{\partial x} + \frac{\partial g_y(k)}{\partial k}\frac{\partial k}{\partial y} \right). \tag{5.20}$$

By substituting Eq. (5.20) into Eq. (5.14) and Eq. (5.16), alternative expressions for $\frac{\partial \psi_x}{\partial t}$ and $\frac{\partial \psi_y}{\partial t}$ are obtained as

$$\frac{\partial \psi_x}{\partial t} = \frac{\partial g_x(k)}{\partial k} \left[s(k) - \left(\frac{\partial g_x(k)}{\partial k}\frac{\partial k}{\partial x} + \frac{\partial g_y(k)}{\partial k}\frac{\partial k}{\partial y} \right) \right], \tag{5.21}$$

$$\frac{\partial \psi_y}{\partial t} = \frac{\partial g_y(k)}{\partial k} \left[s(k) - \left(\frac{\partial g_x(k)}{\partial k}\frac{\partial k}{\partial x} + \frac{\partial g_y(k)}{\partial k}\frac{\partial k}{\partial y} \right) \right]. \tag{5.22}$$

Substituting Eq. (5.21) and Eq. (5.22) into Eq. (5.18) and Eq. (5.19) respectively, gives

$$\begin{aligned} \psi_{x1} &= -\tau_k \left\{ \frac{\partial g_x(k)}{\partial k} \left[s(k) - \left(\frac{\partial g_x(k)}{\partial k}\frac{\partial k}{\partial x} + \frac{\partial g_y(k)}{\partial k}\frac{\partial k}{\partial y} \right) \right] + \frac{\partial f_x(k)}{\partial k}\frac{\partial k}{\partial x} - \frac{\partial g_x(k)}{\partial k} s(k) \right\} \\ &= -\tau_k \left\{ \left[\frac{\partial f_x(k)}{\partial k} - \left(\frac{\partial g_x(k)}{\partial k} \right)^2 \right] \frac{\partial k}{\partial x} - \frac{\partial g_x(k)}{\partial k}\frac{\partial g_y(k)}{\partial k}\frac{\partial k}{\partial y} \right\}, \end{aligned} \tag{5.23}$$

$$\begin{aligned} \psi_{y1} &= -\tau_k \left\{ \frac{\partial g_y(k)}{\partial k} \left[s(k) - \left(\frac{\partial g_x(k)}{\partial k}\frac{\partial k}{\partial x} + \frac{\partial g_y(k)}{\partial k}\frac{\partial k}{\partial y} \right) \right] + \frac{\partial f_y(k)}{\partial k}\frac{\partial k}{\partial y} - \frac{\partial g_y(k)}{\partial k} s(k) \right\} \\ &= -\tau_k \left\{ \left[\frac{\partial f_y(k)}{\partial k} - \left(\frac{\partial g_y(k)}{\partial k} \right)^2 \right] \frac{\partial k}{\partial y} - \frac{\partial g_y(k)}{\partial k}\frac{\partial g_x(k)}{\partial k}\frac{\partial k}{\partial x} \right\}. \end{aligned} \tag{5.24}$$

Now, replacing ψ_{x1} and ψ_{y1} by Eq. (5.23) and Eq. (5.24) in Eq. (5.12) and Eq. (5.13) leads to

$$\psi_x = g_x(k) - \tau_k \left\{ \left[\frac{\partial f_x(k)}{\partial k} - \left(\frac{\partial g_x(k)}{\partial k} \right)^2 \right] \frac{\partial k}{\partial x} - \frac{\partial g_x(k)}{\partial k} \frac{\partial g_y(k)}{\partial k} \frac{\partial k}{\partial y} \right\}, \tag{5.25}$$

$$\psi_y = g_y(k) - \tau_k \left\{ \left[\frac{\partial f_y(k)}{\partial k} - \left(\frac{\partial g_y(k)}{\partial k} \right)^2 \right] \frac{\partial k}{\partial y} - \frac{\partial g_y(k)}{\partial k} \frac{\partial g_x(k)}{\partial k} \frac{\partial k}{\partial x} \right\}. \tag{5.26}$$

Substituting Eq. (5.25) and Eq. (5.26) into Eq. (5.9) gives

$$\begin{aligned} &\frac{\partial k}{\partial t} + \frac{\partial}{\partial x} \left(g_x(k) - \tau_k \left\{ \left[\frac{\partial f_x(k)}{\partial k} - \left(\frac{\partial g_x(k)}{\partial k} \right)^2 \right] \frac{\partial k}{\partial x} - \frac{\partial g_x(k)}{\partial k} \frac{\partial g_y(k)}{\partial k} \frac{\partial k}{\partial y} \right\} \right) \\ &\quad + \frac{\partial}{\partial y} \left(g_y(k) - \tau_k \left\{ \left[\frac{\partial f_y(k)}{\partial k} - \left(\frac{\partial g_y(k)}{\partial k} \right)^2 \right] \frac{\partial k}{\partial y} - \frac{\partial g_y(k)}{\partial k} \frac{\partial g_x(k)}{\partial k} \frac{\partial k}{\partial x} \right\} \right) = s(k) \,. \end{aligned} \tag{5.27}$$

Following a similar derivation, as was used for the convection-diffusion equation [4, 41], the cross-derivative terms are ignored and Eq. (5.27) can be simplified to

$$\begin{aligned} &\frac{\partial k}{\partial t} + \frac{\partial}{\partial x} \left\{ g_x(k) - \tau_k \left[\frac{\partial f_x(k)}{\partial k} - \left(\frac{\partial g_x(k)}{\partial k} \right)^2 \right] \frac{\partial k}{\partial x} \right\} \\ &\qquad + \frac{\partial}{\partial y} \left\{ g_y(k) - \tau_k \left[\frac{\partial f_y(k)}{\partial k} - \left(\frac{\partial g_y(k)}{\partial k} \right)^2 \right] \frac{\partial k}{\partial y} \right\} = s(k) \end{aligned} \tag{5.28}$$

or

$$\begin{aligned} &\frac{\partial k}{\partial t} + \frac{\partial g_x(k)}{\partial x} - \tau_k \frac{\partial}{\partial x} \left\{ \left[\frac{\partial f_x(k)}{\partial k} - \left(\frac{\partial g_x(k)}{\partial k} \right)^2 \right] \frac{\partial k}{\partial x} \right\} \\ &\qquad + \frac{\partial g_y(k)}{\partial y} - \tau_k \frac{\partial}{\partial y} \left\{ \left[\frac{\partial f_y(k)}{\partial k} - \left(\frac{\partial g_y(k)}{\partial k} \right)^2 \right] \frac{\partial k}{\partial y} \right\} = s(k) \,. \end{aligned} \tag{5.29}$$

To match Prandtl's one equation model, Eq. (5.7), the following functions are chosen

$$g_x(k) = \bar{u}_x k \,, \tag{5.30}$$

$$g_y(k) = \bar{u}_y k \,, \tag{5.31}$$

$$f_x(k) = \frac{1}{\tau_k} \left(\nu k + \frac{2}{3} k^{3/2} l \right) + \bar{u}_x^2 k \,, \tag{5.32}$$

$$f_y(k) = \frac{1}{\tau_k} \left(\nu k + \frac{2}{3} k^{3/2} l \right) + \bar{u}_y^2 k \,, \tag{5.33}$$

$$s(k) = \frac{k^{1/2} l}{2\mu^2} \bar{t}_{ij} \bar{t}_{ij} - C_D \frac{k^{3/2}}{l} \,. \tag{5.34}$$

Thus, the equivalent two-dimensional p-system type hyperbolic-relaxation version of Eq. (5.7) is given by

$$\frac{\partial k}{\partial t}+\frac{\partial \psi_x}{\partial x}+\frac{\partial \psi_y}{\partial y}=s\left(k\right)\,, \tag{5.35}$$

$$\frac{\partial \psi_x}{\partial t}+\frac{\partial}{\partial x}\left[\frac{1}{\tau_k}\left(\nu k+\frac{2}{3}k^{3/2}l\right)+\bar{u}_x^2 k\right]=-\frac{1}{\tau_k}\left(\psi_x-\bar{u}_x k\right)+\bar{u}_x s\left(k\right)\,, \tag{5.36}$$

$$\frac{\partial \psi_y}{\partial t}+\frac{\partial}{\partial y}\left[\frac{1}{\tau_k}\left(\nu k+\frac{2}{3}k^{3/2}l\right)+\bar{u}_y^2 k\right]=-\frac{1}{\tau_k}\left(\psi_y-\bar{u}_y k\right)+\bar{u}_y s\left(k\right)\,, \tag{5.37}$$

and the general form with an arbitrary number of spacial dimensions can be written as

$$\frac{\partial k}{\partial t}+\frac{\partial \psi_j}{\partial x_j}=s\left(k\right)\,, \tag{5.38}$$

$$\frac{\partial \psi_i}{\partial t}+\frac{\partial}{\partial x_i}\left[\frac{1}{\tau_k}\left(\nu k+\frac{2}{3}k^{3/2}l\right)+\bar{u}_i^2 k\right]=-\frac{1}{\tau_k}\left(\psi_i-\bar{u}_i k\right)+\bar{u}_i s\left(k\right)\,. \tag{5.39}$$

Instead of one PDE with a second-order derivative, the hyperbolic-relaxation form introduces a set of first-order PDEs that take the form of hyperbolic balance laws. With a small relaxation time, τ_k, the asymptotic behaviour of this hyperbolic system approaches its diffusion limit, where the first-order PDEs provide the same solution as the original model. Thus, this hyperbolic version is indeed equivalent to the original one.

5.1.2 Cattaneo-Vernotte Type Hyperbolic-Relaxation version of Prandtl's One-Equation Model

Based on the Cattaneo-Vernotte model, Eqs. (2.40)–(2.41), of the general convection-diffusion equation, the Cattaneo-Vernotte type hyperbolic-relaxation Prandtl's one-equation model can be easily derived. Its general form can be written as

$$\frac{\partial k}{\partial t}+\frac{\partial}{\partial x_j}\left(k\bar{u}_j-\left(\nu+k^{1/2}l\right)\psi_j\right)=s\left(k\right)\,, \tag{5.40}$$

$$\frac{\partial \psi_i}{\partial t}+\frac{\partial}{\partial x_i}\left(-\frac{k}{\tau_k}\right)=-\frac{\psi_i}{\tau_k}\,. \tag{5.41}$$

The first equation, Eq. (5.40), takes exactly the same form as the original model, Eq. (5.7), except the gradient of turbulence kinetic energy, $\frac{\partial k}{\partial x_j}$, is replaced by the new variable, ψ_j. Similar to the p-system type hyperbolic form, the same number of additional PDEs are introduced, which describe the time evolution of the diffusive flux components. Again, for this model's behaviour to approach that of the original one-equation model, the relaxation time, τ_k, must be small.

5.2 Reynolds-Averaged Gaussian Ten-Moment Model Coupled with the Hyperbolic-Relaxation Prandtl's One-Equation Model

At this point, two first-order hyperbolic-relaxation forms of Prandtl's one-equation model are proposed. The generalized pressure tensor is used to estimate the production term in the turbulence kinetic energy equation, which puts the equations in balance-law form. However, the system of equations is still not closed due to the appearance of the Reynolds-stress tensor in the Reynolds-averaged ten-moment equations. In the traditional one-, two-, and three-equation models, the Boussinesq approximation is used to approximate the Reynolds-stress tensor. However, this approximation is not preferred in the Reynolds-averaged ten-moment equations, since it will bring second-order derivatives into the momentum and energy equations, which will break the form of the first-order hyperbolic equations. Fortunately, the Reynolds-stress always occurs with the generalized pressure tensor in the governing equations, therefore, a new tensor, $\overline{\Psi}_{ij}$, is introduced to represent the summation of the averaged generalized pressure and Reynolds-stress tensors. It is defined as

$$\overline{\Psi}_{ij} = \overline{P}_{ij} + \bar{\rho}\overline{u_i' u_j'} \,. \tag{5.42}$$

According to the constitutive equation for an isotropic Newtonian fluid

$$t_{ij} = \mu \left(\frac{\partial u_i}{\partial x_j} + \frac{\partial u_j}{\partial x_i} \right) , \tag{5.43}$$

and the Boussinesq approximation, Eq. (4.17), the above relation can then be expanded as

$$\overline{\Psi}_{ij} = \frac{1}{3}\overline{P}_{kk}\delta_{ij} - \mu \left(\frac{\partial \bar{u}_i}{\partial x_j} + \frac{\partial \bar{u}_j}{\partial x_i} \right) + \frac{2}{3}\bar{\rho}\bar{k}\delta_{ij} - \bar{\rho}\nu_T \left(\frac{\partial \bar{u}_i}{\partial x_j} + \frac{\partial \bar{u}_j}{\partial x_i} \right) . \tag{5.44}$$

Thus, the averaged thermodynamic pressure, $\bar{p}$, can be extracted as

$$\bar{p} = \frac{1}{3}\overline{P}_{kk} = \frac{1}{3}\left(\overline{\Psi}_{kk} - 2\bar{\rho}\bar{k} \right) , \tag{5.45}$$

the averaged shear stress, $\overline{P}_{ij}$ for $i \neq j$, can be obtained as

$$\overline{P}_{ij} = \frac{\mu}{\mu + \bar{\rho}\nu_T}\overline{\Psi}_{ij} \,. \tag{5.46}$$

The shear Reynolds-stress, $\bar{\rho}\overline{u_i' u_j'}$ for $i \neq j$, can be obtained as

$$\bar{\rho}\overline{u_i' u_j'} = \frac{\bar{\rho}\nu_T}{\mu + \bar{\rho}\nu_T}\overline{\Psi}_{ij} \,, \tag{5.47}$$

and the deviatoric stress tensor can be rewritten as

$$\bar{t}_{ij} = \frac{1}{3}\overline{P}_{kk}\delta_{ij} - \overline{P}_{ij} = -\frac{\mu}{\mu + \bar{\rho}\nu_T}\left(\overline{\Psi}_{ij} - \frac{1}{3}\overline{\Psi}_{kk}\delta_{ij}\right) . \tag{5.48}$$

Finally, the Reynolds-averaged ten-moment equations can be rewritten as

$$\frac{\partial \bar{\rho}}{\partial t} + \frac{\partial}{\partial x_k}\left(\bar{\rho}\bar{u}_k\right) = 0 , \tag{5.49}$$

$$\frac{\partial}{\partial t}\left(\bar{\rho}\bar{u}_i\right) + \frac{\partial}{\partial x_k}\left(\bar{\rho}\bar{u}_i\bar{u}_k + \overline{\Psi}_{ik}\right) = 0 , \tag{5.50}$$

$$\frac{\partial}{\partial t}\left(\bar{\rho}\bar{u}_i\bar{u}_j + \overline{\Psi}_{ij}\right) + \frac{\partial}{\partial x_k}\left(\bar{\rho}\bar{u}_i\bar{u}_j\bar{u}_k + \bar{\rho}\overline{u_i'u_j'u_k'} + \bar{u}_i\overline{\Psi}_{jk} + \bar{u}_j\overline{\Psi}_{ik} + \bar{u}_k\overline{\Psi}_{ij}\right. \tag{5.51}$$

$$\left. + \overline{u_i'P_{jk}'} + \overline{u_j'P_{ik}'} + \overline{u_k'P_{ij}'}\right) = \frac{\bar{t}_{ij}}{\tau_{\mathcal{G}}} .$$

Akin to RANS models, since the effects of the triple velocity perturbation correlation tensor, $\overline{u_i'u_j'u_k'}$, and velocity pressure correlation tensor, $\overline{u_i'P_{jk}'}$, are negligible in many situations [50], they are neglected for now. Finally, the full Reynolds-averaged ten-moment equations are given as

$$\frac{\partial \bar{\rho}}{\partial t} + \frac{\partial}{\partial x_k}\left(\bar{\rho}\bar{u}_k\right) = 0 , \tag{5.52}$$

$$\frac{\partial}{\partial t}\left(\bar{\rho}\bar{u}_i\right) + \frac{\partial}{\partial x_k}\left(\bar{\rho}\bar{u}_i\bar{u}_k + \overline{\Psi}_{ik}\right) = 0 , \tag{5.53}$$

$$\frac{\partial}{\partial t}\left(\bar{\rho}\bar{u}_i\bar{u}_j + \overline{\Psi}_{ij}\right) + \frac{\partial}{\partial x_k}\left(\bar{\rho}\bar{u}_i\bar{u}_j\bar{u}_k + \bar{u}_i\overline{\Psi}_{jk} + \bar{u}_j\overline{\Psi}_{ik} + \bar{u}_k\overline{\Psi}_{ij}\right) = \frac{\bar{t}_{ij}}{\tau_{\mathcal{G}}} . \tag{5.54}$$

In general, these equations can be closed by any turbulence model that provides the approximation of the kinematic eddy viscosity, ν_T. Here, the closure is done by coupling the hyperbolic-relaxation version of Prandtl's one-equation model in the form of the p-system

$$\frac{\partial k}{\partial t} + \frac{\partial \psi_j}{\partial x_j} = S_k , \tag{5.55}$$

$$\frac{\partial \psi_i}{\partial t} + \frac{\partial}{\partial x_i}\left[\frac{1}{\tau_k}\left(\nu k + \frac{2}{3}k^{3/2}l\right) + \bar{u}_i^2 k\right] = -\frac{1}{\tau_k}\left(\psi_i - \bar{u}_i k\right) + \bar{u}_i S_k , \tag{5.56}$$

or in the Cattaneo-Vernotte form

$$\frac{\partial k}{\partial t} + \frac{\partial}{\partial x_j}\left(k\bar{u}_j - \left(\nu + k^{1/2}l\right)\psi_j\right) = S_k , \tag{5.57}$$

$$\frac{\partial \psi_i}{\partial t} + \frac{\partial}{\partial x_i}\left(-\frac{k}{\tau_k}\right) = -\frac{\psi_i}{\tau_k} , \tag{5.58}$$

where

$$S_k = \frac{k^{1/2}l}{2\mu^2}\bar{t}_{ij}\bar{t}_{ij} - C_D\frac{k^{3/2}}{l} , \tag{5.59}$$

$$\bar{t}_{ij} = -\frac{\mu}{\mu + \bar{\rho}k^{1/2}l}\left(\overline{\Psi}_{ij} - \frac{1}{3}\overline{\Psi}_{kk}\delta_{ij}\right) . \tag{5.60}$$

One notes that the Reynolds-averaged ten-moment equations, Eqs. (5.52)–(5.54), exactly recover the laminar Gaussian ten-moment equations, Eqs. (3.43)–(3.45), when the kinematic eddy viscosity is zero. In a practical implementation, this allows the governing equations to be easily switched between the Gaussian ten-moment model and Reynolds-averaged ten-moment model for laminar and turbulent flow.

5.3 Eigenstructure for Two-Dimensional Flow

At this point, the Reynolds-averaged ten-moment equations are closed by the equivalent hyperbolic-relaxation forms of Prandtl's one-equation model. The full system takes the form of hyperbolic-relaxation equations, which predicts that information is propagated in waves with finite speed. In this section, the full Reynolds-averaged ten-moment equations with the p-system type hyperbolic-relaxation Prandlt's one-equation model are studied. To analyse these PDEs, the eigenstructure of the flux Jacobian is first presented. This analysis shows how the fundamental solutions are propagated in different wave modes. Here, the eigenstructure for two-dimensional flow is shown as an example.

For two space dimensions, the Reynolds-averaged ten-moment equations with hyperbolic-relaxation turbulence model, Eqs. (5.52)–(5.56), can be written in balance-law form as

$$\frac{\partial \mathbf{U}}{\partial t} + \frac{\partial \mathbf{F}_x}{\partial x} + \frac{\partial \mathbf{F}_y}{\partial y} = \mathbf{S}\,, \tag{5.61}$$

where the vector of solution variables, $\mathbf{U}$, and source term, $\mathbf{S}$, have the form

$$\mathbf{U} = \begin{bmatrix} \bar{\rho} \\ \bar{\rho}\bar{u}_x \\ \bar{\rho}\bar{u}_y \\ \bar{\rho}\bar{u}_x^2 + \overline{\Psi}_{xx} \\ \bar{\rho}\bar{u}_x\bar{u}_y + \overline{\Psi}_{xy} \\ \bar{\rho}\bar{u}_y^2 + \overline{\Psi}_{yy} \\ \overline{\Psi}_{zz} \\ k \\ \psi_x \\ \psi_y \end{bmatrix}, \mathbf{S} = \begin{bmatrix} 0 \\ 0 \\ 0 \\ -\frac{1}{3\tau_{\mathcal{G}}}\frac{\mu}{\mu+\bar{\rho}k^{1/2}l}\left(2\overline{\Psi}_{xx} - \overline{\Psi}_{yy} - \overline{\Psi}_{zz}\right) \\ -\frac{1}{\tau_{\mathcal{G}}}\frac{\mu}{\mu+\bar{\rho}k^{1/2}l}\overline{\Psi}_{xy} \\ -\frac{1}{3\tau_{\mathcal{G}}}\frac{\mu}{\mu+\bar{\rho}k^{1/2}l}\left(2\overline{\Psi}_{yy} - \overline{\Psi}_{xx} - \overline{\Psi}_{zz}\right) \\ -\frac{1}{3\tau_{\mathcal{G}}}\frac{\mu}{\mu+\bar{\rho}k^{1/2}l}\left(2\overline{\Psi}_{zz} - \overline{\Psi}_{xx} - \overline{\Psi}_{yy}\right) \\ S_k \\ -\frac{1}{\tau_k}\left(\psi_x - \bar{u}_x k\right) + \bar{u}_x S_k \\ -\frac{1}{\tau_k}\left(\psi_y - \bar{u}_y k\right) + \bar{u}_y S_k \end{bmatrix}, \tag{5.62}$$

with

$$S_k = \frac{k^{1/2}l}{\left(\mu + \bar{\rho}k^{1/2}l\right)^2}\left[\frac{1}{3}\left(\overline{\Psi}_{xx}^2 + \overline{\Psi}_{yy}^2 + \overline{\Psi}_{zz}^2 - \overline{\Psi}_{xx}\,\overline{\Psi}_{yy} - \overline{\Psi}_{xx}\,\overline{\Psi}_{zz} - \overline{\Psi}_{yy}\,\overline{\Psi}_{zz}\right) + \overline{\Psi}_{xy}^2\right] - \frac{C_D k^{3/2}}{l}\,. \quad (5.63)$$

The x- and y-direction fluxes, $\mathbf{F}_x$ and $\mathbf{F}_y$, are

$$\mathbf{F}_x = \begin{bmatrix} \bar{\rho}\bar{u}_x \\ \bar{\rho}\bar{u}_x^2 + \overline{\Psi}_{xx} \\ \bar{\rho}\bar{u}_x\bar{u}_y + \overline{\Psi}_{xy} \\ \bar{\rho}\bar{u}_x^3 + 3\overline{\Psi}_{xx}\bar{u}_x \\ \bar{\rho}\bar{u}_x^2\bar{u}_y + \overline{\Psi}_{xx}\bar{u}_y + 2\overline{\Psi}_{xy}\bar{u}_x \\ \bar{\rho}\bar{u}_x\bar{u}_y^2 + \overline{\Psi}_{yy}\bar{u}_x + 2\overline{\Psi}_{xy}\bar{u}_y \\ \overline{\Psi}_{zz}\bar{u}_x \\ \psi_x \\ \left[\frac{1}{\tau_k}\left(\nu k + \frac{2}{3}k^{3/2}l\right) + k\bar{u}_x^2\right] \\ 0 \end{bmatrix}, \mathbf{F}_y = \begin{bmatrix} \bar{\rho}\bar{u}_y \\ \bar{\rho}\bar{u}_x\bar{u}_y + \overline{\Psi}_{xy} \\ \bar{\rho}\bar{u}_y^2 + \overline{\Psi}_{yy} \\ \bar{\rho}\bar{u}_x^2\bar{u}_y + \overline{\Psi}_{xx}\bar{u}_y + 2\overline{\Psi}_{xy}\bar{u}_x \\ \bar{\rho}\bar{u}_x\bar{u}_y^2 + \overline{\Psi}_{yy}\bar{u}_x + 2\overline{\Psi}_{xy}\bar{u}_y \\ \bar{\rho}\bar{u}_y^3 + 3\overline{\Psi}_{yy}\bar{u}_y \\ \overline{\Psi}_{zz}\bar{u}_y \\ \psi_y \\ 0 \\ \left[\frac{1}{\tau_k}\left(\nu k + \frac{2}{3}k^{3/2}l\right) + k\bar{u}_y^2\right] \end{bmatrix}. \quad (5.64)$$

By introducing flux Jacobian matrices $\mathbf{A}_c = \frac{\partial \mathbf{F}_x}{\partial \mathbf{U}}$ and $\mathbf{B}_c = \frac{\partial \mathbf{F}_y}{\partial \mathbf{U}}$, Eq. (5.61) can be rewritten as

$$\frac{\partial \mathbf{U}}{\partial t} + \mathbf{A}_c\frac{\partial \mathbf{U}}{\partial x} + \mathbf{B}_c\frac{\partial \mathbf{U}}{\partial y} = \mathbf{S}\,. \quad (5.65)$$

By similarity transformation, this equation system can also be written in primitive form with mean and turbulent flow properties, $\mathbf{W}$, as the solution vector, where

$$\mathbf{W} = \begin{bmatrix} \bar{\rho} & \bar{u}_x & \bar{u}_y & \overline{\Psi}_{xx} & \overline{\Psi}_{xy} & \overline{\Psi}_{yy} & \overline{\Psi}_{zz} & k & \psi_x & \psi_y \end{bmatrix}^{\mathrm{T}}. \quad (5.66)$$

The rewritten system has the form

$$\frac{\partial \mathbf{W}}{\partial t} + \mathbf{A}_p\frac{\partial \mathbf{W}}{\partial x} + \mathbf{B}_p\frac{\partial \mathbf{W}}{\partial y} = \mathbf{S}\,, \quad (5.67)$$

where $\mathbf{A}_p = \left(\frac{\partial \mathbf{U}}{\partial \mathbf{W}}\right)^{-1}\frac{\partial \mathbf{F}_x}{\partial \mathbf{U}}\frac{\partial \mathbf{U}}{\partial \mathbf{W}}$ and $\mathbf{B}_p = \left(\frac{\partial \mathbf{U}}{\partial \mathbf{W}}\right)^{-1}\frac{\partial \mathbf{F}_y}{\partial \mathbf{U}}\frac{\partial \mathbf{U}}{\partial \mathbf{W}}$. The matrices $\mathbf{A}_p$ and $\mathbf{B}_p$ share the same eigenvalues of the flux Jacobian matrices $\mathbf{A}_c$ and $\mathbf{B}_c$, which represent the wave speeds of the fundamental solution modes for the model. By defining $\bar{\rho}a_{xx}^2 = \overline{\Psi}_{xx}$, the ten

eigenvalues of $\mathbf{A}_p$ and $\mathbf{A}_c$ are

$$\lambda_{1-10} = \left(\bar{u}_x - \sqrt{3}a_{xx}, \bar{u}_x - a_{xx}, -\sqrt{\bar{u}_x^2 + \frac{(k^{1/2}l + \nu)}{\tau_k}}, \bar{u}_x, \bar{u}_x, \bar{u}_x, 0, \right.$$
$$\left. \sqrt{\bar{u}_x^2 + \frac{(k^{1/2}l + \nu)}{\tau_k}}, \bar{u}_x + a_{xx}, \bar{u}_x + \sqrt{3}a_{xx} \right) ,$$

and the matrix, $\mathbf{R}_p$, which is composed of the corresponding right eigenvectors in each column, are

$$r_{p1} = \begin{bmatrix} \frac{\sqrt{3}\bar{\rho}}{3a_{xx}} \\ -1 \\ -\frac{\bar{\rho}\overline{\Psi}_{xy}}{a_{xx}^2} \\ \sqrt{3}\bar{\rho}a_{xx} \\ \frac{\sqrt{3}\,\overline{\Psi}_{xy}}{a_{xx}} \\ \frac{\sqrt{3}\bar{\rho}\left(\bar{\rho}^2 a_{xx}^2 a_{yy}^2 + 2\overline{\Psi}_{xy}^2\right)}{3a_{xx}^3} \\ \frac{\sqrt{3}\bar{\rho}a_{zz}^2}{3a_{xx}} \\ \frac{2k\tau_k\bar{u}_x}{2\sqrt{3}a_{xx}\tau_k\bar{u}_x + \sqrt{kl} + \nu - 3a_{xx}^2\tau_k} \\ \frac{2k\tau_k\bar{u}_x\left(\bar{u}_x - \sqrt{3}a_{xx}\right)}{2\sqrt{3}a_{xx}\tau_k\bar{u}_x + \sqrt{kl} + \nu - 3a_{xx}^2\tau_k} \\ 0 \end{bmatrix} , \; r_{p2} = \begin{bmatrix} 0 \\ 0 \\ -1 \\ 0 \\ \bar{\rho}a_{xx} \\ 1 \\ 0 \\ 0 \\ 0 \\ 0 \end{bmatrix} , \; r_{p3} = \begin{bmatrix} 0 \\ 0 \\ 0 \\ 0 \\ 0 \\ 0 \\ 0 \\ 1 \\ -\sqrt{\bar{u}_x^2 + \frac{\left(k^{1/2}l + \nu\right)}{\tau_k}} \\ 0 \end{bmatrix} ,$$

$$r_{p4} = \begin{bmatrix} 0 \\ 0 \\ 0 \\ 0 \\ 0 \\ 0 \\ 1 \\ 0 \\ 0 \\ 0 \\ 0 \end{bmatrix} , \; r_{p5} = \begin{bmatrix} 0 \\ 0 \\ 0 \\ 0 \\ 0 \\ 1 \\ 0 \\ 0 \\ 0 \\ 0 \\ 0 \end{bmatrix} , \; r_{p6} = \begin{bmatrix} 1 \\ 0 \\ 0 \\ 0 \\ 0 \\ 0 \\ 0 \\ 0 \\ 0 \\ 0 \\ 0 \end{bmatrix} , \; r_{p7} = \begin{bmatrix} 0 \\ 0 \\ 0 \\ 0 \\ 0 \\ 0 \\ 0 \\ 0 \\ 0 \\ 0 \\ 1 \end{bmatrix} ,$$

$$r_{p8} = \begin{bmatrix} 0 \\ 0 \\ 0 \\ 0 \\ 0 \\ 0 \\ 0 \\ 1 \\ \sqrt{\bar{u}_x^2 + \frac{\left(k^{1/2}l+\nu\right)}{\tau_k}} \\ 0 \end{bmatrix}, \; r_{p9} = \begin{bmatrix} 0 \\ 0 \\ 1 \\ 0 \\ \bar{\rho}a_{xx} \\ 1 \\ 0 \\ 0 \\ 0 \\ 0 \end{bmatrix}, \; r_{p10} = \begin{bmatrix} -\frac{\sqrt{3}\bar{\rho}}{3a_{xx}} \\ -1 \\ -\frac{\bar{\rho}\overline{\Psi}_{xy}}{a_{xx}^2} \\ -\sqrt{3}\bar{\rho}a_{xx} \\ -\frac{\sqrt{3}\,\overline{\Psi}_{xy}}{a_{xx}} \\ -\frac{\sqrt{3}\bar{\rho}\left(\bar{\rho}^2 a_{xx}^2 a_{yy}^2 + 2\overline{\Psi}_{xy}^2\right)}{3a_{xx}^3} \\ -\frac{\sqrt{3}\bar{\rho}a_{zz}^2}{3a_{xx}} \\ \frac{2k\tau_k\bar{u}_x}{-2\sqrt{3}a_{xx}\tau_k\bar{u}_x + \sqrt{k}l + \nu - 3a_{xx}^2\tau_k} \\ \frac{2k\tau_k\bar{u}_x\left(\bar{u}_x + \sqrt{3}a_{xx}\right)}{-2\sqrt{3}a_{xx}\tau_k\bar{u}_x + \sqrt{k}l + \nu - 3a_{xx}^2\tau_k} \\ 0 \end{bmatrix}.$$

The matrix with corresponding left eigenvectors in each row, $\mathbf{L}_p$, can be determined by $\mathbf{L}_p = \mathbf{R}_p^{-1}$, which has form as

$$l_{p1}^{\mathrm{T}} = \begin{bmatrix} 0 \\ -\frac{\sqrt{3}\bar{\rho}}{6a_{xx}} \\ 0 \\ \frac{1}{6a_{xx}^2} \\ 0 \\ 0 \\ 0 \\ 0 \\ 0 \\ 0 \end{bmatrix}, \; l_{p2}^{\mathrm{T}} = \begin{bmatrix} 0 \\ -\frac{\overline{\Psi}_{xy}}{2a_{xx}^2} \\ \frac{\bar{\rho}}{2} \\ \frac{\overline{\Psi}_{xy}}{2\bar{\rho}a_{xx}^3} \\ -\frac{1}{2a_{xx}} \\ 0 \\ 0 \\ 0 \\ 0 \\ 0 \end{bmatrix},$$

$$
l_{p3}^{\mathrm{T}}=\begin{bmatrix}
0\\
\frac{k\tau_k\bar{u}_x\left[\sqrt{\tau_k\left(\bar{u}_x^2\tau_k+\sqrt{k}l+\nu\right)}\left(\sqrt{k}l+\nu-3a_{xx}^2\tau_k\right)-\tau_k\bar{u}_x\left(\sqrt{k}l+\nu+3a_{xx}^2\tau_k\right)\right]}{\sqrt{\tau_k\left(\bar{u}_x^2\tau_k+\sqrt{k}l+\nu\right)}\left[\left(\sqrt{k}l+\nu-3a_{xx}^2\tau_k\right)^2-\left(2\sqrt{3}a_{xx}\tau_k\bar{u}_x\right)^2\right]}\\
0\\
-\frac{k\tau_k^2\bar{u}_x\left[2\tau_k\bar{u}_x^2-2\sqrt{\tau_k\left(\bar{u}_x^2\tau_k+\sqrt{k}l+\nu\right)}\bar{u}_x+\left(\sqrt{k}l+\nu-3a_{xx}^2\tau_k\right)\right]}{\rho\sqrt{\tau_k\left(\bar{u}_x^2\tau_k+\sqrt{k}l+\nu\right)}\left[\left(\sqrt{k}l+\nu-3a_{xx}^2\tau_k\right)^2-\left(2\sqrt{3}a_{xx}\tau_k\bar{u}_x\right)^2\right]}\\
0\\
0\\
0\\
\frac{1}{2}\\
-\frac{\tau_k}{2\sqrt{\tau_k\left(\bar{u}_x^2\tau_k+\sqrt{k}l+\nu\right)}}\\
0
\end{bmatrix},
$$

$$
l_{p4}^{\mathrm{T}}=\begin{bmatrix}
0\\0\\0\\-\frac{a_{zz}^2}{3a_{xx}^2}\\0\\0\\1\\0\\0\\0
\end{bmatrix},\ l_{p5}^{\mathrm{T}}=\begin{bmatrix}
0\\0\\0\\\frac{-\bar{\rho}^2a_{xx}^2a_{yy}^2+4\overline{\Psi}_{xy}^2}{3\bar{\rho}^2a_{xx}^4}\\-\frac{2\overline{\Psi}_{xy}}{\bar{\rho}a_{xx}^2}\\1\\0\\0\\0\\0
\end{bmatrix},\ l_{p6}^{\mathrm{T}}=\begin{bmatrix}
1\\0\\0\\-\frac{1}{3a_{xx}^2}\\0\\0\\0\\0\\0\\0
\end{bmatrix},\ l_{p7}^{\mathrm{T}}=\begin{bmatrix}
0\\0\\0\\0\\0\\0\\0\\0\\0\\1
\end{bmatrix},
$$

$$l_{p8}^{\mathrm{T}} = \begin{bmatrix} 0 \\ \frac{k\tau_k\bar{u}_x\left[\sqrt{\tau_k\left(\bar{u}_x^2\tau_k+\sqrt{k}l+\nu\right)}\left(\sqrt{k}l+\nu-3a_{xx}^2\tau_k\right)+\tau_k\bar{u}_x\left(\sqrt{k}l+\nu+3a_{xx}^2\tau_k\right)\right]}{\sqrt{\tau_k\left(\bar{u}_x^2\tau_k+\sqrt{k}l+\nu\right)}\left[\left(\sqrt{k}l+\nu-3a_{xx}^2\tau_k\right)^2-\left(2\sqrt{3}a_{xx}\tau_k\bar{u}_x\right)^2\right]} \\ 0 \\ \frac{k\tau_k^2\bar{u}_x\left[2\tau_k\bar{u}_x^2+2\sqrt{\tau_k\left(\bar{u}_x^2\tau_k+\sqrt{k}l+\nu\right)}\bar{u}_x+\left(\sqrt{k}l+\nu-3a_{xx}^2\tau_k\right)\right]}{\bar{\rho}\sqrt{\tau_k\left(\bar{u}_x^2\tau_k+\sqrt{k}l+\nu\right)}\left[\left(\sqrt{k}l+\nu-3a_{xx}^2\tau_k\right)^2-\left(2\sqrt{3}a_{xx}\tau_k\bar{u}_x\right)^2\right]} \\ 0 \\ 0 \\ 0 \\ \frac{1}{2} \\ \frac{\tau_k}{2\sqrt{\tau_k\left(\bar{u}_x^2\tau_k+\sqrt{k}l+\nu\right)}} \\ 0 \end{bmatrix},$$

$$l_{p9}^{\mathrm{T}} = \begin{bmatrix} 0 \\ -\frac{\overline{\Psi}_{xy}}{2a_{xx}^2} \\ \frac{\bar{\rho}}{2} \\ -\frac{\overline{\Psi}_{xy}}{2\bar{\rho}a_{xx}^3} \\ \frac{1}{2a_{xx}} \\ 0 \\ 0 \\ 0 \\ 0 \\ 0 \end{bmatrix}, \; l_{p10}^{\mathrm{T}} = \begin{bmatrix} 0 \\ \frac{\sqrt{3}\bar{\rho}}{6a_{xx}} \\ 0 \\ \frac{1}{6a_{xx}^2} \\ 0 \\ 0 \\ 0 \\ 0 \\ 0 \\ 0 \end{bmatrix}.$$

As discussed, the right eigenvector shows which quantities are affected by each wave and the left eigenvectors are associated with the wave strength. In comparison with the ten-moment model, the flux Jacobian of the Reynolds-averaged ten-moment model has very similar eigenstructure, except for the fundamental wave modes associated with $\lambda_{3,7,8}$, which carry the information related to the turbulent kinetic energy. It is notable that, $\lambda_7 = 0$ is because the fluxes of the turbulence kinetic energy in different physical directions are described by separated equations, Eqs. (5.36)–(5.37), where Eq. (5.37) contains zero flux in the x direction.

One notes that this model is unfortunately, not Galilean invariant, because the eigenvalues of the hyperbolic-relaxation turbulence model, $\lambda_{3,8}$, do not follow the form of $\bar{u}_i \pm c$. The form of eigenvalues $\lambda_{3,8}$ is inherited from the natural structure of the p-system—which

is not Galilean invariant [31]. This implies that, to obtain a Galilean invariant hyperbolic form, the relaxation method must be reconsidered. To develop a model which maintains the hyperbolicity and Galilean invariance is a challenge for future work.

5.4 Dispersion Analysis

Following the same procedure as introduced in Section 2.2, a dispersion analysis is applied to the Reynolds-averaged ten-moment equations with p-system type hyperbolic-relaxation Prandtl's one-equation model, Eqs. (5.52)–(5.56), and the corresponding dispersion relation can be easily found. To explore the influence of a small perturbation on the full Reynolds-averaged ten-moment equations, the full system must first be linearized about a quiescent equilibrium state. This state can be written as

$$\mathbf{W}_0 = \begin{bmatrix} \bar{\rho}_0 & \bar{u}_0 & 0 & \overline{\Psi}_0 & 0 & \overline{\Psi}_0 & \overline{\Psi}_0 & 0 & 0 & 0 \end{bmatrix}^{\mathrm{T}} ,$$

in two-dimensional form. The vector, $\mathbf{W}_0$, indicates the quiescent equilibrium state of the vector of primitive variables, $\mathbf{W}$, which was defined earlier by (5.66).

As defined by Eq. (5.42), $\overline{\Psi}_{ij}$ is the summation of the averaged generalized pressure tensor, $\overline{P}_{ij}$, and the Reynolds-stress tensor, $\bar{\rho}\overline{u_i' u_j'}$. In the state of quiescent equilibrium, $\overline{P}_{ij} = \bar{p}_0 \delta_{ij}$, and the turbulence is assumed to be absent, which leads to all the components of Reynolds-stress being zero, therefore, $\overline{\Psi}_0 = \bar{p}_0$. In order to investigate the dispersion relation in a non-dimensional setting, the following characteristic scales for velocity, relaxation time, and length scale are chosen:

$$a_0 = \sqrt{\frac{3\overline{\Psi}_0}{\bar{\rho}_0}} , \qquad \tau_0 = \frac{\mu_0}{\overline{\Psi}_0} , \qquad L_0 = a_0 \tau_0 , \tag{5.68}$$

where μ_0 is the dynamic viscosity in the equilibrium state. The time and space variables are non-dimensionalized as

$$\frac{t}{\tau_0} = t^* , \qquad \frac{x_i}{L_0} = x_i^* . \tag{5.69}$$

Here, the starred variables are non-dimensionalized.

A small perturbation in the x direction about the state $\mathbf{W}_0$ is of interest, which can be

written as

$$\bar{\rho}\left(x_i,t\right)=\bar{\rho}_0\left(1+\alpha\bar{\rho}^*\left(x_i^*,t^*\right)+O\left(\alpha^2\right)\right)\,, \tag{5.70}$$

$$\overline{\Psi}_{ij}\left(x_i,t\right)=\overline{\Psi}_0\left(\delta_{ij}+\alpha\overline{\Psi}_{ij}^*\left(x_i^*,t^*\right)+O\left(\alpha^2\right)\right)\,, \tag{5.71}$$

$$\bar{u}_i\left(x_i,t\right)=a_0\left(\mathrm{Ma}\,e_i+\alpha\bar{u}_i^*\left(x_i^*,t^*\right)+O\left(\alpha^2\right)\right)\,, \tag{5.72}$$

$$k\left(x_i,t\right)=a_0^2\left(\alpha k^*\left(x_i^*,t^*\right)+O\left(\alpha^2\right)\right)\,, \tag{5.73}$$

$$\psi_i\left(x_i,t\right)=a_0^3\left(\alpha\psi_i^*\left(x_i^*,t^*\right)+O\left(\alpha^2\right)\right)\,, \tag{5.74}$$

where e_i is the unit vector in the direction of the velocity, and the Mach number is defined as the ratio of the bulk velocity to the fastest acoustic-like speed in the system, $\mathrm{Ma}=\bar{u}_0/a_0$, and $0<\alpha\ll 1$. Based on the above assumption, the relaxation time can be written as

$$\tau_{\mathcal{G}}\left(x_i,t\right)=\tau_0\left(1+\alpha\tau_{\mathcal{G}}^*\left(x_i^*,t^*\right)+O\left(\alpha^2\right)\right)\,, \tag{5.75}$$

$$\tau_k\left(x_i,t\right)=\tau_0\,. \tag{5.76}$$

One notes that, τ_k is a constant, which takes the same value as τ_0 in this analysis. Equations (5.70)–(5.76) can be substituted into the full Reynolds-averaged ten-moment equations, Eqs. (5.52)–(5.56). Since the leading order satisfies the equations and only the perturbation in the x direction is of interest, the system of equations for the perturbations can be written as

$$\frac{\partial\mathbf{U}^*}{\partial t^*}+\frac{\partial\mathbf{F}^*}{\partial x^*}=\mathbf{S}^*\,, \tag{5.77}$$

which can also be written as a linear operator acting on a solution vector containing the perturbations

$$\left(\mathbf{I}\frac{\partial}{\partial t^*}+\mathbf{A}^*\frac{\partial}{\partial x^*}-\mathbf{Q}^*\right)\mathbf{U}^*=\mathbf{0}\,, \tag{5.78}$$

where the matrix $\mathbf{A}^*$ is defined as $\frac{\partial\mathbf{F}^*}{\partial\mathbf{U}^*}$ evaluated at the non-dimensional state and, similarly, the matrix $\mathbf{Q}^*$ is $\frac{\partial\mathbf{S}^*}{\partial\mathbf{U}^*}$ evaluated at the same state. Akin to the one-dimension hyperbolic-relaxation model, the influence of the linear operator, $\left(\mathbf{I}\frac{\partial}{\partial t^*}+\mathbf{A}^*\frac{\partial}{\partial x^*}-\mathbf{Q}^*\right)$, acting on the Fourier mode of the perturbed solution vector, $\mathbf{U}^*$, with dimensionless wavenumber, ξ, is of interest in this analysis. This is a similar initial-value problem as introduced earlier. If the form of the initial condition is assumed to be

$$\mathbf{U}^*\left(x^*,0\right)=\mathbf{U}_0^*e^{-i\xi x^*}\,, \tag{5.79}$$

based on the same derivation, the complete solution has form

$$\mathbf{U}^*\left(x^*,t^*\right)=\mathbf{R}^*e^{i\left(t^*\mathbf{\Omega}^*-\xi x^*\right)}\mathbf{L}^*\mathbf{U}_0^*\,, \tag{5.80}$$

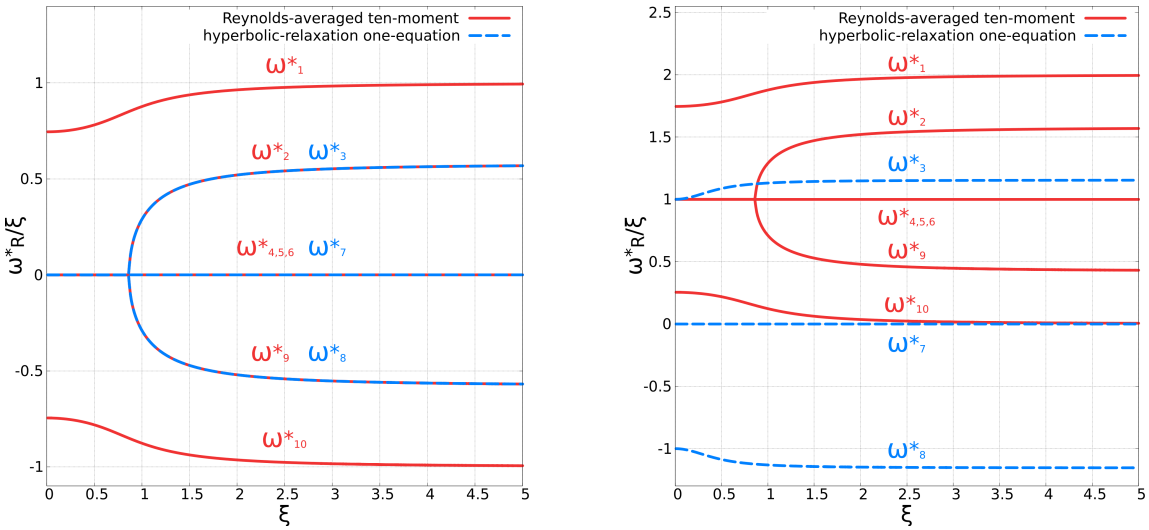

(a) Ma = 0 (b) Ma = 1

Figure 5.1: Variation with wave number of the phase speed for the Reynolds-averaged ten-moment equations coupled with p-system type hyperbolic-relaxation Prandtl's one-equation model for zero and non-zero background velocity

where $\mathbf{\Omega}^*$ is the diagonal matrix of the eigenvalues of the matrix, $\xi\mathbf{A}^* - i\mathbf{Q}^*$. By solving the characteristic equation,

$$\det\left(\xi\mathbf{A}^* - i\mathbf{Q}^* - \omega^*\mathbf{I}\right) = 0\,, \tag{5.81}$$

the eigenvalues, $\omega^* = \omega^*_{\mathrm{R}} + i\,\omega^*_{\mathrm{I}}$, of the matrix $\xi\mathbf{A}^* - i\mathbf{Q}^*$ can be found. The wave speed, $\omega^*_{\mathrm{R}}/\xi$, and the attenuation rate, $e^{-\omega^*_{\mathrm{I}}}$, can then be determined. In this analysis, the non-dimensional relaxation time, τ_0, is chosen as 1. Two choices of Mach number, Ma = 0 and Ma = 1, are selected, so that the dispersion relations for zero and non-zero bulk velocity can be investigated. The phase speeds and attenuation rates over wave number are plotted in Figs. 5.1 and 5.2 respectively.

Obviously, the system is dispersive since the phase speeds are dependent on the wave number and, in general, the waves are damped at different rates. A similar analysis on the Chen-Levermore-Liu p-system [15] and previous study on the laminar ten-moment model has been done by Hittinger and Brown [9, 22]. In comparison with their analysis, the dispersion relation corresponding to the eigenvalues of the Reynolds-averaged ten-moment equations, which are plotted by red solid lines in the figures, parallels the behaviour of the modes associated with the base ten-moment model, while the ones corresponding to the eigenvalues of the p-system type hyperbolic-relaxation Prandtl's one-equation model,

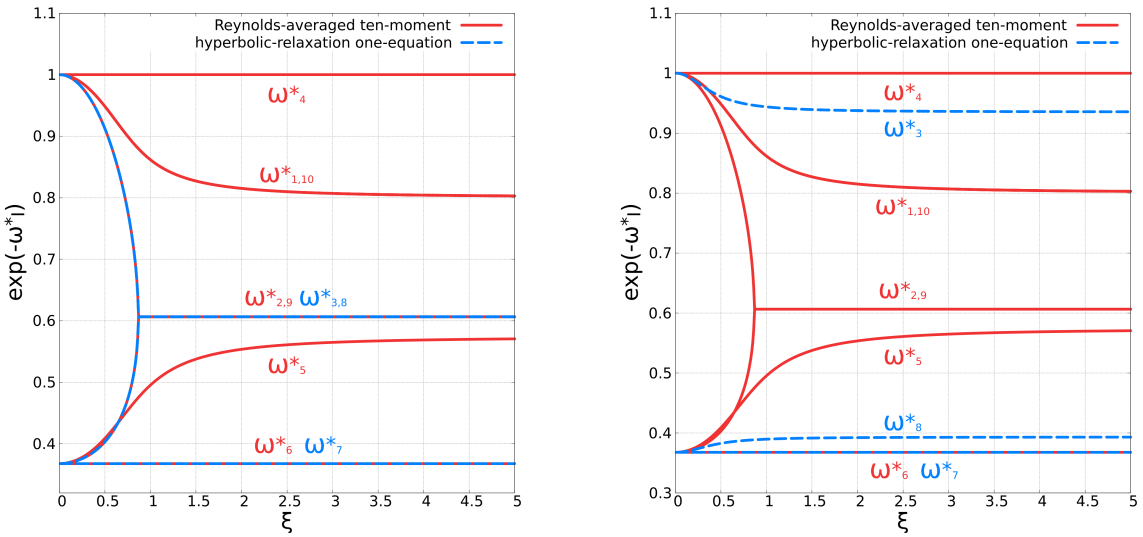

(a) Ma = 0 (b) Ma = 1

Figure 5.2: Variation with wave number of the attenuation rate for the Reynolds-averaged ten-moment equations coupled with p-system type hyperbolic-relaxation Prandtl's one-equation model for zero and non-zero background velocity

which are plotted by blue dashed lines, parallels the behaviour of the modes associated with the original p-system [15]. One notable feature is the bifurcation points. In the case of zero bulk velocity, in the long-wave region of the plot, the shear modes corresponding to the eigenvalues $\omega^*_{2,3}$ and $\omega^*_{8,9}$ propagate with the same speed as $\omega^*_{4,5,6,7}$. All these waves have a velocity of zero in the long-wavelength limit, however they are damped at different rates. For shorter waves above the bifurcation points, the modes propagate with different speeds, but dampen at the same rate. In the case of non-zero bulk velocity, even though the magnitudes of the phase speeds are changed, this feature is maintained for those modes associated with the Reynolds-averaged ten-moment equations. However, the waves speed associated with the translation of turbulence kinetic energy now smoothly vary in the range of low wave number. Similarly, the damping rate of the waves belonging to the Reynolds-averaged ten-moment equations maintain the same feature, but the modes corresponding to the eigenvalues $\omega^*_{3,8}$ are no longer damped at the same rate in the range of high wave numbers.

It is clear to see that the attenuation rate of the disturbed solutions never crosses the boundary of the stability region, $e^{-\omega^*_{\mathrm{I}}} \in [0\ ,\ 1]$, either in the limit of low wave number, which represents the flow being source-term dominated, or in the limit of high wave number, which is the purely hyperbolic limit. This means that the perturbed solution is linearly

stable.

Chapter 6

Reynolds-Averaged Ten-Moment Model with Hyperbolic-Relaxation Two-Equation Models

The typical one-equation models are rarely used in real applications. This is because the description of the turbulence kinetic energy by this single equation can be said to be incomplete. In this model, the eddy viscosity relates the turbulence length scale to some typical flow dimension. In other words, the model relies on apriori knowledge of the characteristic size or structure of the flow turbulence. By contrast, in two-equation models, an extra equation provides the evolution of the turbulence length scale, or its equivalent. This allows direct modelling of the energy dissipation and eddy viscosity [50].

The k-ϵ and k-ω models are the most popular two-equation models. They have been continually refined and widely implemented in industry over the past several decades. In this chapter, the standard k-ϵ and Wilcox k-ω models [50] are discussed as examples. To obtain the appropriate turbulence model for the Reynolds-averaged ten-moment equations, these models are reformulated into their equivalent hyperbolic-relaxation form using the Cattaneo-Vernotte approach. As mentioned in earlier chapters, due to the fact that diffusion coefficients are typically variable in the two-equation models, building the equivalent p-system type hyperbolic-relaxation form is very difficult. The details of such difficulty are discussed in this chapter as well. The hyperbolic-relaxation versions of the two-equation models are then coupled to the Reynolds-averaged ten-moment equations. The corresponding eigenstructure and dispersion analysis of the resulting first-order PDEs systems

are studied and presented.

6.1 Hyperbolic-Relaxation Version of the Standard k-ϵ Model

The earliest development of the k-ϵ model can be traced back to 1940s [50], however, it has been widely used since the version introduced by Jones and Launder in 1972 [25]. After Launder and Sharma's adjustment of the closure coefficients, the standard k-ϵ model was created in 1974 [27]. This model completes the model of eddy viscosity by providing an extra equation for the dissipation rate of turbulent kinetic energy, ϵ. It has the form

$$\frac{\partial k}{\partial t} + \bar{u}_j \frac{\partial k}{\partial x_j} = \tau_{ij} \frac{\partial \bar{u}_i}{\partial x_j} - \epsilon + \frac{\partial}{\partial x_j} \left[\left(\nu + \nu_T / \sigma_k \right) \frac{\partial k}{\partial x_j} \right] , \tag{6.1}$$

$$\frac{\partial \epsilon}{\partial t} + \bar{u}_j \frac{\partial \epsilon}{\partial x_j} = C_{\epsilon 1} \frac{\epsilon}{k} \tau_{ij} \frac{\partial \bar{u}_i}{\partial x_j} - C_{\epsilon 2} \frac{\epsilon^2}{k} + \frac{\partial}{\partial x_j} \left[\left(\nu + \nu_T / \sigma_\epsilon \right) \frac{\partial \epsilon}{\partial x_j} \right] , \tag{6.2}$$

with kinematic eddy viscosity modelled as

$$\nu_T = C_\mu k^2 / \epsilon \, . \tag{6.3}$$

The standard values of the closure coefficients are

$$C_\mu = 0.09 \, , \quad C_{\epsilon 1} = 1.44 \, , \quad C_{\epsilon 2} = 1.92 \, , \quad \sigma_k = 1.0 \, , \quad \sigma_\epsilon = 1.3 \, . \tag{6.4}$$

As discussed, in the case of low-speed flow, the production term can be replaced by an algebraic expression, Eq. (5.6). Therefore, the k-ϵ model, Eqs. (6.1)–(6.2), can be rewritten as

$$\frac{\partial k}{\partial t} + \bar{u}_j \frac{\partial k}{\partial x_j} = \frac{C_\mu k^2}{2\mu^2 \epsilon} \bar{t}_{ij} \bar{t}_{ij} - \epsilon + \frac{\partial}{\partial x_j} \left[\left(\nu + \frac{C_\mu k^2}{\epsilon \sigma_k} \right) \frac{\partial k}{\partial x_j} \right] , \tag{6.5}$$

$$\frac{\partial \epsilon}{\partial t} + \bar{u}_j \frac{\partial \epsilon}{\partial x_j} = \frac{C_{\epsilon 1} C_\mu k}{2\mu^2} \bar{t}_{ij} \bar{t}_{ij} - C_{\epsilon 2} \frac{\epsilon^2}{k} + \frac{\partial}{\partial x_j} \left[\left(\nu + \frac{C_\mu k^2}{\epsilon \sigma_\epsilon} \right) \frac{\partial \epsilon}{\partial x_j} \right] . \tag{6.6}$$

In comparison with the one-equation model, since the number of original convection-diffusion equations is doubled, the number of equations in the equivalent hyperbolic-relaxation system is doubled as well. Another important distinction between these models is the diffusion coefficient. In two-equation models, ν_T is formulated as a function of two variables, $k\left(x_i, t\right)$ and $\epsilon\left(x_i, t\right)$, due to the extra PDE. This extra dependency brings added difficulty to formulate the equivalent hyperbolic-relaxation system in the form of the p-system.

6.1.1 Difficulties of P-System Type Two-Equation Models

According to the derivation of one-dimensional hyperbolic-relaxation version of convection-diffusion equation in Section 2.1.3, to match the original equations, the diffusion coefficient, $\tau\left[\left(\frac{\partial g(\phi)}{\partial \phi}\right)^2 - \frac{\partial f(\phi)}{\partial \phi}\right]$, from the asymptotic form of hyperbolic-relaxation equations, Eq. (2.26), must be identical to μ. However, this asymptotic form is only valid for $f(\phi)$ and $g(\phi)$, which are functions of a single variable. In the case of a constant diffusion coefficient μ, it is easy to find the proper $f(\phi)$ and $g(\phi)$, as given by Eqs. (2.27)–(2.28). In Prandtl's one-equation model, the diffusion coefficient, $\mu(\phi)$, is a function of ϕ. This is still achievable by the appropriate selections of $f(\phi)$ and $g(\phi)$, as discussed in the Section 5.1.1. However, in the case of two-equation models, the diffusion coefficient, $\mu(\phi, \varphi)$, is, in general, a function of ϕ and φ, which are time and space dependent. There is no degree of freedom to introduce the new dependency into Eq. (2.26) while maintaining the same asymptotic form. Matching this asymptotic form to Eq. (2.16), $g(\phi)$ is chosen to be the convection term, which is the only function of ϕ. If $f(\phi)$ is replaced by $f(\phi, \varphi)$ to introduce the new variable, φ, into the diffusion coefficient, the expression of ψ_1 in Eq. (2.24) is not longer valid, since

$$\frac{\partial f(\phi, \varphi)}{\partial x} = \frac{\partial f(\phi, \varphi)}{\partial \phi}\frac{\partial \phi}{\partial x} + \frac{\partial f(\phi, \varphi)}{\partial \varphi}\frac{\partial \varphi}{\partial x}\,. \tag{6.7}$$

Then, ψ_1 becomes

$$\psi_1 = \tau\left\{\left[\left(\frac{\partial g(\phi)}{\partial \phi}\right)^2 - \frac{\partial f(\phi, \varphi)}{\partial \phi}\right]\frac{\partial \phi}{\partial x} - \frac{\partial f(\phi, \varphi)}{\partial \varphi}\frac{\partial \varphi}{\partial x}\right\}, \tag{6.8}$$

which gives a totally different asymptotic form as

$$\frac{\partial \phi}{\partial t} + \frac{\partial g(\phi)}{\partial x} + \tau\frac{\partial}{\partial x}\left\{\left[\left(\frac{\partial g(\phi)}{\partial \phi}\right)^2 - \frac{\partial f(\phi, \varphi)}{\partial \phi}\right]\frac{\partial \phi}{\partial x} - \frac{\partial f(\phi, \varphi)}{\partial \varphi}\frac{\partial \varphi}{\partial x}\right\} = 0\,. \tag{6.9}$$

The last term of Eq. (6.9) introduces a second-order derivative of φ, which is undesirable to match the original convection-diffusion equation. In the two-equation model, the diffusion coefficients in, for example, the k-ϵ model, are $(\nu + \nu_T/\sigma_k)$ and $(\nu + \nu_T/\sigma_\epsilon)$, where the kinematic eddy viscosity is a function of k and ϵ, $\nu_T = C_\mu k^2/\epsilon$. The hyperbolization by the p-system is, therefore, difficult. However, this feature of the diffusion coefficient does not affect the hyperbolization using the Cattaneo-Vernotte approach.

6.1.2 Cattaneo-Vernotte Type Two-Equation Models

For the standard k-ϵ model, the reformulation by the Cattaneo-Vernotte relaxation method is very straightforward. It has the form

$$\frac{\partial k}{\partial t} + \frac{\partial}{\partial x_j}\left[\bar{u}_j k - \left(\nu + \frac{C_\mu k^2}{\epsilon \sigma_k}\right)\psi_j\right] = \frac{C_\mu k^2}{2\mu^2 \epsilon}\bar{t}_{ij}\bar{t}_{ij} - \epsilon\,, \tag{6.10}$$

$$\frac{\partial \psi_i}{\partial t} + \frac{\partial}{\partial x_i}\left(-\frac{k}{\tau_k}\right) = -\frac{\psi_i}{\tau_k}\,, \tag{6.11}$$

for the turbulence kinetic energy and

$$\frac{\partial \epsilon}{\partial t} + \frac{\partial}{\partial x_j}\left[\bar{u}_j \epsilon - \left(\nu + \frac{C_\mu k^2}{\epsilon \sigma_\epsilon}\right)\phi_j\right] = \frac{C_{\epsilon 1} C_\mu k}{2\mu^2}\bar{t}_{ij}\bar{t}_{ij} - C_{\epsilon 2}\frac{\epsilon^2}{k}\,, \tag{6.12}$$

$$\frac{\partial \phi_i}{\partial t} + \frac{\partial}{\partial x_i}\left(-\frac{\epsilon}{\tau_\epsilon}\right) = -\frac{\phi_i}{\tau_\epsilon}\,, \tag{6.13}$$

for the dissipation rate. Obviously, the extra equations are only responsible for the relaxation procedure between the relaxation variables, ψ_i and ϕ_i, and corresponding spacial derivatives, $\frac{\partial k}{\partial x_i}$ and $\frac{\partial \epsilon}{\partial x_i}$. This hyperbolic form provides the same solution as the original model in the limit of small relaxation times, τ_k and τ_ϵ.

6.2 Hyperbolic-Relaxation Version of the Wilcox k-ω Model

Akin to the k-ϵ model, the k-ω model completes the modelling of energy dissipation and eddy viscosity by providing an extra equation for specific dissipation, ω. This model has a similar history of development since the 1940s [50]. Kolmogorov is the pioneer who proposed the first k-ω model. This model was subsequently developed by Launder and Spalding (1972) [28], Wilcox and Alber (1972) [51], Staffman and Wilcox (1974) [39], Wilcox and Rubesin (1980) [52], Wilcox (1988a) and Wilcox (1988) [49]. In this section, the version of Wilcox (1988) is taken as the example from the k-ω family, which is further referred to as the Wilcox k-ω model, since most of the later developed versions are based on it. The Wilcox k-ω model is expressed as

$$\frac{\partial k}{\partial t} + \bar{u}_j \frac{\partial k}{\partial x_j} = \tau_{ij}\frac{\partial \bar{u}_i}{\partial x_j} - \beta^* \omega k + \frac{\partial}{\partial x_j}\left[(\nu + \sigma_k \nu_T)\frac{\partial k}{\partial x_j}\right]\,, \tag{6.14}$$

$$\frac{\partial \omega}{\partial t} + \bar{u}_j \frac{\partial \omega}{\partial x_j} = \frac{\gamma \omega}{k}\tau_{ij}\frac{\partial \bar{u}_i}{\partial x_j} - \beta \omega^2 + \frac{\partial}{\partial x_j}\left[(\nu + \sigma_\omega \nu_T)\frac{\partial \omega}{\partial x_j}\right]\,, \tag{6.15}$$

with kinematic eddy viscosity

$$\nu_T = k/\omega\,, \tag{6.16}$$

where the closure coefficients are

$$\sigma_k = 0.5\,, \quad \sigma_\omega = 0.5\,, \quad \beta_* = 0.09\,, \quad \beta = \frac{3}{40}\,, \quad \gamma = \frac{5}{9}\,. \tag{6.17}$$

Replacing the production term by the algebraic expression, Eq. (5.6), Eqs. (6.14)–(6.15) can be rewritten as

$$\frac{\partial k}{\partial t} + \bar{u}_j \frac{\partial k}{\partial x_j} = \frac{\nu_T}{2\mu^2}\bar{t}_{ij}\bar{t}_{ij} - \beta^*\omega k + \frac{\partial}{\partial x_j}\left[(\nu + \sigma_k \nu_T)\frac{\partial k}{\partial x_j}\right], \tag{6.18}$$

$$\frac{\partial \omega}{\partial t} + \bar{u}_j \frac{\partial \omega}{\partial x_j} = \frac{\gamma\omega}{k}\frac{\nu_T}{2\mu^2}\bar{t}_{ij}\bar{t}_{ij} - \beta\omega^2 + \frac{\partial}{\partial x_j}\left[(\nu + \sigma_\omega \nu_T)\frac{\partial \omega}{\partial x_j}\right]. \tag{6.19}$$

As noted, since the diffusion coefficient is dependent on multiple variables, k and ω, the k-ω model is also only hyperbolized in the Cattaneo-Vernotte form. The equivalent hyperbolic-relaxation system has the form

$$\frac{\partial k}{\partial t} + \frac{\partial}{\partial x_j}\left[\bar{u}_j k - \left(\nu + \sigma_k \frac{k}{\omega}\right)\psi_j\right] = \frac{k}{2\mu^2\omega}\bar{t}_{ij}\bar{t}_{ij} - \beta^*\omega k\,, \tag{6.20}$$

$$\frac{\partial \psi_i}{\partial t} + \frac{\partial}{\partial x_i}\left(-\frac{k}{\tau_k}\right) = -\frac{\psi_i}{\tau_k}\,, \tag{6.21}$$

for turbulence kinetic energy and

$$\frac{\partial \omega}{\partial t} + \frac{\partial}{\partial x_j}\left[\bar{u}_j \omega - \left(\nu + \sigma_\omega \frac{k}{\omega}\right)\phi_j\right] = \frac{\gamma}{2\mu^2}\bar{t}_{ij}\bar{t}_{ij} - \beta\omega^2\,, \tag{6.22}$$

$$\frac{\partial \phi_i}{\partial t} + \frac{\partial}{\partial x_i}\left(-\frac{\omega}{\tau_\omega}\right) = -\frac{\phi_i}{\tau_\omega}\,, \tag{6.23}$$

for specific dissipation rate.

6.3 Dispersion Analysis

One notes that, finding analytical expressions for the full eigenstructure of the Cattaneo-Vernotte type hyperbolic-relaxation equations is very difficult. Therefore, the eigenvalues of the corresponding flux Jacobian are calculated through algorithmic differentiation in this project. The dispersive behaviour of the system can, however, still be analysed.

To explore the dispersive wave behaviour of the Cattaneo-Vernotte type hyperbolic-relaxation two-equation models, the dispersion relation of the PDEs has to be found. In

this section, a similar dispersion analysis is done for the hyperbolic-relaxation form of the standard k-ϵ model and the Wilcox k-ω model.

The same technique introduced in Section 5.4 is used. To study the influence of a small perturbation on the Reynolds-averaged ten-moment equations with Cattaneo-Vernotte type hyperbolic-relaxation two-equation models, the full system is first linearized about a quiescent equilibrium state, which can be written as

$$\mathbf{W}_0 = \begin{bmatrix} \bar{\rho}_0 & \bar{u}_0 & 0 & \overline{\Psi}_0 & 0 & \overline{\Psi}_0 & \overline{\Psi}_0 & 0 & 0 & 0 & 0 & 0 & 0 \end{bmatrix}^{\mathrm{T}} .$$

The vector $\mathbf{W}_0$ indicates the quiescent equilibrium state of the vector of primitive variables, $\mathbf{W}$, which is defined as

$$\mathbf{W} = \begin{bmatrix} \bar{\rho} & \bar{u}_x & \bar{u}_y & \overline{\Psi}_{xx} & \overline{\Psi}_{xy} & \overline{\Psi}_{yy} & \overline{\Psi}_{zz} & k & \psi_x & \psi_y & \epsilon & \phi_x & \phi_y \end{bmatrix}^{\mathrm{T}} ,$$

for the k-ϵ model, or

$$\mathbf{W} = \begin{bmatrix} \bar{\rho} & \bar{u}_x & \bar{u}_y & \overline{\Psi}_{xx} & \overline{\Psi}_{xy} & \overline{\Psi}_{yy} & \overline{\Psi}_{zz} & k & \psi_x & \psi_y & \omega & \phi_x & \phi_y \end{bmatrix}^{\mathrm{T}} ,$$

for the k-ω model.

Again, a small perturbation in the x direction about the state, $\mathbf{W}_0$, is of interest. In addition to the variables introduced in Eqs. (5.70)–(5.72), the perturbed version of the new variables can be written as

$$k\left(x_i, t\right) = a_0^2 \left(\alpha k^*\left(x_i^*, t^*\right) + O\left(\alpha^2\right)\right) , \tag{6.24}$$

$$\psi_i\left(x_i, t\right) = \frac{a_0}{\tau_0} \left(\alpha \psi_i^*\left(x_i^*, t^*\right) + O\left(\alpha^2\right)\right) , \tag{6.25}$$

for the hyperbolic-relaxation k-ϵ model, one uses

$$\epsilon\left(x_i, t\right) = \frac{a_0^2}{\tau_0} \left(\alpha \epsilon^*\left(x_i^*, t^*\right) + O\left(\alpha^2\right)\right) , \tag{6.26}$$

$$\phi_i\left(x_i, t\right) = \frac{a_0}{\tau_0^2} \left(\alpha \phi_i^*\left(x_i^*, t^*\right) + O\left(\alpha^2\right)\right) , \tag{6.27}$$

while for the hyperbolic-relaxation k-ω model, one uses

$$\omega\left(x_i, t\right) = \frac{1}{\tau_0} \left(\alpha \omega^*\left(x_i^*, t^*\right) + O\left(\alpha^2\right)\right) , \tag{6.28}$$

$$\phi_i\left(x_i, t\right) = \frac{1}{a_0 \tau_0^2} \left(\alpha \phi_i^*\left(x_i^*, t^*\right) + O\left(\alpha^2\right)\right) . \tag{6.29}$$

In addition to the previously introduced relaxation time, Eqs. (5.75)–(5.76), the other new relaxation times, τ_ϵ and τ_ω, are constants, which take the same value as τ_0 in this analysis,

$$\tau_\epsilon \left(x_i, t\right) = \tau_0 \,, \tag{6.30}$$

$$\tau_\omega \left(x_i, t\right) = \tau_0 \,. \tag{6.31}$$

All above mentioned variables are then substituted into the Reynolds-averaged ten-moment equations coupled with the Cattaneo-Vernotte type hyperbolic-relaxation two-equation models. Similarly to the previous analysis, as the leading order satisfies the equations, the equations of the non-dimensional perturbed variables can then be obtained. The full equations of the system,

$$\frac{\partial \mathbf{U}^*}{\partial t^*} + \frac{\partial \mathbf{F}^*}{\partial x^*} = \mathbf{S}^* \,, \tag{6.32}$$

can again be expressed as a linear operator acting on a solution vector containing the perturbations,

$$\left(\mathbf{I} \frac{\partial}{\partial t^*} + \mathbf{A}^* \frac{\partial}{\partial x^*} - \mathbf{Q}^* \right) \mathbf{U}^* = \mathbf{0} \,, \tag{6.33}$$

where the matrix $\mathbf{A}^*$ and $\mathbf{Q}^*$ are defined as $\frac{\partial \mathbf{F}^*}{\partial \mathbf{U}^*}$ and $\frac{\partial \mathbf{S}^*}{\partial \mathbf{U}^*}$, which are evaluated at the non-dimensional equilibrium state.

One notes that, in this analysis, the eddy viscosity, ν_T, is assumed to be zero at the equilibrium state. This is because there is no effect of turbulence mixing when turbulence is absent. The production and dissipation terms of the turbulence models are assumed to be zero at the equilibrium state as well. Moreover, the singularity caused by the inverse terms, $\frac{1}{k}$, $\frac{1}{\epsilon}$ and $\frac{1}{\omega}$, at the equilibrium state, is avoided by this assumption as well.

Following the same steps as introduced in Section 5.4, the eigenvalues, $\omega^* = \omega_{\mathrm{R}}^* + i\,\omega_{\mathrm{I}}^*$, of the matrix $\xi \mathbf{A}^* - i\mathbf{Q}^*$ must be found first, the wave speed, $\omega_{\mathrm{R}}^*/\xi$, and the attenuation rate, $e^{-\omega_{\mathrm{I}}^*}$, can then be determined. Again, the relaxation time, τ_0, is chosen as 1 in this analysis. The same choices of Mach number, $\mathrm{Ma} = 0$ and $\mathrm{Ma} = 1$, are selected. One notes that, the non-dimensional flux Jacobian matrix, $\mathbf{A}^*$, and the matrix $\mathbf{Q}^*$ of the Reynolds-averaged ten-moment equations coupled with hyperbolic-relaxation form of the standard k-ϵ and Wilcox k-ω models are exactly the same in equilibrium. Therefore, the matrix, $\xi \mathbf{A}^* - i\mathbf{Q}^*$, of the two-equation models shares the same eigenvalues, ω^*. Consequently, the phase speed and attenuation rate distributions over wave number of these two-equation models are exactly the same, which are plotted in Figs. 6.1 and 6.2 respectively. In these figures, the eigenvalues ω_{1-7}^* belong to the Reynolds-averaged ten-moment equations, which are

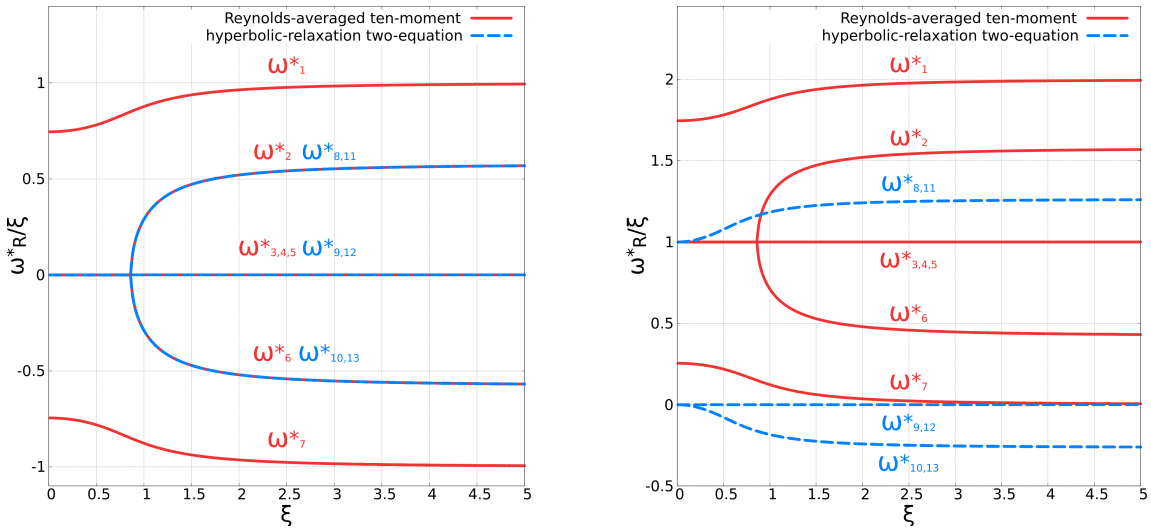

(a) Ma = 0 (b) Ma = 1

Figure 6.1: Variation with wave number of the phase speed for the Reynolds-averaged ten-moment equations coupled with Cattaneo-Vernotte type two-equation models for zero and non-zero background velocity

plotted as the red solid lines, and the eigenvalues ω^*_{8-13} belong to the hyperbolic-relaxation two-equation models, which are plotted as the blue dashed lines.

As shown, the dispersive behaviour of the Cattaneo-Vernotte type hyperbolic-relaxation two-equation models is the same as that of the p-system type hyperbolic-relaxation one-equation model, when the bulk velocity is zero, Ma = 0. In the case of Ma = 1, and the limit of the long-wave region of the plot, the eigenvalues $\omega^*_{10,13}$ and $\omega^*_{9,12}$ have the same propagation speed as well as the same damping rate, which is different from the one in the p-system. This feature implies that the Cattaneo-Vernotte type hyperbolic-relaxation model is not Galilean invariant either. Obviously, the attenuation rate of the perturbation always stays in the stability region, $e^{-\omega^*_{\mathrm{I}}} \in [0\ ,\ 1]$, which means that the disturbed solution is linearly stable.

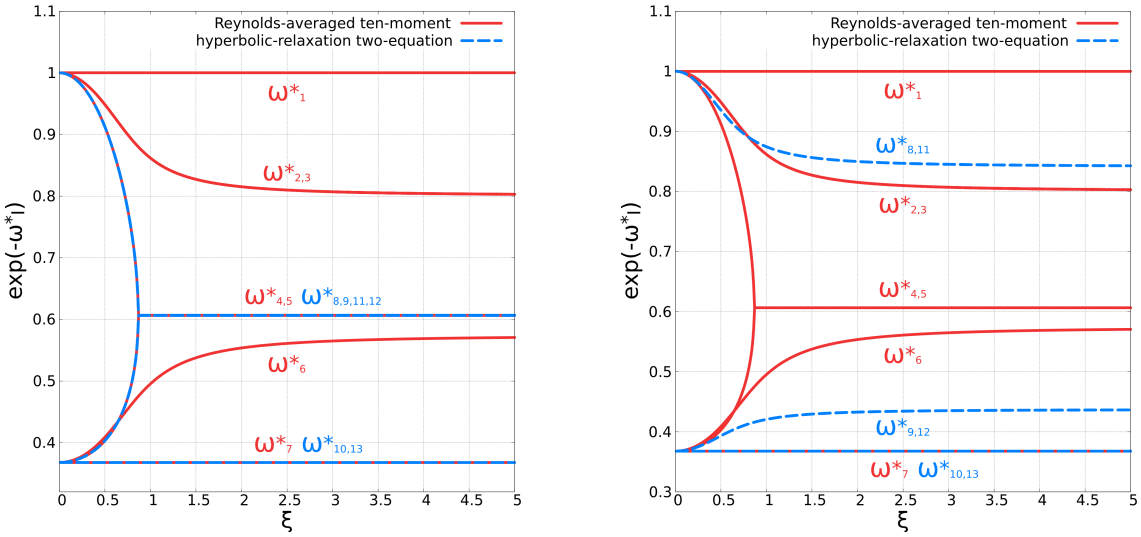

(a) Ma = 0 (b) Ma = 1

Figure 6.2: Variation with wave number of the attenuation rate for the Reynolds-averaged ten-moment equations coupled with Cattaneo-Vernotte type two-equation models for zero and non-zero background velocity

Chapter 7

Axisymmetric Form

In this chapter, the axisymmetric form of the Reynolds-averaged ten-moment equations coupled with the derived hyperbolic-relaxation turbulence models is introduced. This two-dimensional form can be used to solve axisymmetric flow problems. Unlike in Cartesian coordinates, in cylindrical coordinates the divergence of the flux tensor generates a more complicated form, due to the non-zero derivatives of the metric tensor for the coordinate frame. For general coordinates, the divergence of tensors of various orders can be expressed as

$$\nabla \cdot \mathbf{A}_i = \frac{\partial \mathbf{A}_i}{\partial x_i} + \Gamma^i_{li}\mathbf{A}_l \,, \tag{7.1}$$

$$\nabla \cdot \mathbf{B}_{ij} = \frac{\partial \mathbf{B}_{ij}}{\partial x_j} + \Gamma^i_{lj}\mathbf{B}_{lj} + \Gamma^j_{lj}\mathbf{B}_{il} \,, \tag{7.2}$$

$$\nabla \cdot \mathbf{C}_{ijk} = \frac{\partial \mathbf{C}_{ijk}}{\partial x_k} + \Gamma^i_{lk}\mathbf{C}_{ljk} + \Gamma^j_{lk}\mathbf{C}_{ilk} + \Gamma^k_{lk}\mathbf{C}_{ijl} \,, \tag{7.3}$$

where $\mathbf{A}_i$, $\mathbf{B}_{ij}$ and $\mathbf{C}_{ijk}$ are first-, second-, and third-order tensors, and Γ^i_{jk} indicates the Christoffel symbols or connection coefficients. In cylindrical coordinates, the connection coefficients are

$$\Gamma^r = \begin{bmatrix} 0 & 0 & 0 \\ 0 & -\frac{1}{r} & 0 \\ 0 & 0 & 0 \end{bmatrix} , \Gamma^\theta = \begin{bmatrix} 0 & \frac{1}{r} & 0 \\ 0 & 0 & 0 \\ 0 & 0 & 0 \end{bmatrix} , \Gamma^z = \begin{bmatrix} 0 & 0 & 0 \\ 0 & 0 & 0 \\ 0 & 0 & 0 \end{bmatrix} . \tag{7.4}$$

Applying Eqs.(7.1)–(7.3) to the Reynolds-averaged ten-moment equations with hyperbolic-relaxation turbulence models, the resulting governing equations can be written as

$$\frac{\partial \mathbf{U}}{\partial t} + \frac{\partial \mathbf{F}_r}{\partial r} + \frac{\partial \mathbf{F}_z}{\partial z} = \frac{\mathbf{S}_a}{r} + \mathbf{S} \,, \tag{7.5}$$

where $\mathbf{U}$ is the vector of conserved variables, $\mathbf{F}_r$ and $\mathbf{F}_z$ are the fluxes in r and z directions respectively, $\mathbf{S}_a$ is the source term due to the cylindrical coordinates and $\mathbf{S}$ is the relaxation source term from the original models.

7.1 Axisymmetric Version of the Reynolds-Averaged Ten-Moment Equations with P-System Type Hyperbolic-Relaxation Prandtl's One-Equation Model

For the Reynolds-averaged ten-moment equations coupled with the p-system type hyperbolic-relaxation Prandtl's one-equation model, the above mentioned vectors are given by

$$\mathbf{U} = \begin{bmatrix} \bar{\rho} \\ \bar{\rho}\bar{u}_r \\ \bar{\rho}\bar{u}_z \\ \bar{\rho}\bar{u}_r^2 + \overline{\Psi}_{rr} \\ \bar{\rho}\bar{u}_r\bar{u}_z + \overline{\Psi}_{rz} \\ \bar{\rho}\bar{u}_z^2 + \overline{\Psi}_{zz} \\ \overline{\Psi}_{\theta\theta} \\ k \\ \psi_r \\ \psi_z \end{bmatrix}, \mathbf{S} = \begin{bmatrix} 0 \\ 0 \\ 0 \\ -\frac{1}{3\tau_{\mathcal{G}}}\frac{\mu}{\mu+\bar{\rho}k^{1/2}l}\left(2\overline{\Psi}_{rr} - \overline{\Psi}_{zz} - \overline{\Psi}_{\theta\theta}\right) \\ -\frac{1}{\tau_{\mathcal{G}}}\frac{\mu}{\mu+\bar{\rho}k^{1/2}l}\overline{\Psi}_{rz} \\ -\frac{1}{3\tau_{\mathcal{G}}}\frac{\mu}{\mu+\bar{\rho}k^{1/2}l}\left(2\overline{\Psi}_{zz} - \overline{\Psi}_{rr} - \overline{\Psi}_{\theta\theta}\right) \\ -\frac{1}{3\tau_{\mathcal{G}}}\frac{\mu}{\mu+\bar{\rho}k^{1/2}l}\left(2\overline{\Psi}_{\theta\theta} - \overline{\Psi}_{rr} - \overline{\Psi}_{zz}\right) \\ S_k \\ -\frac{1}{\tau_k}\left(\psi_r - \bar{u}_r k\right) + \bar{u}_r S_k \\ -\frac{1}{\tau_k}\left(\psi_z - \bar{u}_z k\right) + \bar{u}_z S_k \end{bmatrix}, \tag{7.6}$$

with

$$S_k = \frac{k^{1/2}l}{\left(\mu + \bar{\rho}k^{1/2}l\right)^2}\left[\frac{1}{3}\left(\overline{\Psi}_{rr}^2 + \overline{\Psi}_{zz}^2 + \overline{\Psi}_{\theta\theta}^2 - \overline{\Psi}_{rr}\,\overline{\Psi}_{zz} - \overline{\Psi}_{rr}\,\overline{\Psi}_{\theta\theta} - \overline{\Psi}_{zz}\,\overline{\Psi}_{\theta\theta}\right) + \overline{\Psi}_{rz}^2\right] - \frac{C_D k^{3/2}}{l}, \tag{7.7}$$

and

$$\mathbf{S}_a = \begin{bmatrix} -\rho\bar{u}_r \\ -\left(\rho\bar{u}_r^2 + \overline{\Psi}_{rr} - \overline{\Psi}_{\theta\theta}\right) \\ -\left(\rho\bar{u}_r\bar{u}_z + \overline{\Psi}_{rz}\right) \\ 2\bar{u}_r\overline{\Psi}_{\theta\theta} - \left(\rho\bar{u}_r^3 + 3\bar{u}_r\overline{\Psi}_{rr}\right) \\ \bar{u}_z\overline{\Psi}_{\theta\theta} - \left(\rho\bar{u}_r^2\bar{u}_z + 2\bar{u}_r\overline{\Psi}_{rz} + \bar{u}_z\overline{\Psi}_{rr}\right) \\ -\left(\rho\bar{u}_z^2\bar{u}_r + 2\bar{u}_z\overline{\Psi}_{rz} + \bar{u}_r\overline{\Psi}_{zz}\right) \\ -3\bar{u}_r\overline{\Psi}_{\theta\theta} \\ -\psi_r \\ -\bar{u}_r^2 k \\ 0 \end{bmatrix}, \tag{7.8}$$

$$\mathbf{F}_r = \begin{bmatrix} \bar{\rho}\bar{u}_r \\ \bar{\rho}\bar{u}_r^2 + \overline{\Psi}_{rr} \\ \bar{\rho}\bar{u}_r\bar{u}_z + \overline{\Psi}_{rz} \\ \bar{\rho}\bar{u}_r^3 + 3\overline{\Psi}_{rr}\bar{u}_r \\ \bar{\rho}\bar{u}_r^2\bar{u}_z + \overline{\Psi}_{rr}\bar{u}_z + 2\overline{\Psi}_{rz}\bar{u}_r \\ \bar{\rho}\bar{u}_r\bar{u}_z^2 + \overline{\Psi}_{zz}\bar{u}_r + 2\overline{\Psi}_{rz}\bar{u}_z \\ \overline{\Psi}_{\theta\theta}\bar{u}_r \\ \psi_r \\ \left[\frac{1}{\tau_k}\left(\nu k + \frac{2}{3}k^{3/2}l\right) + k\bar{u}_r^2\right] \\ 0 \end{bmatrix}, \mathbf{F}_z = \begin{bmatrix} \bar{\rho}\bar{u}_z \\ \bar{\rho}\bar{u}_r\bar{u}_z + \overline{\Psi}_{rz} \\ \bar{\rho}\bar{u}_z^2 + \overline{\Psi}_{zz} \\ \bar{\rho}\bar{u}_r^2\bar{u}_z + \overline{\Psi}_{rr}\bar{u}_z + 2\overline{\Psi}_{rz}\bar{u}_r \\ \bar{\rho}\bar{u}_r\bar{u}_z^2 + \overline{\Psi}_{zz}\bar{u}_r + 2\overline{\Psi}_{rz}\bar{u}_z \\ \bar{\rho}\bar{u}_z^3 + 3\overline{\Psi}_{zz}\bar{u}_z \\ \overline{\Psi}_{\theta\theta}\bar{u}_z \\ \psi_z \\ 0 \\ \left[\frac{1}{\tau_k}\left(\nu k + \frac{2}{3}k^{3/2}l\right) + k\bar{u}_z^2\right] \end{bmatrix}. \tag{7.9}$$

7.2 Axisymmetric Version of the Reynolds-Averaged Ten-Moment Equations with Cattaneo-Vernotte Type Hyperbolic-Relaxation Two-Equation Models

For the Reynolds-averaged ten-moment equations coupled with Cattaneo-Vernotte type two-equation models, these vectors can be found in the same manner,

$$\mathbf{U} = \begin{bmatrix} \bar{\rho} \\ \bar{\rho}\bar{u}_r \\ \bar{\rho}\bar{u}_z \\ \bar{\rho}\bar{u}_r^2 + \overline{\Psi}_{rr} \\ \bar{\rho}\bar{u}_r\bar{u}_z + \overline{\Psi}_{rz} \\ \bar{\rho}\bar{u}_z^2 + \overline{\Psi}_{zz} \\ \overline{\Psi}_{\theta\theta} \\ k \\ \psi_r \\ \psi_z \\ \epsilon \\ \phi_r \\ \phi_z \end{bmatrix}, \mathbf{S} = \begin{bmatrix} 0 \\ 0 \\ 0 \\ -\frac{1}{3\tau_{\mathcal{G}}}\frac{\mu}{\mu+\bar{\rho}C_\mu k^2/\epsilon}\left(2\overline{\Psi}_{rr} - \overline{\Psi}_{zz} - \overline{\Psi}_{\theta\theta}\right) \\ -\frac{1}{\tau_{\mathcal{G}}}\frac{\mu}{\mu+\bar{\rho}C_\mu k^2/\epsilon}\overline{\Psi}_{rz} \\ -\frac{1}{3\tau_{\mathcal{G}}}\frac{\mu}{\mu+\bar{\rho}C_\mu k^2/\epsilon}\left(2\overline{\Psi}_{zz} - \overline{\Psi}_{rr} - \overline{\Psi}_{\theta\theta}\right) \\ -\frac{1}{3\tau_{\mathcal{G}}}\frac{\mu}{\mu+\bar{\rho}C_\mu k^2/\epsilon}\left(2\overline{\Psi}_{\theta\theta} - \overline{\Psi}_{rr} - \overline{\Psi}_{zz}\right) \\ S_k \\ -\frac{\psi_r}{\tau_k} \\ -\frac{\psi_z}{\tau_k} \\ S_\epsilon \\ -\frac{\phi_r}{\tau_\epsilon} \\ -\frac{\phi_z}{\tau_\epsilon} \end{bmatrix}, \tag{7.10}$$

with

$$S_k = \frac{C_\mu k^2/\epsilon}{\left(\mu + \bar{\rho}C_\mu k^2/\epsilon\right)^2}\left[\frac{1}{3}\left(\overline{\Psi}_{rr}^2 + \overline{\Psi}_{zz}^2 + \overline{\Psi}_{\theta\theta}^2 - \overline{\Psi}_{rr}\,\overline{\Psi}_{zz} - \overline{\Psi}_{rr}\,\overline{\Psi}_{\theta\theta} - \overline{\Psi}_{zz}\,\overline{\Psi}_{\theta\theta}\right) + \overline{\Psi}_{rz}^2\right] - \epsilon\,, \tag{7.11}$$

$$S_\epsilon = \frac{C_{\epsilon 1}C_\mu k}{\left(\mu + \bar{\rho}C_\mu k^2/\epsilon\right)^2}\left[\frac{1}{3}\left(\overline{\Psi}_{rr}^2 + \overline{\Psi}_{zz}^2 + \overline{\Psi}_{\theta\theta}^2 - \overline{\Psi}_{rr}\,\overline{\Psi}_{zz} - \overline{\Psi}_{rr}\,\overline{\Psi}_{\theta\theta} - \overline{\Psi}_{zz}\,\overline{\Psi}_{\theta\theta}\right) + \overline{\Psi}_{rz}^2\right] - C_{\epsilon 2}\frac{\epsilon^2}{k}\,, \tag{7.12}$$

and

$$\mathbf{S}_a = \begin{bmatrix} -\rho\bar{u}_r \\ -\left(\rho\bar{u}_r^2 + \overline{\Psi}_{rr} - \overline{\Psi}_{\theta\theta}\right) \\ -\left(\rho\bar{u}_r\bar{u}_z + \overline{\Psi}_{rz}\right) \\ 2\bar{u}_r\overline{\Psi}_{\theta\theta} - \left(\rho\bar{u}_r^3 + 3\bar{u}_r\overline{\Psi}_{rr}\right) \\ \bar{u}_z\overline{\Psi}_{\theta\theta} - \left(\rho\bar{u}_r^2\bar{u}_z + 2\bar{u}_r\overline{\Psi}_{rz} + \bar{u}_z\overline{\Psi}_{rr}\right) \\ -\left(\rho\bar{u}_z^2\bar{u}_r + 2\bar{u}_z\overline{\Psi}_{rz} + \bar{u}_r\overline{\Psi}_{zz}\right) \\ -3\bar{u}_r\overline{\Psi}_{\theta\theta} \\ -\left[\bar{u}_r k - \left(\nu + \frac{C_\mu k^2}{\epsilon\sigma_k}\right)\psi_r\right] \\ 0 \\ 0 \\ -\left[\bar{u}_r\epsilon - \left(\nu + \frac{C_\mu k^2}{\epsilon\sigma_\epsilon}\right)\phi_r\right] \\ 0 \\ 0 \end{bmatrix}, \tag{7.13}$$

$$\mathbf{F}_r = \begin{bmatrix} \bar{\rho}\bar{u}_r \\ \bar{\rho}\bar{u}_r^2 + \overline{\Psi}_{rr} \\ \bar{\rho}\bar{u}_r\bar{u}_z + \overline{\Psi}_{rz} \\ \bar{\rho}\bar{u}_r^3 + 3\overline{\Psi}_{rr}\bar{u}_r \\ \bar{\rho}\bar{u}_r^2\bar{u}_z + \overline{\Psi}_{rr}\bar{u}_z + 2\overline{\Psi}_{rz}\bar{u}_r \\ \bar{\rho}\bar{u}_r\bar{u}_z^2 + \overline{\Psi}_{zz}\bar{u}_r + 2\overline{\Psi}_{rz}\bar{u}_z \\ \overline{\Psi}_{\theta\theta}\bar{u}_r \\ \bar{u}_r k - \left(\nu + \frac{C_\mu k^2}{\epsilon\sigma_k}\right)\psi_r \\ -\frac{k}{\tau_k} \\ 0 \\ \bar{u}_r\epsilon - \left(\nu + \frac{C_\mu k^2}{\epsilon\sigma_\epsilon}\right)\phi_r \\ -\frac{\epsilon}{\tau_\epsilon} \\ 0 \end{bmatrix}, \mathbf{F}_z = \begin{bmatrix} \bar{\rho}\bar{u}_z \\ \bar{\rho}\bar{u}_r\bar{u}_z + \overline{\Psi}_{rz} \\ \bar{\rho}\bar{u}_z^2 + \overline{\Psi}_{zz} \\ \bar{\rho}\bar{u}_r^2\bar{u}_z + \overline{\Psi}_{rr}\bar{u}_z + 2\overline{\Psi}_{rz}\bar{u}_r \\ \bar{\rho}\bar{u}_r\bar{u}_z^2 + \overline{\Psi}_{zz}\bar{u}_r + 2\overline{\Psi}_{rz}\bar{u}_z \\ \bar{\rho}\bar{u}_z^3 + 3\overline{\Psi}_{zz}\bar{u}_z \\ \overline{\Psi}_{\theta\theta}\bar{u}_z \\ \bar{u}_z k - \left(\nu + \frac{C_\mu k^2}{\epsilon\sigma_k}\right)\psi_z \\ 0 \\ -\frac{k}{\tau_k} \\ \bar{u}_z\epsilon - \left(\nu + \frac{C_\mu k^2}{\epsilon\sigma_\epsilon}\right)\phi_z \\ 0 \\ -\frac{\epsilon}{\tau_\epsilon} \end{bmatrix}, \tag{7.14}$$

for the k-ϵ model and

$$\mathbf{U} = \begin{bmatrix} \bar{\rho} \\ \bar{\rho}\bar{u}_r \\ \bar{\rho}\bar{u}_z \\ \bar{\rho}\bar{u}_r^2 + \overline{\Psi}_{rr} \\ \bar{\rho}\bar{u}_r\bar{u}_z + \overline{\Psi}_{rz} \\ \bar{\rho}\bar{u}_z^2 + \overline{\Psi}_{zz} \\ \overline{\Psi}_{\theta\theta} \\ k \\ \psi_r \\ \psi_z \\ \omega \\ \phi_r \\ \phi_z \end{bmatrix}, \mathbf{S} = \begin{bmatrix} 0 \\ 0 \\ 0 \\ -\frac{1}{3\tau_{\mathcal{G}}}\frac{\mu}{\mu+\bar{\rho}k/\omega}\left(2\overline{\Psi}_{rr} - \overline{\Psi}_{zz} - \overline{\Psi}_{\theta\theta}\right) \\ -\frac{1}{\tau_{\mathcal{G}}}\frac{\mu}{\mu+\bar{\rho}k/\omega}\overline{\Psi}_{rz} \\ -\frac{1}{3\tau_{\mathcal{G}}}\frac{\mu}{\mu+\bar{\rho}k/\omega}\left(2\overline{\Psi}_{zz} - \overline{\Psi}_{rr} - \overline{\Psi}_{\theta\theta}\right) \\ -\frac{1}{3\tau_{\mathcal{G}}}\frac{\mu}{\mu+\bar{\rho}k/\omega}\left(2\overline{\Psi}_{\theta\theta} - \overline{\Psi}_{rr} - \overline{\Psi}_{zz}\right) \\ S_k \\ -\frac{\psi_r}{\tau_k} \\ -\frac{\psi_z}{\tau_k} \\ S_\omega \\ -\frac{\phi_r}{\tau_\omega} \\ -\frac{\phi_z}{\tau_\omega} \end{bmatrix}, \tag{7.15}$$

with

$$S_k = \frac{k/\omega}{\left(\mu + \bar{\rho}k/\omega\right)^2}\left[\frac{1}{3}\left(\overline{\Psi}_{rr}^2 + \overline{\Psi}_{zz}^2 + \overline{\Psi}_{\theta\theta}^2 - \overline{\Psi}_{rr}\,\overline{\Psi}_{zz} - \overline{\Psi}_{rr}\,\overline{\Psi}_{\theta\theta} - \overline{\Psi}_{zz}\,\overline{\Psi}_{\theta\theta}\right) + \overline{\Psi}_{rz}^2\right] - \beta^*\omega k\,, \tag{7.16}$$

$$S_\omega = \frac{\gamma}{\left(\mu + \bar{\rho}k/\omega\right)^2}\left[\frac{1}{3}\left(\overline{\Psi}_{rr}^2 + \overline{\Psi}_{zz}^2 + \overline{\Psi}_{\theta\theta}^2 - \overline{\Psi}_{rr}\,\overline{\Psi}_{zz} - \overline{\Psi}_{rr}\,\overline{\Psi}_{\theta\theta} - \overline{\Psi}_{zz}\,\overline{\Psi}_{\theta\theta}\right) + \overline{\Psi}_{rz}^2\right] - \beta\omega^2\,, \tag{7.17}$$

and

$$\mathbf{S}_a = \begin{bmatrix} -\rho\bar{u}_r \\ -\left(\rho\bar{u}_r^2 + \overline{\Psi}_{rr} - \overline{\Psi}_{\theta\theta}\right) \\ -\left(\rho\bar{u}_r\bar{u}_z + \overline{\Psi}_{rz}\right) \\ 2\bar{u}_r\overline{\Psi}_{\theta\theta} - \left(\rho\bar{u}_r^3 + 3\bar{u}_r\overline{\Psi}_{rr}\right) \\ \bar{u}_z\overline{\Psi}_{\theta\theta} - \left(\rho\bar{u}_r^2\bar{u}_z + 2\bar{u}_r\overline{\Psi}_{rz} + \bar{u}_z\overline{\Psi}_{rr}\right) \\ -\left(\rho\bar{u}_z^2\bar{u}_r + 2\bar{u}_z\overline{\Psi}_{rz} + \bar{u}_r\overline{\Psi}_{zz}\right) \\ -3\bar{u}_r\overline{\Psi}_{\theta\theta} \\ -\left[\bar{u}_r k - \left(\nu + \sigma_k\frac{k}{\omega}\right)\psi_r\right] \\ 0 \\ 0 \\ -\left[\bar{u}_r\omega - \left(\nu + \sigma_\omega\frac{k}{\omega}\right)\phi_r\right] \\ 0 \\ 0 \end{bmatrix}, \tag{7.18}$$

$$\mathbf{F}_r = \begin{bmatrix} \bar{\rho}\bar{u}_r \\ \bar{\rho}\bar{u}_r^2 + \overline{\Psi}_{rr} \\ \bar{\rho}\bar{u}_r\bar{u}_z + \overline{\Psi}_{rz} \\ \bar{\rho}\bar{u}_r^3 + 3\overline{\Psi}_{rr}\bar{u}_r \\ \bar{\rho}\bar{u}_r^2\bar{u}_z + \overline{\Psi}_{rr}\bar{u}_z + 2\overline{\Psi}_{rz}\bar{u}_r \\ \bar{\rho}\bar{u}_r\bar{u}_z^2 + \overline{\Psi}_{zz}\bar{u}_r + 2\overline{\Psi}_{rz}\bar{u}_z \\ \overline{\Psi}_{\theta\theta}\bar{u}_r \\ \bar{u}_r k - \left(\nu + \sigma_k\frac{k}{\omega}\right)\psi_r \\ -\frac{k}{\tau_k} \\ 0 \\ \bar{u}_r\omega - \left(\nu + \sigma_\omega\frac{k}{\omega}\right)\phi_r \\ -\frac{\omega}{\tau_\omega} \\ 0 \end{bmatrix}, \mathbf{F}_z = \begin{bmatrix} \bar{\rho}\bar{u}_z \\ \bar{\rho}\bar{u}_r\bar{u}_z + \overline{\Psi}_{rz} \\ \bar{\rho}\bar{u}_z^2 + \overline{\Psi}_{zz} \\ \bar{\rho}\bar{u}_r^2\bar{u}_z + \overline{\Psi}_{rr}\bar{u}_z + 2\overline{\Psi}_{rz}\bar{u}_r \\ \bar{\rho}\bar{u}_r\bar{u}_z^2 + \overline{\Psi}_{zz}\bar{u}_r + 2\overline{\Psi}_{rz}\bar{u}_z \\ \bar{\rho}\bar{u}_z^3 + 3\overline{\Psi}_{zz}\bar{u}_z \\ \overline{\Psi}_{\theta\theta}\bar{u}_z \\ \bar{u}_z k - \left(\nu + \sigma_k\frac{k}{\omega}\right)\psi_z \\ 0 \\ -\frac{k}{\tau_k} \\ \bar{u}_z\omega - \left(\nu + \sigma_\omega\frac{k}{\omega}\right)\phi_z \\ 0 \\ -\frac{\omega}{\tau_\omega} \end{bmatrix}, \tag{7.19}$$

for the k-ω model.

Chapter 8

Numerical Experiments

In this chapter, several numerical experiments are designed to demonstrate the behaviour of the proposed hyperbolic-relaxation turbulence models.

In the first set of numerical tests, the recovery of the original Prandtl's one-equation model, Eq. (5.7), by the new hyperbolic-relaxation model, Eqs. (5.38)–(5.39), in the p-system form, and Eqs. (5.40)–(5.41), in the Cattaneo-Vernotte form, is demonstrated. This is done by demonstrating that both types of hyperbolic-relaxation versions predict the same solutions for a simple one-dimensional initial-value problem. The selection of the appropriate relaxation time for both types of hyperbolic-relaxation models is discussed. The effect of formulation error caused by variable velocity is also investigated. Similar initial-value problems are solved by the original two-equation models, the standard k-ϵ model, Eqs. (6.5)–(6.6), and the Wilcox k-ω model, Eqs. (6.18)–(6.19), and the corresponding Cattaneo-Vernotte type hyperbolic-relaxation forms, Eqs. (6.10)–(6.13) and Eqs. (6.20)–(6.23). The final solutions at various times are compared.

In the second set of numerical tests, two-dimensional initial-value problems are solved by the same original one- and two-equation models and the corresponding hyperbolic-relaxation versions. The final solutions along the translational direction of the background flow at various times are sampled and compared. The relaxation time that is appropriate for the two-dimensional p-system type hyperbolic-relaxation model is investigated.

In the rest of the numerical tests, the Reynolds-averaged ten-moment equations, Eqs. (5.52)–(5.54), coupled with the p-system type hyperbolic-relaxation Prandtl's one-equation model, Eqs. (5.55)–(5.56), the Cattaneo-Vernotte type hyperbolic-relaxation standard k-ϵ model, Eqs. (6.10)–(6.13), and Wilcox k-ω model, Eqs. (6.20)–(6.23), are validated through the

solutions of a two-dimensional planar turbulent mixing-layer, planar turbulent free-jet, and circular turbulent free-jet. The numerical solutions at steady state are investigated, where the velocity and shear Reynolds-stress profiles at various locations are sampled and compared to existing experimental measurements.

8.1 Numerical Approximation by Godunov-Type Finite-Volume Scheme

Many numerical techniques exist to approximate the solution of hyperbolic PDEs with stiff relaxation source terms. In this project, the computational domain of all numerical tests is decomposed into a structured mesh, where the index i, j denotes the row and column of each computational cell. A second-order accurate finite-volume scheme is applied and the flux of conserved quantities between computational cells is computed by the approximate solution of Riemann problems. A point-implicit time marching method is applied to integrate the set of ordinary differential equations that is generated by the spatial discretization of the governing equations.

The update procedure for the average solution in cell i, j is given by a fully-discrete finite-volume scheme with second-order semi-implicit time marching, which can be written as

$$\widehat{\mathbf{U}}_{i,j}^{n+1} = \mathbf{U}_{i,j}^{n} - \frac{\Delta t}{A_{i,j}} \left[\sum_{k} \left(\mathbf{F} \cdot \mathbf{n} \, \Delta l \right)_{i,j,k}^{n} \right] + \Delta t \widehat{\mathbf{S}}_{i,j}^{n+1} , \tag{8.1}$$

$$\mathbf{U}_{i,j}^{n+1} = \mathbf{U}_{i,j}^{n} - \frac{\Delta t}{2A_{i,j}} \left[\sum_{k} \left(\mathbf{F} \cdot \mathbf{n} \, \Delta l \right)_{i,j,k}^{n} + \sum_{k} \left(\widehat{\mathbf{F}} \cdot \mathbf{n} \, \Delta l \right)_{i,j,k}^{n+1} \right] + \frac{\Delta t}{2} \left(\mathbf{S}_{i,j}^{n} + \mathbf{S}_{i,j}^{n+1} \right) . \tag{8.2}$$

In the validation tests, where the Reynolds-averaged ten-moment equations coupled with different type of hyperbolic-relaxation turbulence models are solved, due to the complexity of the non-linear source term, a Newton method is used to iteratively find the next time step solution [11]. In the expressions, $\mathbf{U}_{i,j}$ is a vector containing the average value of solution quantities in cell i, j, $\mathbf{F}$ is a vector of corresponding flux through the kth cell face, A_{ij} is the area of the cell, Δl and $\mathbf{n}_k$ are the length and the normal unit vector of the cell face, and $\mathbf{S}_{i,j}$ is the vector of the local source term. The superscript n is the index for the time step of size Δt. The symbol $\widehat{(\cdot)}$ denotes the evaluation at the predictor step. Piece-wise limited-linear reconstruction is used along with the van-Albada slope limiter [2]. Inter-cell fluxes are computed using the HLL approximate Riemann solver [21].

One could reasonably be worried about stiffness caused by the factor $1/\tau$ that has been added to the flux. As τ must be small to ensure the correct asymptotic behaviour is modelled, any possibility of stiffness of the flux terms should be considered. Fortunately, in the wavespeed of the p-system type hyperbolic-relaxation Prandtl's one-equation model, $1/\tau_k$ always appears under a square root, which greatly reduces the worry of stiffness. Also, in practice, it has been found that τ_k can normally be chosen to be much larger than $\tau_{\mathcal{G}}$ while still maintaining good results. For the Cattaneo-Vernotte type hyperbolic-relaxation two-equation models, the same conclusion for choosing the relaxation times, τ_k, τ_ϵ and τ_ω, can be made in practice. Moreover, good results can be obtained in the higher dimensional form for the same value of the relaxation times as are appropriate for one dimension, which is discussed later in the following sections. Therefore, for all numerical solutions in this project, no special treatment of the flux terms was needed and no stiffness-related problems due to fluxes were encountered.

8.2 Equivalence between the One-Dimensional Turbulence Models and the Hyperbolic-Relaxation Forms

In this section, several one-dimensional initial-value problems are investigated using one-equation and two-equation models. The goal is to verify the equivalence between the original turbulence models and corresponding hyperbolic-relaxation systems.

8.2.1 Prandtl's One-Equation Model and the Hyperbolic-Relaxation Versions

The first numerical experiment aims to show that the one-dimensional form of the p-system type hyperbolic-relaxation version, Eqs. (5.38)–(5.39), and the Cattaneo-Vernotte type hyperbolic-relaxation version, Eqs. (5.40)–(5.41), is equivalent (in the sense defined in Section 2.1.3) to the original one-equation model, Eq. (5.7). An initial-value problem is designed to be solved by these models. The computational domain, $x \in [0\ ,\ 4]\,\mathrm{m}$, is decomposed into equally spaced cells. The original one-equation model is solved by a simple fourth-order accurate finite-difference scheme in space and explicit-Euler time marching. Two grid resolutions, 1000 and 2000 cells, are tested. The maximum difference

Table 8.1: Numerical setup for the one-dimensional one-equation model

$\bar{u}_x$	ν	l	$\bar{t}_{ij}\ \bar{t}_{ij}$	C_d
$1.5\,\mathrm{m/s}$	$0.05\,\mathrm{m^2/s}$	$0.03\,\mathrm{m}$	$1.0\,\mathrm{kg^2/m^2s^4}$	0.01

between the final solutions, in magnitude, is less than 10^{-3}, therefore, the solution on the former grid is considered accurate and is further used as the reference solution of the one-equation model. The hyperbolic-relaxation system has been solved by the above mentioned numerical method on the same two grid resolutions. The maximum difference between the final solutions, in magnitude, is less than 10^{-4}, therefore, the same grid resolution of the original model is used for the further computations.

A one-dimensional Gaussian pulse is selected as the initial condition of the turbulence kinetic energy, which is defined by the function

$$k\left(x,0\right)=\left\{10\ \exp\left[-\frac{\left(x-x_0\right)^2}{\kappa}\right]+0.01\right\}\ \ \mathrm{m^2/s^2}\,, \tag{8.3}$$

where $\kappa=0.1\,\mathrm{m}^2$. A small value, $0.01\,\mathrm{m^2/s^2}$, is added to guarantee the positive non-zero initial distribution within the computational domain. The centre of the pulse is initially located at the coordinate, $x_0=1\,\mathrm{m}$, and moves with the background flow over the positive direction of the x axis. In order to investigate observable rates of production, dissipation and diffusion while the initial Gaussian pulse translates, the magnitude of coefficients must be carefully selected. The selection of parameter values for the computation is summarized in Table 8.1.

One notes that the variable ψ in the hyperbolic-relaxation systems is initialized differently for each model. In the form of the p-system, ψ represents the flux of the turbulence kinetic energy, which is initialized as $\psi=\bar{u}_x k$. However, in Cattaneo-Vernotte form, ψ represents the spacial gradient of the turbulence kinetic energy, which is therefore initialized as $\psi=\frac{\partial k}{\partial x}$. The relaxation time $\tau_k=1\times10^{-3}\,\mathrm{s}$ is chosen for the computation.

The numerical solutions at $t=0.2\,\mathrm{s}$, $0.4\,\mathrm{s}$, $0.6\,\mathrm{s}$, $0.8\,\mathrm{s}$ and $1.0\,\mathrm{s}$ are plotted in Fig. 8.1. The reference solutions of the original one-equation model are plotted with red solid lines, which show the initial pulse undergoes production, dissipation and diffusion during the translation, as expected. The solutions of both hyperbolic-relaxation forms, with a value of $1\times10^{-3}\,\mathrm{s}$ for the relaxation time, agree with the solution of the original one-equation model, which demonstrates the equivalence between these models.

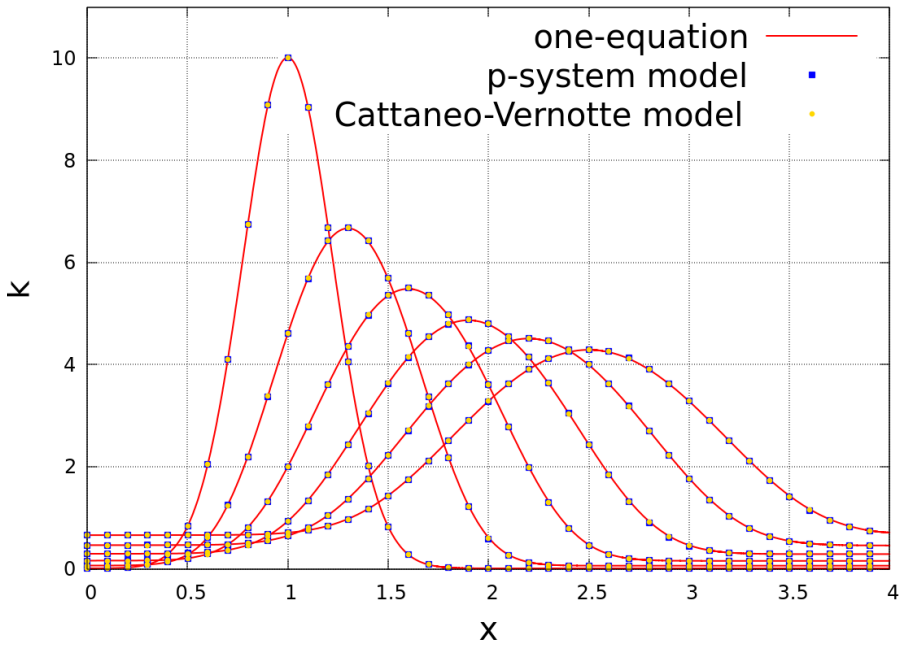

Figure 8.1: Numerical solutions of Prandtl's one-equation model and the equivalent hyperbolic-relaxation forms at $t = 0.1\,\mathrm{s}$, $0.2\,\mathrm{s}$, $0.3\,\mathrm{s}$, $0.4\,\mathrm{s}$ and $0.5\,\mathrm{s}$

Investigation of the relaxation time for the one-dimensional form

Until now, the specific value of the relaxation time, τ_k, has not been discussed. According to the asymptotic analysis, one notes that the hyperbolic-relaxation systems exhibit diffusion behaviour in the limit of small relaxation time. But, some questions arise—how small does the relaxation time have to be? Does the formulation error caused by the velocity variable affect the selection of relaxation time? Is the value equally applicable in the form of higher spacial dimensions?

In order to determine the appropriate limit of acceptable relaxation time, several values of τ_k are tested here. The above mentioned initial-value problem is solved by the hyperbolic-relaxation systems with $\tau_k = 1 \times 10^{-1}\,\mathrm{s}$, $1 \times 10^{-2}\,\mathrm{s}$, $1 \times 10^{-3}\,\mathrm{s}$ and $1 \times 10^{-4}\,\mathrm{s}$. Again, the numerical solutions of the original one-equation model and the hyperbolic-relaxation forms at $t = 0.2\,\mathrm{s}$, $0.4\,\mathrm{s}$, $0.6\,\mathrm{s}$, $0.8\,\mathrm{s}$ and $1.0\,\mathrm{s}$ are plotted in Figs. 8.2.

With different choices of relaxation time, the solutions exhibits different levels of equivalence between the hyperbolic-relaxation models, but, in general, they follow the same trend of equivalence. One notices that, for smaller values of τ_k, the agreement with the original model is better. Obviously, in the case of $\tau_k = 1 \times 10^{-1}\,\mathrm{s}$, the solutions of both hyperbolic-

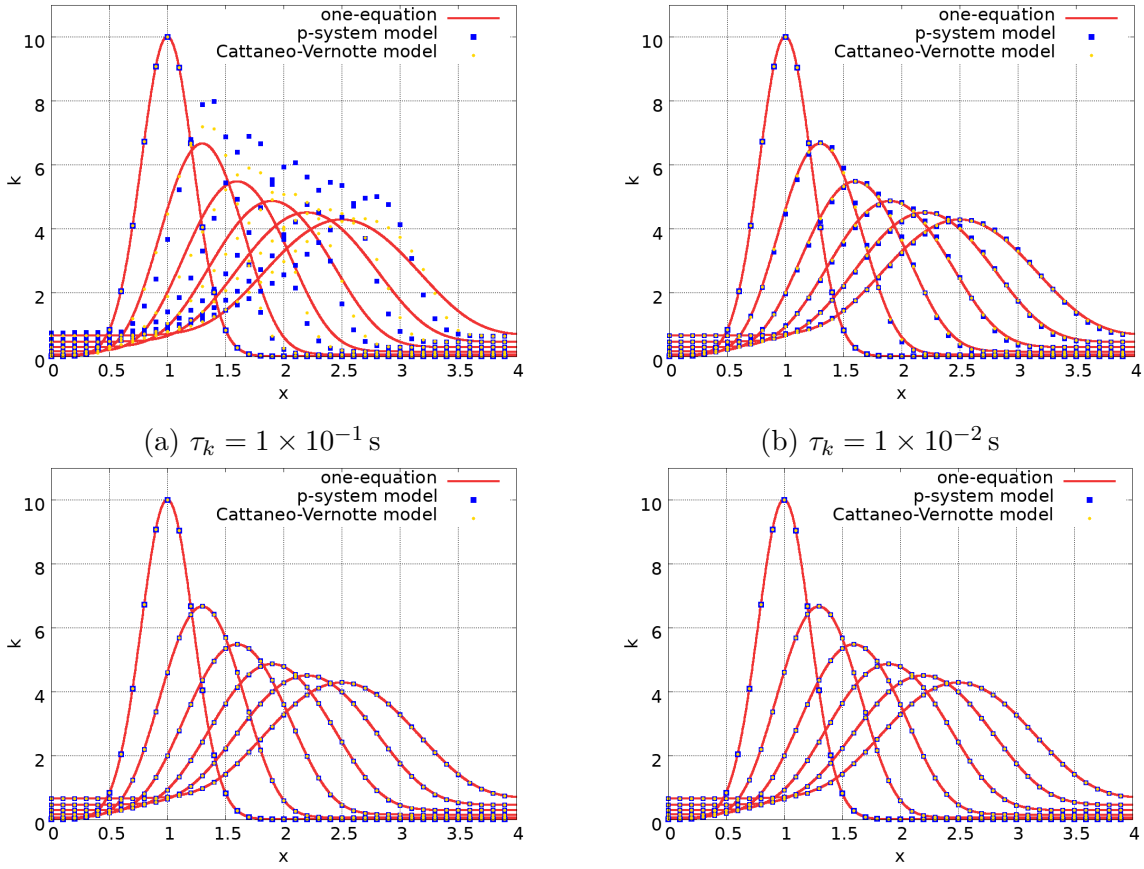

(a) $\tau_k = 1 \times 10^{-1}\,\mathrm{s}$

(b) $\tau_k = 1 \times 10^{-2}\,\mathrm{s}$

(c) $\tau_k = 1 \times 10^{-3}\,\mathrm{s}$

(d) $\tau_k = 1 \times 10^{-4}\,\mathrm{s}$

Figure 8.2: Numerical solutions of the one-dimensional p-system and Cattaneo-Vernotte type hyperbolic-relaxation Prandtl's one-equation model (constant velocity) with multiple choices of τ_k at $t = 0.2\,\mathrm{s}$, $0.4\,\mathrm{s}$, $0.6\,\mathrm{s}$, $0.8\,\mathrm{s}$ and $1.0\,\mathrm{s}$

relaxation systems disagree with the reference solutions. However, when $\tau_k = 1 \times 10^{-2}\,\mathrm{s}$, the solutions start to match quite well, and, in the case of $\tau_k = 1 \times 10^{-3}\,\mathrm{s}$ and $\tau_k = 1 \times 10^{-4}\,\mathrm{s}$ the solutions of both models match the reference solutions almost perfectly. To conclude, for the one-dimensional hyperbolic-relaxation systems, $\tau_k \leqslant 1 \times 10^{-3}\,\mathrm{s}$ is sufficient to provide equivalent solution to the original model for the considered test case.

The above numerical tests give a good baseline for selecting the appropriate relaxation time when the velocity field remains unchanged. In most practical problems, the velocity can be a complicated function dependent on time and space. As discussed in Section 2.1.3, the time and space dependent velocity changes the asymptotic form of the p-system type hyperbolic-relaxation system by adding an extra formulation error. Theoretically, the effect of this error can be neglected when the small relaxation time is selected. Therefore, it is also important to check if the selected relaxation time, in the case of constant velocity, is small enough to suppress the effect of such a formulation error. The study can be done by investigating the solutions of the same initial-value problem, but with variable velocity field.

In this test, instead of using a constant velocity, a new variable velocity is defined by a wave function, which is time and space dependent. The velocity function is given as

$$\bar{u}_x\,(x,t) = a\;x\;\sin\left(k\;x\;t - w\;t\right) + e\,, \tag{8.4}$$

where the value of the parameters that partially control the amplitude, frequency and phase shift are chosen as

$$a = 0.2\,\mathrm{s}^{-1}\,, \quad k = 4.0\,\mathrm{m}^{-1}\mathrm{s}^{-1}\,, \quad w = 8.0\,\mathrm{s}^{-1}\,, \quad e = 1.5\,\mathrm{m/s}\,. \tag{8.5}$$

The aim is to define a velocity function whose temporal and spatial gradient is significant, so that the corresponding contribution on the extra formulation error is remarkable. In this situation, the baseline of the safer relaxation time can be found, whose value should also be applicable to the situation with lower formulation error caused by the variable velocity. The defined variable velocity is plotted at instants $t = 0.2\,\mathrm{s}$, $0.4\,\mathrm{s}$, $0.6\,\mathrm{s}$, $0.8\,\mathrm{s}$ and $1.0\,\mathrm{s}$ in Fig. 8.3.

The same choice of relaxation times $\tau_k = 1 \times 10^{-1}\,\mathrm{s}$, $1 \times 10^{-2}\,\mathrm{s}$, $1 \times 10^{-3}\,\mathrm{s}$ and $1 \times 10^{-4}\,\mathrm{s}$ is used for the tests. The reference solutions and the solutions of the equivalent hyperbolic-relaxation systems are plotted in the set of Figs. 8.4.

As expected, a similar trend of equivalence can be observed: with the smaller relaxation time the solution of any types of hyperbolic-relaxation forms agrees better with the solution

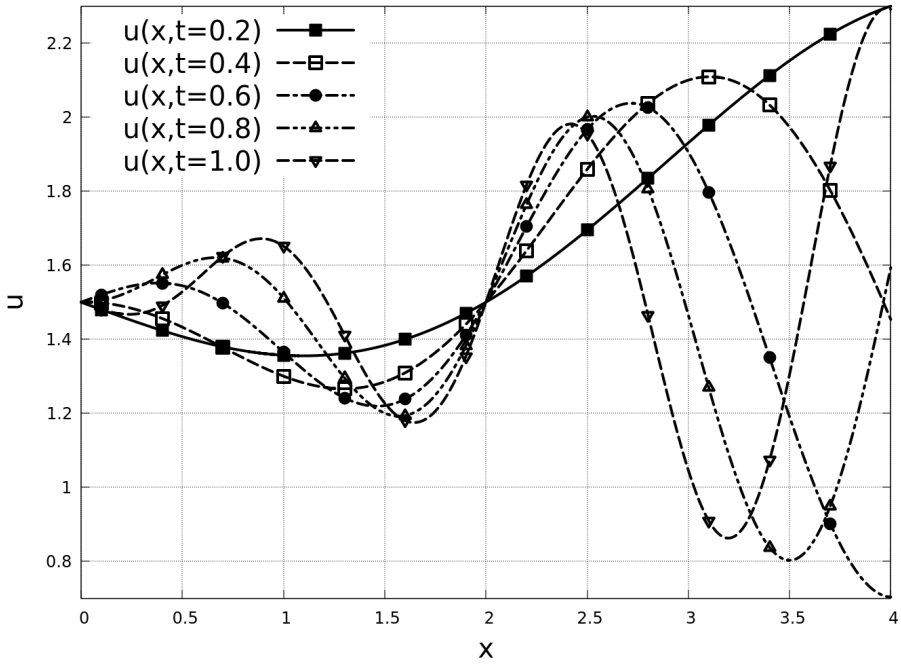

Figure 8.3: Variable velocity, $\bar{u}_x$, at $t = 0.2\,\text{s}$, $0.4\,\text{s}$, $0.6\,\text{s}$, $0.8\,\text{s}$ and $1.0\,\text{s}$

of the original equation. As shown, the solutions with $\tau_k = 1\times10^{-3}\,\text{s}$ still match the original equation very well, in spite of the presence of an added formulation error. This illustrates that the value of the relaxation time, $\tau_k = 1 \times 10^{-3}\,\text{s}$, is sufficiently small that the effect of total formulation error from the one-dimensional hyperbolic-relaxation forms can be neglected. To conclude, this value can be considered as an appropriate reference value of the relaxation time for the other similar one-dimensional applications.

It is worth remembering, the asymptotic form of p-system type hyperbolic-relaxation systems is derived based on the assumption that the deviation ψ_{i1} is small and its time and space derivatives are negligible. If the derivative terms of ψ_{i1} remain in the asymptotic derivation, correlations of these terms will occur in the final asymptotic form and will multiply τ_k. Thus, as long as τ_k is sufficiently small, the effect of those correlations is negligible. For higher spacial dimensions, more correlations of ψ_{i1} and cross derivatives exist; it is therefore expected that a smaller value of this relaxation time may be required in the multi-dimensional setting. This is investigated in Section 8.3.1.

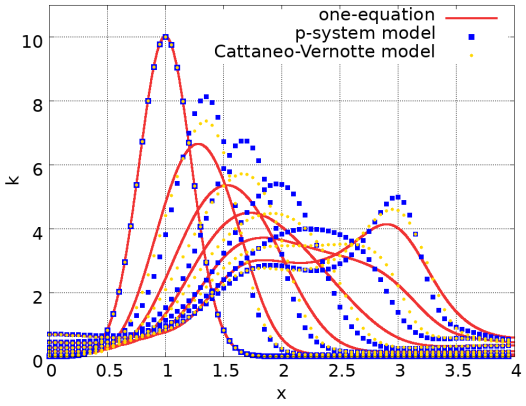

(a) $\tau_k = 1 \times 10^{-1}\,\mathrm{s}$

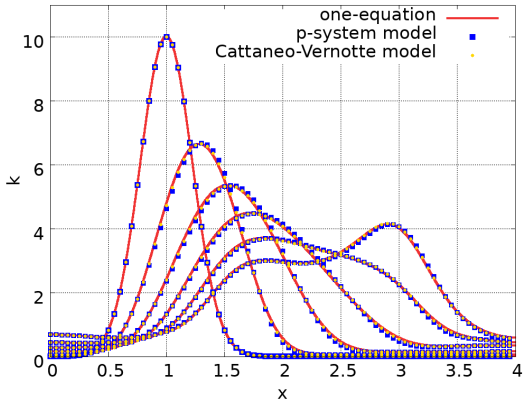

(b) $\tau_k = 1 \times 10^{-2}\,\mathrm{s}$

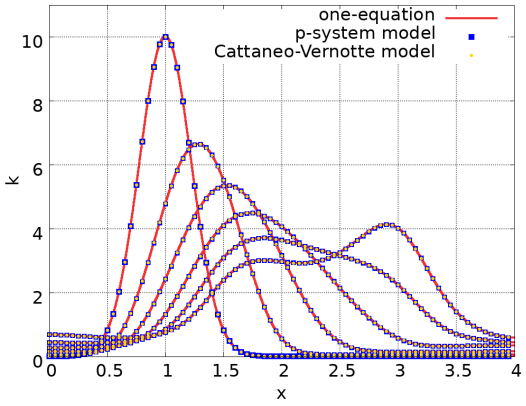

(c) $\tau_k = 1 \times 10^{-3}\,\mathrm{s}$

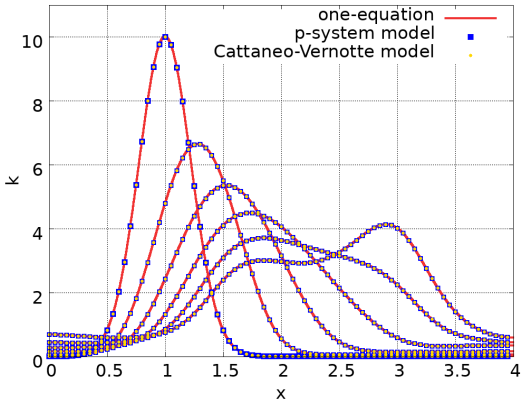

(d) $\tau_k = 1 \times 10^{-4}\,\mathrm{s}$

Figure 8.4: Numerical solutions of one-dimensional p-system and Cattaneo-Vernotte type hyperbolic-relaxation Prandtl's one-equation model (variable velocity) with multiple choices of τ_k at $t = 0.2\,\mathrm{s}$, $0.4\,\mathrm{s}$, $0.6\,\mathrm{s}$, $0.8\,\mathrm{s}$ and $1.0\,\mathrm{s}$

Table 8.2: Numerical setup for the one-dimensional standard k-ϵ model

$\bar{u}_x$	ν	$\bar{t}_{ij}\ \bar{t}_{ij}$	l	C_μ	$C_{\epsilon 1}$	$C_{\epsilon 2}$	σ_k	σ_ϵ
$1.5\,\mathrm{m/s}$	$0.05\,\mathrm{m^2/s}$	$1.0\,\mathrm{kg^2/m^2s^4}$	$0.03\,\mathrm{m}$	0.01	2.0	0.01	1.0	5.0

8.2.2 Two-Equation Models and the Hyperbolic-Relaxation Versions

In this section, similar one-dimensional initial-value problems are solved by the two-equation models and their equivalent hyperbolic-relaxation forms. As discussed, only the Cattaneo-Vernotte type hyperbolic-relaxation systems are derived and tested for the two-equation models in this project.

A similar one-dimensional Gaussian pulse is selected as the initial condition of the turbulence kinetic energy for both two-equation models, which is defined by function

$$k\left(x,0\right)=\left\{2\ \exp\left[-\frac{\left(x-x_0\right)^2}{\kappa}\right]+0.01\right\}\ \ \mathrm{m^2/s^2}\,, \tag{8.6}$$

where $x_0=1\,\mathrm{m}$ and $\kappa=0.1\,\mathrm{m^2}$. The computation is carried out within the same computational domain, and according to the mesh convergence study, the same grid resolution as previously introduced is used. The same numerical methods are applied to solve the original and hyperbolic-relaxation models.

In the first numerical test, the standard k-ϵ model, Eqs. (6.5)–(6.6), and the Cattaneo-Vernotte type hyperbolic-relaxation version, Eqs. (6.10)–(6.13), are demonstrated to be equivalent. The initial dissipation rate, ϵ, is defined by the function

$$\epsilon=C_\mu\frac{k^{3/2}}{l}\,. \tag{8.7}$$

The selection of parameter values for the computation is summarized in Table 8.2. The solutions of k and ϵ at $t=0.2\,\mathrm{s}$, $0.4\,\mathrm{s}$, $0.6\,\mathrm{s}$, $0.8\,\mathrm{s}$ and $1.0\,\mathrm{s}$ are shown in Figs. 8.5

In the second numerical test, the Wilcox k-ω model, Eqs. (6.18)–(6.19), and the Cattaneo-Vernotte type hyperbolic-relaxation systems, Eqs. (6.20)–(6.23), are demonstrated to be equivalent. The initial specific dissipation rate, ω, is defined by function

$$\omega=\frac{\sqrt{k}}{l}\,. \tag{8.8}$$

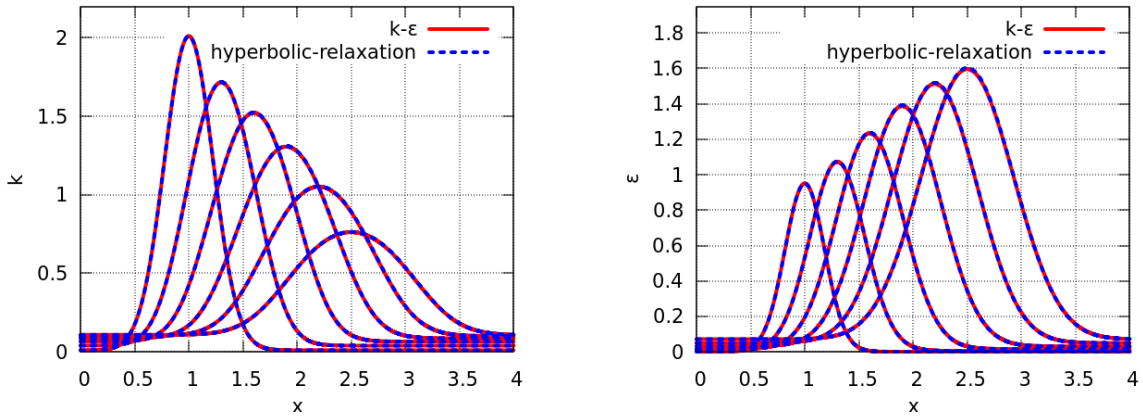

(a) k (b) ϵ

Figure 8.5: Numerical solutions of the standard k-ϵ model and the equivalent hyperbolic-relaxation form at $t = 0.2\,\mathrm{s}$, $0.4\,\mathrm{s}$, $0.6\,\mathrm{s}$, $0.8\,\mathrm{s}$ and $1.0\,\mathrm{s}$

Table 8.3: Numerical setup for the one-dimensional Wilcox k-ω model

$\bar{u}_x$	ν	$\bar{t}_{ij}\ \bar{t}_{ij}$	l	γ	β	β_*	σ_k	σ_ω
$1.5\,\mathrm{m/s}$	$0.05\,\mathrm{m^2/s}$	$0.002\,\mathrm{kg^2/m^2s^4}$	$3.0\,\mathrm{m}$	0.5	0.1	0.1	0.01	0.01

The selection of parameter values for the computation is summarized in Table 8.3. Again, the solutions of k and ω at $t = 0.2\,\mathrm{s}$, $0.4\,\mathrm{s}$, $0.6\,\mathrm{s}$, $0.8\,\mathrm{s}$ and $1.0\,\mathrm{s}$ are sampled and shown in Figs. 8.6.

According to the study in the previous case, the constant value, $1 \times 10^{-3}\,\mathrm{s}$, is chosen for the relaxation times, τ_k, τ_ϵ and τ_ω. Good agreement between the solutions can be observed, which again demonstrates the equivalence between the original model and corresponding hyperbolic-relaxation system in the selected relaxation limit.

8.3 Equivalence between the Two-Dimensional Turbulence Models and the Hyperbolic-Relaxation Forms

In this section, similar two-dimensional initial-value problems are designed for the one-equation and two-equation models. The goal is to further verify the equivalence between

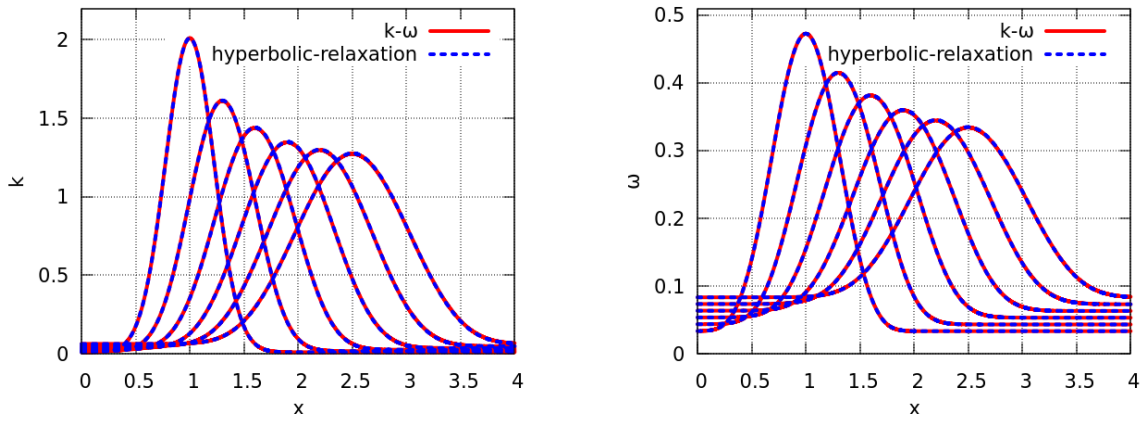

(a) k (b) ω

Figure 8.6: Numerical solutions of Wilcox k-ω model and the equivalent hyperbolic-relaxation form at $t = 0.2\,\mathrm{s}$, $0.4\,\mathrm{s}$, $0.6\,\mathrm{s}$, $0.8\,\mathrm{s}$ and $1.0\,\mathrm{s}$

the original turbulence models and corresponding hyperbolic-relaxation systems in two-dimensional form. A study of the relaxation limit is also presented, which shows that a different value of the appropriate relaxation time is required for the two-dimensional form of the p-system type hyperbolic-relaxation model.

8.3.1 Prandtl's One-Equation Model and the Hyperbolic-Relaxation Versions

This numerical experiment aims to show that the two-dimensional form of the hyperbolic-relaxation systems, is equivalent to the original Prandtl's one-equation model as well. Similarly, all models are applied to solve the same initial-value problem within a two-dimensional square computational domain, $x, y \in [0\ ,\ 2]\,\mathrm{m}$. This computational domain is decomposed into a structured grid, which consists of the same number of cells in each direction. The same numerical method as introduced is used. To determine resolution requirements, the models are again solved on meshes of different resolutions, (1000×1000) and (2000×2000). For the original model, the maximum difference between final solutions with different grid resolutions, in magnitude, is less than 1×10^{-3}, therefore, the solution on the former grid is considered accurate and this resolution is used for further computations. For the hyperbolic-relaxation system, the maximum solution difference between the same choice of grids, in magnitude, is less than 5×10^{-3}, therefore, the solutions on grids of (1000×1000) are used going forward.

Table 8.4: Numerical setup for the two-dimensional one-equation model

$\bar{u}_x$	$\bar{u}_y$	ν	l	$\bar{t}_{ij}\ \bar{t}_{ij}$	C_d
$1.5\,\mathrm{m/s}$	$1.5\,\mathrm{m/s}$	$0.001\,\mathrm{m^2/s}$	$0.003\,\mathrm{m}$	$1.0\,\mathrm{kg^2/m^2s^4}$	0.005

A two-dimensional Gaussian pulse is chosen as the initial condition, with its centre located at the coordinate, $(x_0\ ,\ y_0)$. It is transported diagonally, while it undergoes production, dissipation and diffusion. The initial Gaussian pulse of turbulent kinetic energy is defined by the function

$$k\,(x,y,0) = \left\{ 10\ \exp\left[-\frac{(x-x_0)^2 + (y-y_0)^2}{\kappa} \right] + 0.01 \right\}\ \mathrm{m^2/s^2}\,, \tag{8.9}$$

where $x_0 = 0.5\,\mathrm{m}$, $y_0 = 0.5\,\mathrm{m}$, $\kappa = 0.02\,\mathrm{m^2}$, and the small value $0.01\,\mathrm{m^2/s^2}$ is again added to guarantee non-zero initial distribution within the entire computational domain. The variables ψ_i are initialized as $\bar{u}_i k$ and $\frac{\partial k}{\partial x_i}$ in the p-system and Cattaneo-Vernotte type model respectively.

Investigation of the relaxation time for two-dimensional form

The selection of parameter values for the numerical test is collected in Table 8.4. The contour plot of the initial condition and the numerical solutions of the original model at $t = 0.1\,\mathrm{s}$, $0.3\,\mathrm{s}$ and $0.5\,\mathrm{s}$ are shown in Figs. 8.7. It is clear to see that the initial concentration moves with the background flow over the diagonal direction, while it dissipates and diffuses with a finite rate. The solutions of two choices of the relaxation time, $\tau_k = 1 \times 10^{-3}\,\mathrm{s}$ and $1 \times 10^{-4}\,\mathrm{s}$, are compared. The solution's contour plots of the p-system type and Cattaneo-Vernotte type hyperbolic-relaxation systems at $t = 0.5\,\mathrm{s}$ are shown in Figs. 8.8 and Figs. 8.10. The cell-wise solution data over the translating direction are presented in Figs. 8.9 and Figs. 8.11.

Akin to the one-dimensional model, a similar trend of equivalence can be clearly investigated. However, for the p-system type hyperbolic-relaxation model, the value of relaxation time that gives acceptable equivalence in one-dimensional form no longer provides the same agreement in two-dimensional form. As shown in Figs. 8.8 and 8.9, the solutions of the p-system type model with relaxation time, $\tau_k = 1 \times 10^{-3}\,\mathrm{s}$, show obvious deviations from the reference solutions of the original model, especially at instant $t = 0.5\,\mathrm{s}$. The pulse

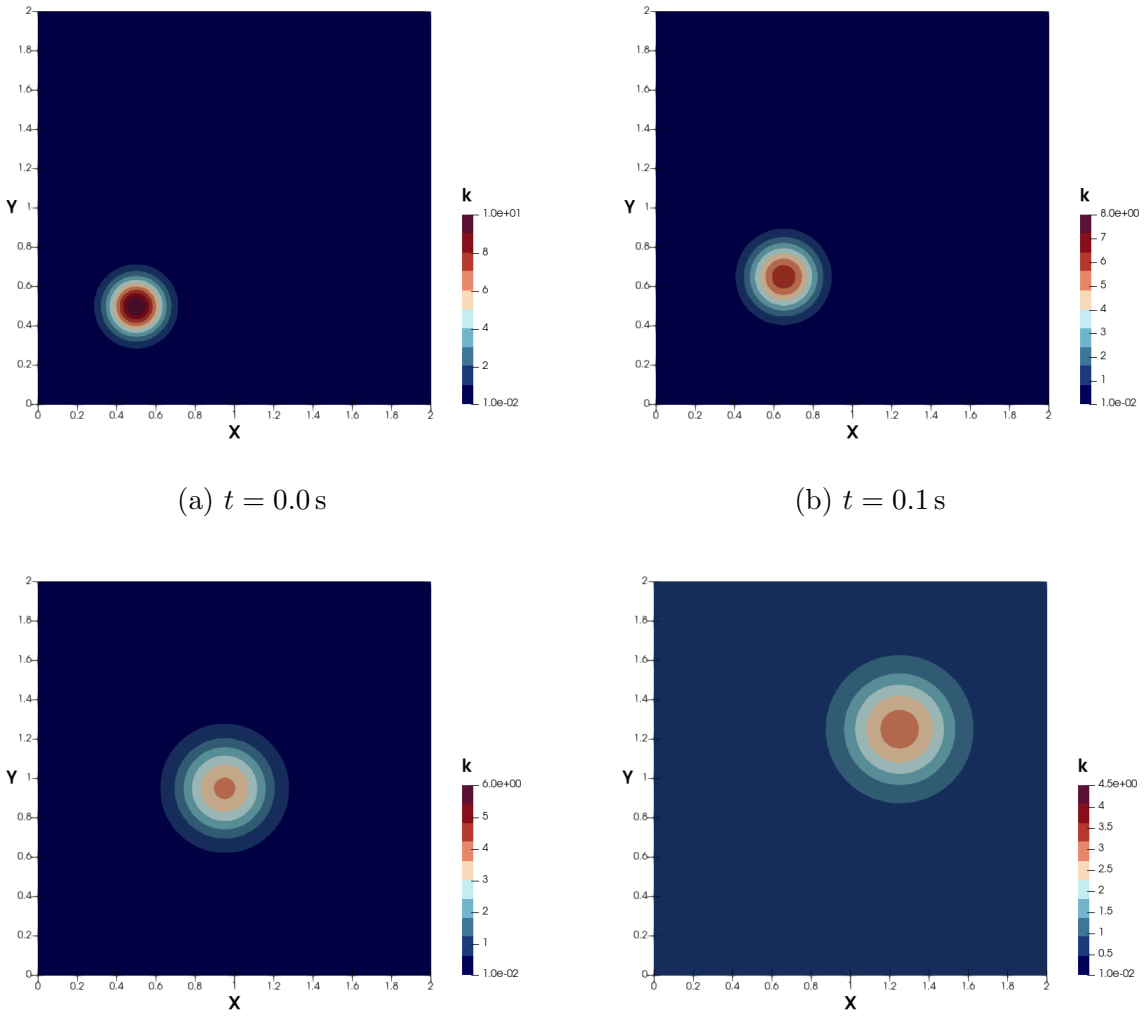

(a) $t = 0.0\,\mathrm{s}$

(b) $t = 0.1\,\mathrm{s}$

(c) $t = 0.3\,\mathrm{s}$

(d) $t = 0.5\,\mathrm{s}$

Figure 8.7: Contour plot of initial condition and reference solutions of k at $t = 0.1\,\mathrm{s}$, $0.3\,\mathrm{s}$ and $0.5\,\mathrm{s}$ for Prandtl's one-equation model

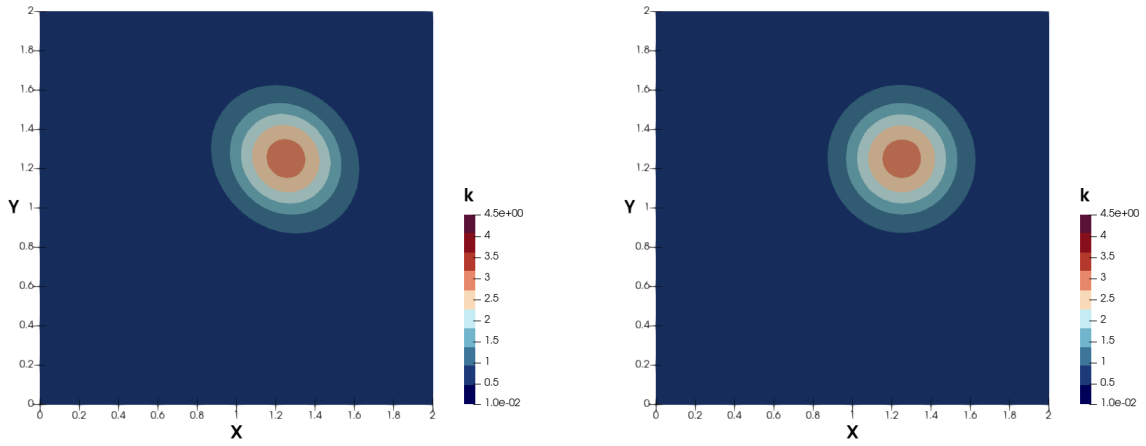

(a) $\tau_k = 1 \times 10^{-3}\,\mathrm{s}$ (b) $\tau_k = 1 \times 10^{-4}\,\mathrm{s}$

Figure 8.8: Two-dimensional numerical solutions of the p-system type hyperbolic-relaxation Prandtl's one-equation model at $t = 0.5\,\mathrm{s}$ for $\tau_k = 1 \times 10^{-3}\,\mathrm{s}$ and $1 \times 10^{-4}\,\mathrm{s}$

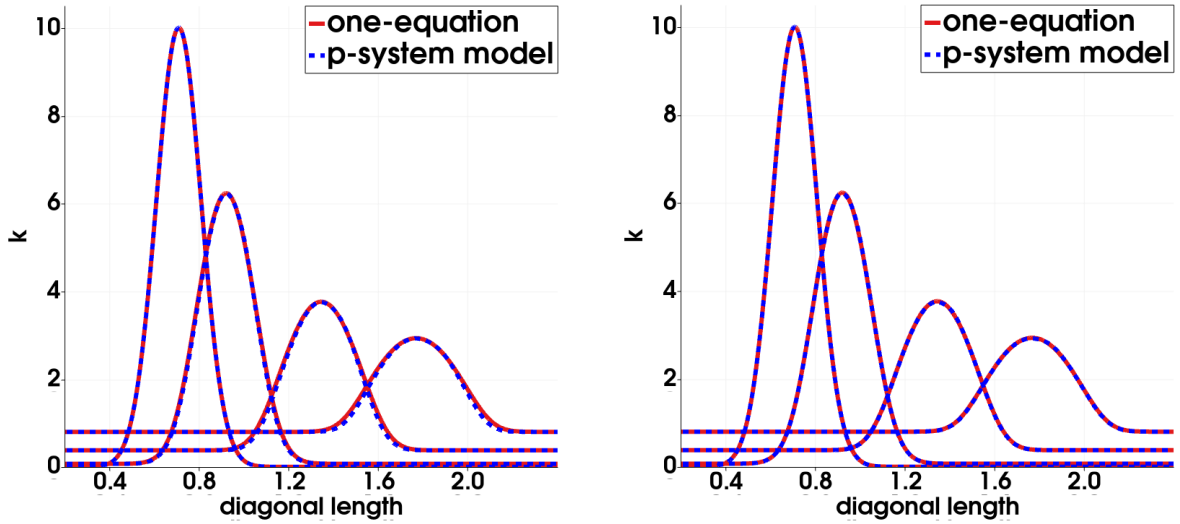

(a) $\tau_k = 1 \times 10^{-3}\,\mathrm{s}$ (b) $\tau_k = 1 \times 10^{-4}\,\mathrm{s}$

Figure 8.9: Two-dimensional numerical solutions of the p-system type hyperbolic-relaxation Prandtl's one-equation model over the translational direction for $\tau_k = 1 \times 10^{-3}\,\mathrm{s}$ and $1 \times 10^{-4}\,\mathrm{s}$

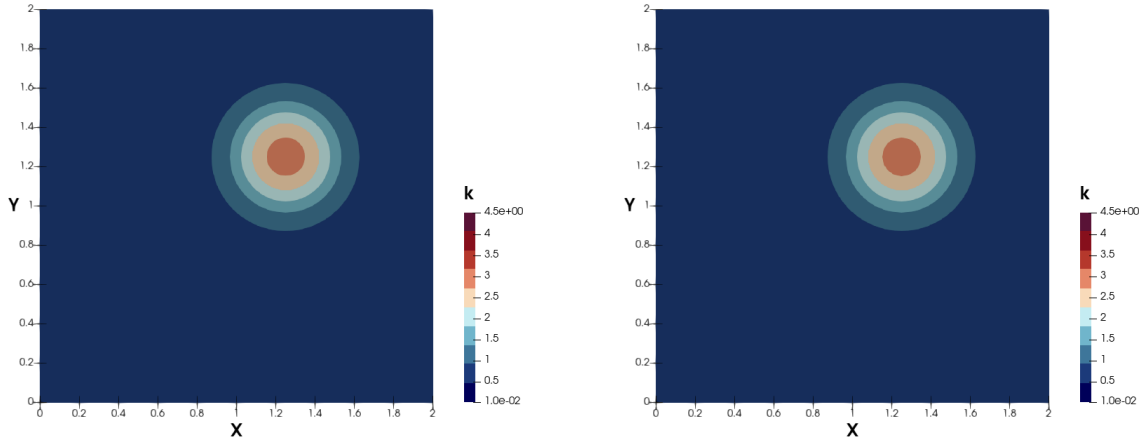

(a) $\tau_k = 1 \times 10^{-3}\,\mathrm{s}$ (b) $\tau_k = 1 \times 10^{-4}\,\mathrm{s}$

Figure 8.10: Two-dimensional numerical solutions of the Cattaneo-Vernotte type hyperbolic-relaxation Prandtl's one-equation model at $t = 0.5\,\mathrm{s}$ for $\tau_k = 1 \times 10^{-3}\,\mathrm{s}$ and $1 \times 10^{-4}\,\mathrm{s}$

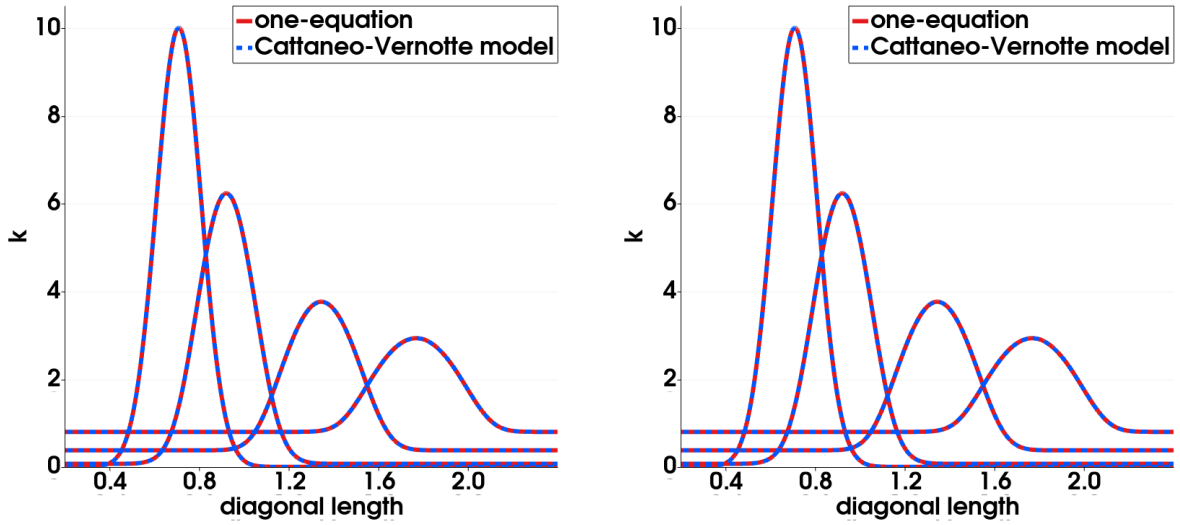

(a) $\tau_k = 1 \times 10^{-3}\,\mathrm{s}$ (b) $\tau_k = 1 \times 10^{-4}\,\mathrm{s}$

Figure 8.11: Two-dimensional numerical solutions of the Cattaneo-Vernotte type hyperbolic-relaxation Prandtl's one-equation model over the translational direction for $\tau_k = 1 \times 10^{-3}\,\mathrm{s}$ and $1 \times 10^{-4}\,\mathrm{s}$

undergoes less diffusion over the diagonal direction even though the constant isotropic diffusivity is specified for the computation. An elliptic shape of the pulse is therefore formed. This is likely due to the presence of more correlations between the various deviations that occur in the final asymptotic form of the hyperbolic-relaxation model—as discussed in the previous section. In addition to this, various spurious cross-derivative terms present in the multi-dimensional case, as seen in Eq. (5.27). The value of relaxation time, τ_k, also serves to suppress the influence of these terms. Therefore, to achieve the acceptable equivalence a smaller value of τ_k is desired in the two-dimensional form of the p-system type model. Based on the existing numerical results, $\tau_k = 1 \times 10^{-4}\,\mathrm{s}$ is considered appropriate for the two-dimensional p-system type hyperbolic-relaxation model for this problem, when the velocity vector is constant, as it provides an equivalent solution to that of the original model.

The solutions of the two-dimensional Cattaneo-Vernotte type hyperbolic-relaxation model with relaxation time, $\tau_k = 1 \times 10^{-3}\,\mathrm{s}$, show acceptable equivalence, as it does for the one-dimensional form. This is because the additional equations in such a model, are responsible for the relaxation of the new variables independently. The formulation of the equations in higher dimensional form does not contribute to any extra formulation error. In the other words, the asymptotic form of the Cattaneo-Vernotte type hyperbolic-relaxation equation has the same general structure in the different dimensions. To conclude, the relaxation time, $\tau_k = 1 \times 10^{-3}\,\mathrm{s}$, can be treated as a proper limit for the two-dimensional form of the Cattaneo-Vernotte type hyperbolic-relaxation model, in the case of constant velocity.

At this point, the selected relaxation values can be considered as appropriate only for the situation with constant velocity. To investigate the proper value of relaxation time for more general situation, where the velocity is a time and space dependent variable, more investigations must be done. Similar to the one-dimensional case, a function of velocity vector is designed for the same two-dimensional initial value problem. It aims to determine if the selected relaxation values are still valid for variable velocity in the two-dimensional form of the hyperbolic-relaxation models. The velocity functions are again defined by wave function as

$$\bar{u}_i\,(x_i, t) = a\; x_i \sin\left(k\; x_i\; t - w\; t\right) + e\,, \tag{8.10}$$

where the value of the parameters are chosen as

$$a = 0.2\,\mathrm{s}^{-1}\,, \quad k = 9.0\,\mathrm{m}^{-1}\mathrm{s}^{-1}\,, \quad w = 7.0\,\mathrm{s}^{-1}\,, \quad e = 1.5\,\mathrm{m/s}\,. \tag{8.11}$$

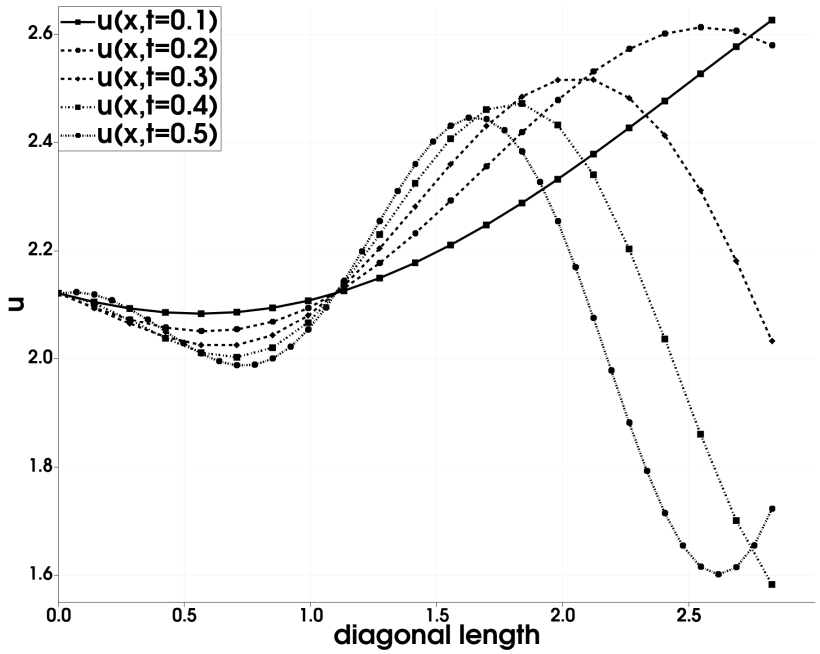

Figure 8.12: Variable velocity, $\bar{u}$, over the diagonal direction at $t = 0.1\,\mathrm{s}$, $0.2\,\mathrm{s}$, $0.3\,\mathrm{s}$, $0.4\,\mathrm{s}$ and $0.5\,\mathrm{s}$

The defined velocity over the diagonal direction at $t = 0.2\,\mathrm{s}$, $0.4\,\mathrm{s}$, $0.6\,\mathrm{s}$, $0.8\,\mathrm{s}$ and $1.0\,\mathrm{s}$ is plotted in Fig. 8.12, which shows the velocity variance over time and space.

In this test, only the selected relaxation values from the previous tests are studied, which includes $\tau_k = 1 \times 10^{-4}\,\mathrm{s}$ and $1 \times 10^{-3}\,\mathrm{s}$ for the p-system and Cattaneo-Vernotte type model respectively. The solution data of the original equation and hyperbolic-relaxation versions over the diagonal direction are again sampled and plotted in Fig. 8.13.

Akin to the one-dimensional case, the selected relaxation values, which are appropriate for the test with constant velocity vector, also provide acceptable equivalent solutions with variable velocity vector. In other words, the effect of additional formulation error caused by the variable velocity can be suppressed by the selected relaxation time. To summarize, for the two-dimensional form, the relaxation values, $\tau_k = 1 \times 10^{-4}\,\mathrm{s}$ and $1 \times 10^{-3}\,\mathrm{s}$, are considered as the appropriate limit for the p-system and Cattaneo-Vernotte type hyperbolic-relaxation model respectively. These values are further used for the other two-dimensional tests and validation cases.

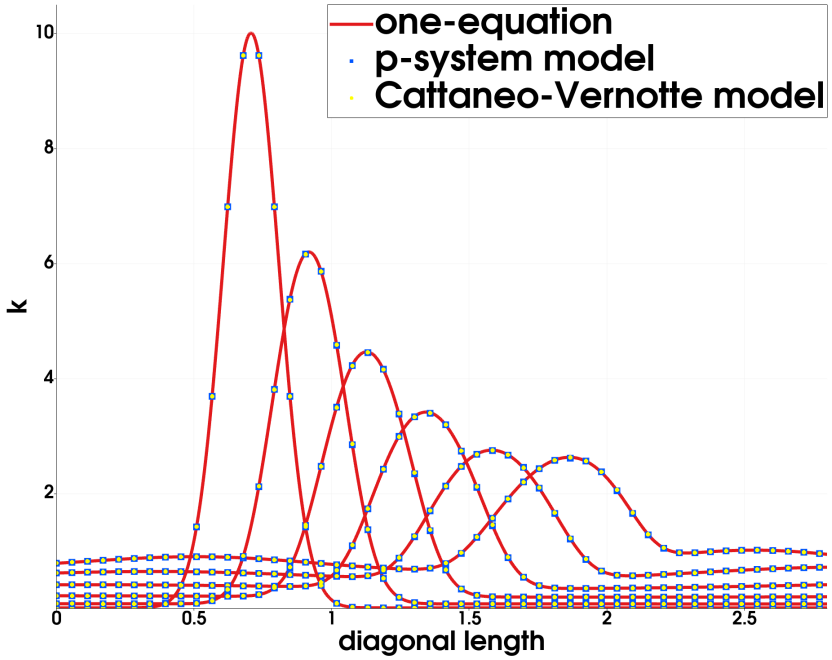

Figure 8.13: Two-dimensional numerical solutions of the p-system type ($\tau_k = 1 \times 10^{-4}\,\mathrm{s}$) and Cattaneo-Vernotte type ($\tau_k = 1 \times 10^{-3}\,\mathrm{s}$) hyperbolic-relaxation Prandtl's one-equation model with variable velocity over the translational direction

Table 8.5: Numerical setup for the two-dimensional standard k-ϵ model

$\bar{u}_x$	$\bar{u}_y$	ν	$\bar{t}_{ij}\ \bar{t}_{ij}$	l	C_μ	$C_{\epsilon 1}$	$C_{\epsilon 2}$	σ_k	σ_ϵ
$1.5\,\mathrm{m/s}$	$1.5\,\mathrm{m/s}$	$0.05\,\mathrm{m^2/s}$	$0.1\,\mathrm{kg^2/m^2s^4}$	$0.02\,\mathrm{m}$	0.01	3.0	0.5	1.0	5.0

Table 8.6: Numerical setup for the two-dimensional Wilcox k-ω model

$\bar{u}_x$	$\bar{u}_y$	ν	$\bar{t}_{ij}\ \bar{t}_{ij}$	l	γ	β	β_*	σ_k	σ_ω
$1.5\,\mathrm{m/s}$	$1.5\,\mathrm{m/s}$	$0.05\,\mathrm{m^2/s}$	$0.001\,\mathrm{kg^2/m^2s^4}$	$3.0\,\mathrm{m}$	0.5	0.1	0.1	0.001	0.001

8.3.2 Two-Equation Models and the Hyperbolic-Relaxation Versions

In this section, the same numerical experiments are carried out for the two-dimensional form of the two-equation models, the standard k-ϵ model and the Wilcox k-ω models. Again, the aim is to show the Cattaneo-Vernotte type hyperbolic-relaxation systems are equivalent to the original two-equation models with the selected relaxation limit. The models are applied to solve a similar initial-value problem within the same two-dimensional computational domain as the one-equation model. Based on the same mesh convergence study, the solutions of grid resolution, (1000×1000), are considered to be representative.

A similar two-dimensional Gaussian pulse is chosen as the initial condition of turbulence kinetic energy at the same location. It is defined by the function

$$k\,(x, y, 0) = \left\{ 2\,\exp\left[-\frac{(x - x_0)^2 + (y - y_0)^2}{\kappa} \right] + 0.01 \right\}\ \mathrm{m^2/s^2}\,, \tag{8.12}$$

where $x_0 = 0.5\,\mathrm{m}$, $y_0 = 0.5\,\mathrm{m}$ and $\kappa = 0.02\,\mathrm{m^2}$. The initial dissipation rate, ϵ, and specific dissipation rate, ω, are defined by the same functions, Eq. (8.7) and Eq. (8.8), respectively. The variables ψ_i and ϕ_i are initialized as $\frac{\partial k}{\partial x_i}$ and $\frac{\partial \epsilon}{\partial x_i}$ or $\frac{\partial \omega}{\partial x_i}$ respectively. The selected values of parameters are summarized in Tables 8.5 and 8.6. Based on the study of the relaxation limit concluded in the previous section, the constant value $1 \times 10^{-3}\,\mathrm{s}$ is used for the relaxation times, τ_k, τ_ϵ and τ_ω.

The contour plot of initial conditions and the numerical solutions of the original model at $t = 0.1\,\mathrm{s}$, $0.3\,\mathrm{s}$ and $0.5\,\mathrm{s}$ are plotted in Figs. 8.14–8.17 for the k-ϵ model, and in Figs. 8.19–

8.22 for the k-ω model. The cell-wise solution data of the original standard k-ϵ model, Wilcox k-ω model and corresponding hyperbolic-relaxation versions over the translational direction are presented in Figs. 8.18 and 8.23 respectively.

Good agreement between the solutions of the original two-equation models and the Cattaneo-Vernotte type hyperbolic-relaxation systems illustrate these models are, in fact, equivalent. It demonstrates again the chosen value of the relaxation times are appropriate for this problem.

8.4 Two-Dimensional Mixing-Layer

The next numerical experiment is designed to simulate a full two-dimensional turbulent plane mixing-layer generated by two separate planar air jets. The experimental measurement was collected by Delville from C.E.A.T. Poitiers in 1995 [17]. This data is commonly used for turbulence-model verification and validation tests.

The wind tunnel for the experimental measurement is designed as shown in Fig. 8.24. Low-turbulence plane air jets are generated by a fan at one side of the wind tunnel, which are further split by a thin flat plate. Head loss filters are placed at one side of the splitting plate to create a velocity difference between the separated flows. Sand paper is used on both sides of the long plate, which allows the boundary layers to be fully turbulent at the trailing edge of the plate. A mixing-layer flow is then created by merging these two air streams with different velocity at the end of the plate. The profile of velocity, $\bar{u}_x$, shear Reynolds-stress, $\overline{u'_x u'_y}$, and turbulence kinetic energy, k are measured at various locations.

According to the geometry of the wind tunnel, a Cartesian coordinate system is built with the origin of the coordinate located at the end of the plate and the flowing direction is defined as the positive direction of x axis. For the present computations, a two-dimensional rectangular computational domain, within $x \in [0\ ,\ 0.3]\,\mathrm{m}$ and $y \in [-0.05\ ,\ 0.05]\,\mathrm{m}$, is built at the end of the plate, where the two air streams just merge. This is shown as the dashed rectangle region in Fig. 8.24. The computational domain is covered by a structured mesh with a resolution of (1500×500).

The measured profile of velocity, $\bar{u}_x$, and Reynolds-stress, $\overline{u'_x u'_x}$, at location $x = 1\,\mathrm{mm}$, are taken as the inlet boundary conditions for the computation, which are plotted in Figs. 8.25. A zero-gradient boundary condition is applied on the top and bottom boundaries, where the air streams maintain constant velocity with top flow velocity, $U_a =$

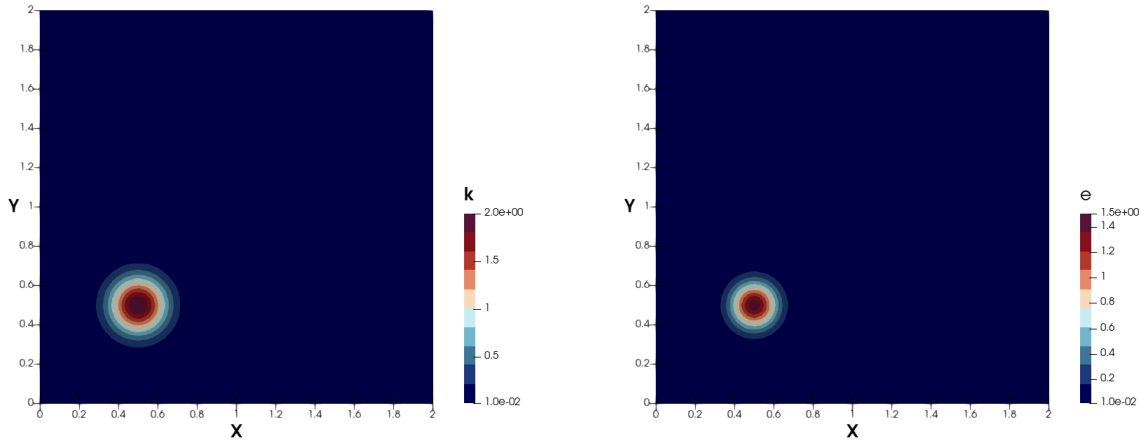

(a) k (b) ϵ

Figure 8.14: Contour plot of initial condition of k and ϵ at $t = 0.0\,\mathrm{s}$

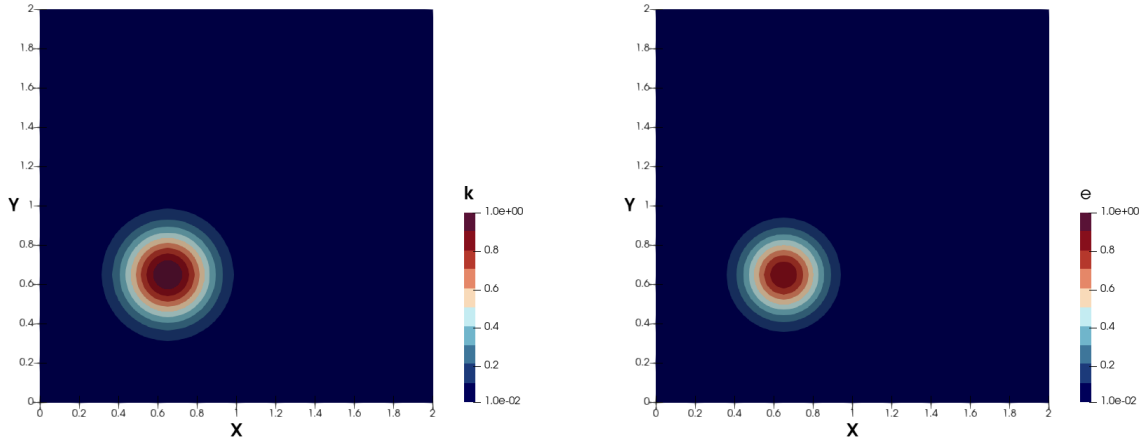

(a) k (b) ϵ

Figure 8.15: Contour plot of reference solution of k and ϵ at $t = 0.1\,\mathrm{s}$

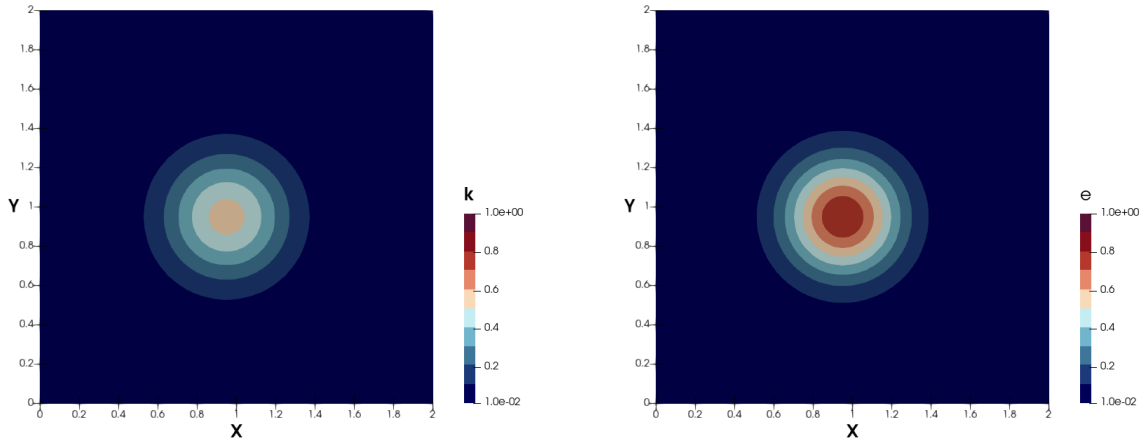

(a) k (b) ϵ

Figure 8.16: Contour plot of reference solution of k and ϵ at $t = 0.3\,\mathrm{s}$

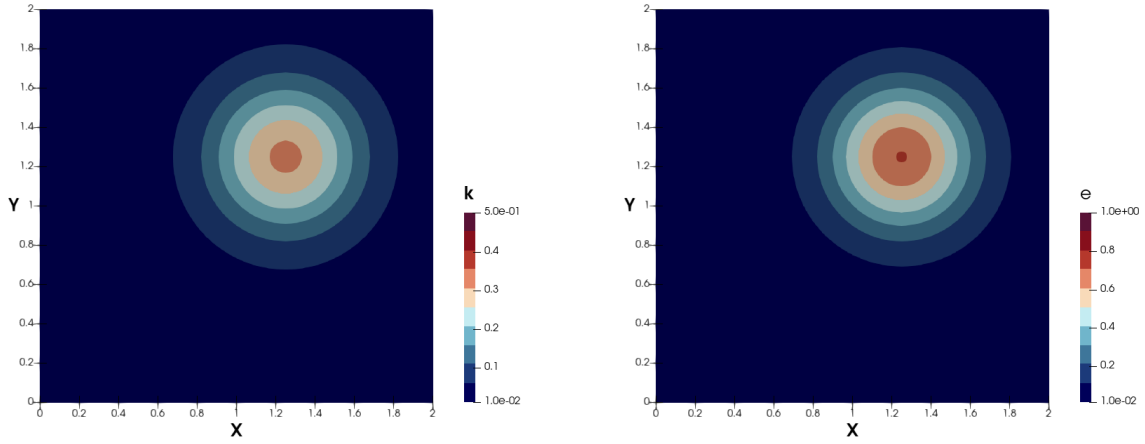

(a) k (b) ϵ

Figure 8.17: Contour plot of reference solution of k and ϵ at $t = 0.5\,\mathrm{s}$

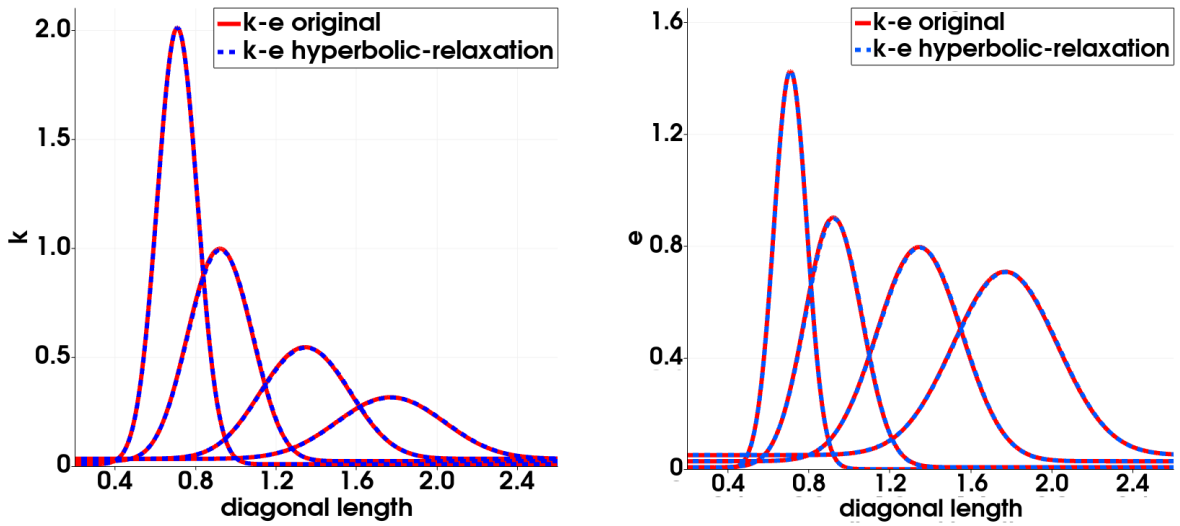

(a) k (b) ϵ

Figure 8.18: Two-dimensional numerical solutions of the hyperbolic-relaxation standard k-ϵ model over the diagonal line

41.69 m/s, and bottom flow velocity, $U_b = 22.51$ m/s. The downstream boundary is treated as an outlet boundary, where the air flow exits. However, due to the flow conditions are unknown at the outlet boundary, zero-gradient boundary condition is used for all conserved variables. The inlet boundary condition is also extruded and taken as the initial condition over the entire computational domain, as shown in Fig. 8.26. To coincide with the experimental environment, where the atmospheric pressure is approximately maintained, a constant atmospheric pressure is taken in this numerical test, $p = 101\,325$ Pa. The mean experimental temperature is kept at $T = 293$ K, therefore, in this test, the initial flow is assumed to be at the same temperature, such that the flow density is $\rho = 1.204\,\mathrm{kg/m^3}$ and viscosity is $\mu = 1.82 \times 10^{-5}$ kg/ms. As discussed, the relaxation time, τ_k, is chosen as 1×10^{-4} s for the p-system type hyperbolic-relaxation Prandtl's one-equation model, and τ_k, τ_ϵ and τ_ω are chosen as 1×10^{-3} s for the Cattaneo-Vernotte type hyperbolic-relaxation two-equation models in this test.

8.4.1 Numerical Approximations by the P-System Type Hyperbolic-Relaxation Prandtl's One-Equation Model

In the Prandtl's one-equation model, the turbulence length scale, l, is a free parameter, which can significantly affect the production, dissipation, and diffusion of turbulence kinetic

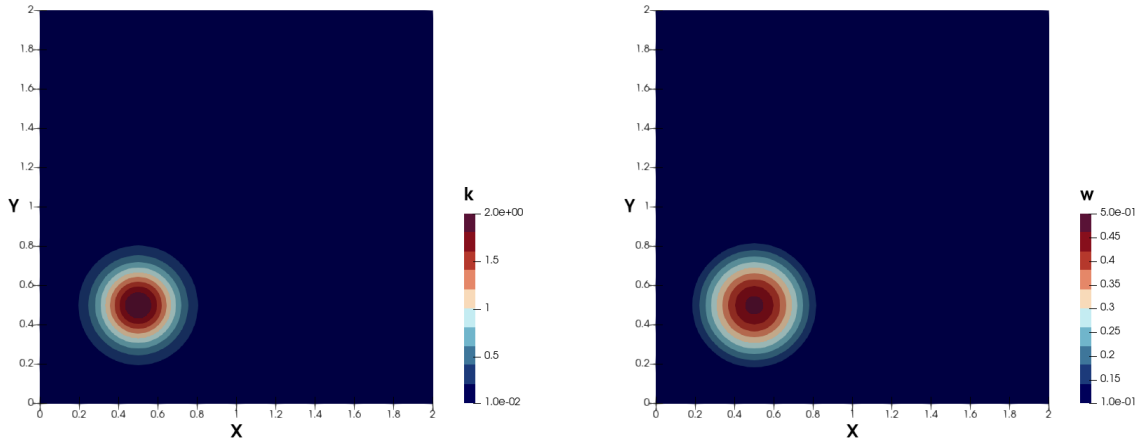

(a) k (b) ω

Figure 8.19: Contour plot of initial condition of k and ω at $t = 0.0\,\mathrm{s}$

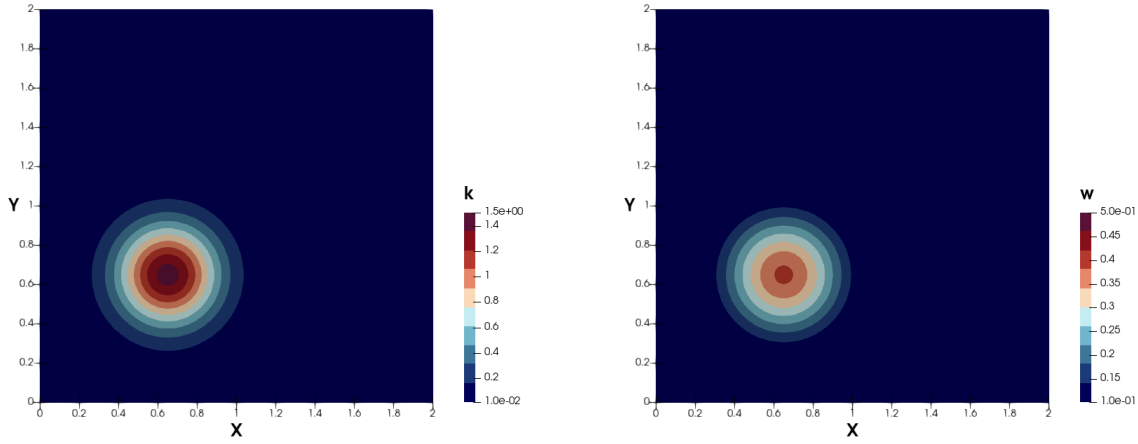

(a) k (b) ω

Figure 8.20: Contour plot of reference solution of k and ω at $t = 0.1\,\mathrm{s}$

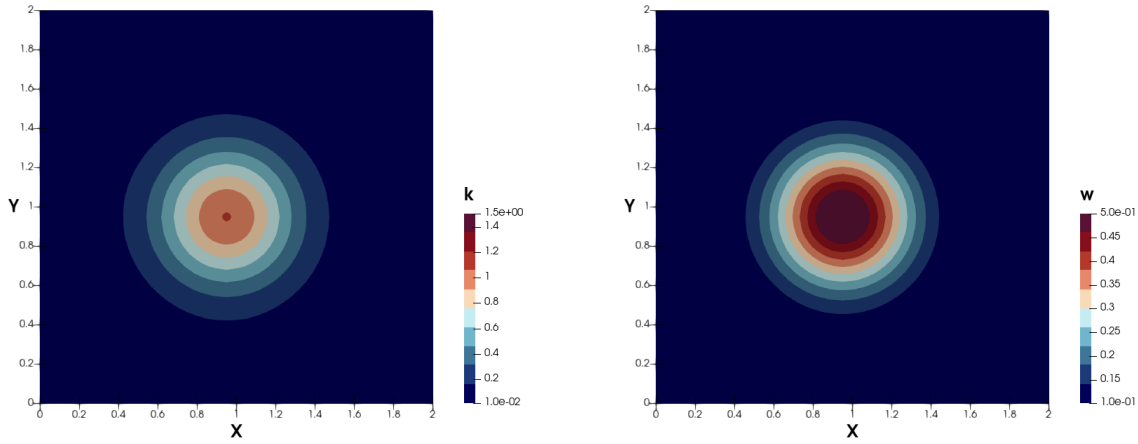

(a) k (b) ω

Figure 8.21: Contour plot of reference solution of k and ω at $t = 0.3\,\mathrm{s}$

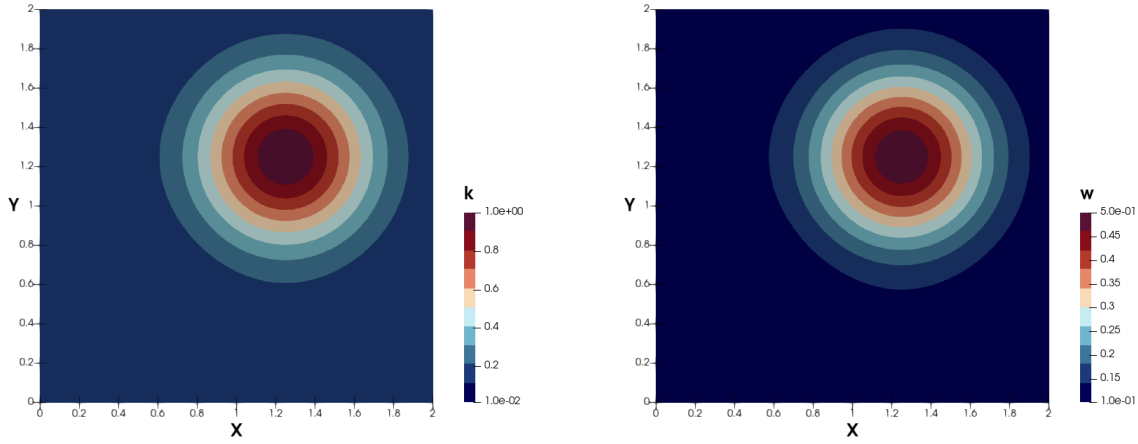

(a) k (b) ω

Figure 8.22: Contour plot of reference solution of k and ω at $t = 0.5\,\mathrm{s}$

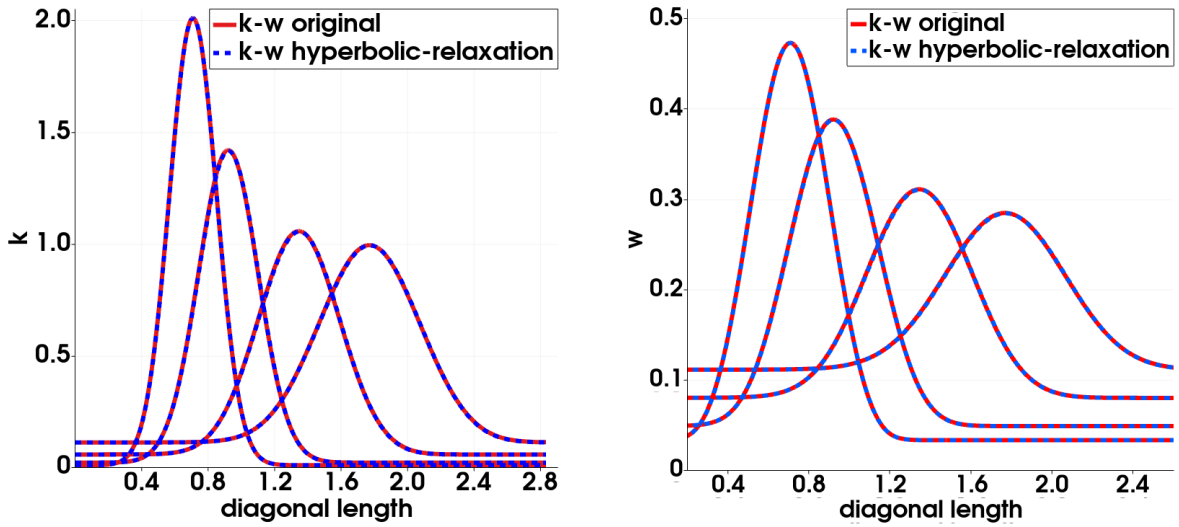

(a) k (b) ω

Figure 8.23: Two-dimensional Numerical solutions of the hyperbolic-relaxation Wilcox k-ω model over the diagonal line

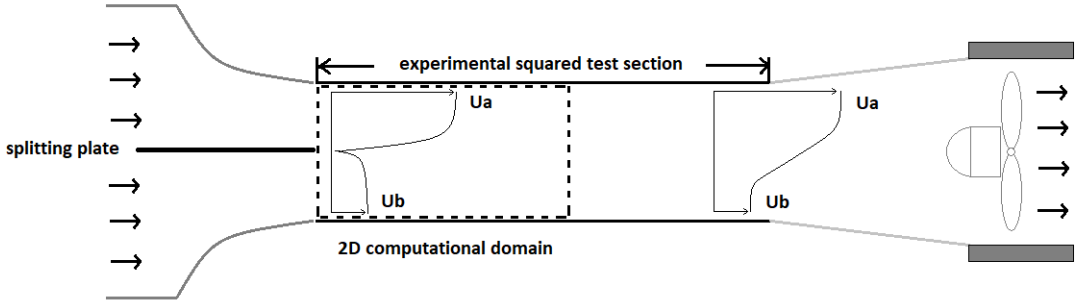

Figure 8.24: Experimental setup by C.E.A.T. Poitiers and two-dimensional computational domain for the plane mixing-layer

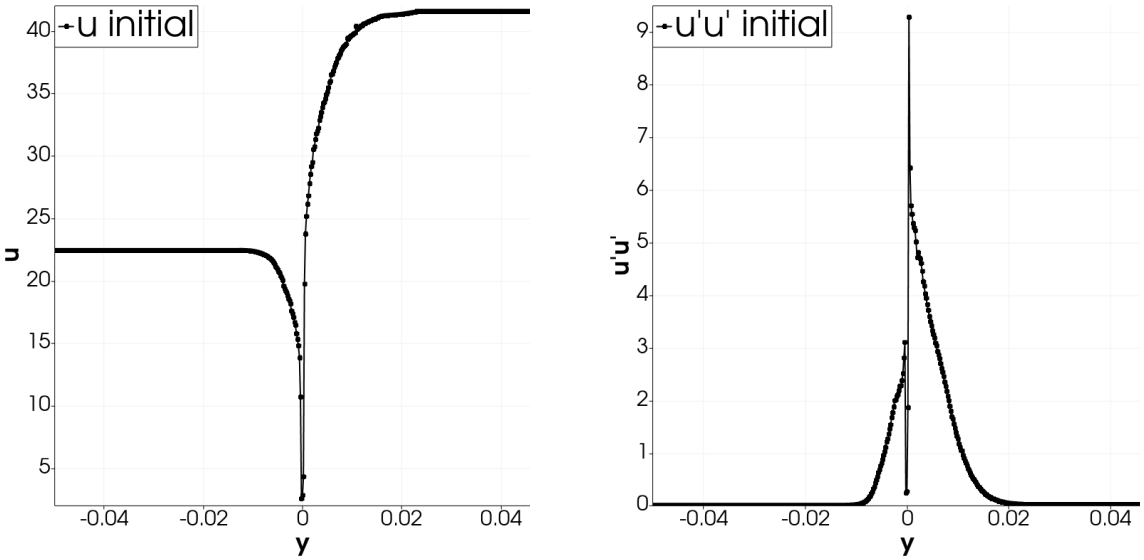

(a) Profile of velocity $\bar{u}_x$ (b) Profile of Reynolds-stress $\overline{u'_x u'_x}$

Figure 8.25: Profile of inlet boundary conditions for the plane mixing-layer

energy. Due to the appearance of the eddy viscosity, ν_T, in the source term of the Reynolds-averaged ten-moment equations, the length scale also affects the other conserved variables. Here, different values of the length scale are tested to estimate the effect on the solution.

Contour plots of velocity, $\bar{u}_x$, shear Reynolds-stress, $\overline{u'_x u'_y}$, and turbulence kinetic energy, k, at steady state are shown in Figs. 8.27–8.29. It is clear to observe that the mixing-layer is generated once the air streams merge at the inlet boundary. At the same location of the shear layer, turbulence kinetic energy is produced, which further dissipates and diffuses over the cross stream-wise direction.

The cell-wise numerical solutions, including the profile of horizontal velocity, $\bar{u}_x$, shear Reynolds-stress, $\overline{u'_x u'_y}$, and turbulence kinetic energy, k, over the vertical direction at location $x = 150\,\text{mm}$, $200\,\text{mm}$ and $250\,\text{mm}$ are plotted in Figs. 8.30–8.31. The black circles denote the experimental measurements and the red dashed line and blue dashed dotted line denote the numerical solution of Reynolds-averaged ten-moment equations coupled with the p-system type hyperbolic-relaxation one-equation model with two choices of turbulence length scale $l = 7 \times 10^{-4}\,\text{m}$ and $1 \times 10^{-3}\,\text{m}$ respectively.

As shown in the profile of horizontal velocity, in the case of $l = 1 \times 10^{-3}\,\text{m}$, the diffusion seems to be overpredicted at all chosen locations, while the shear Reynolds-stress seems to be overpredicted at the location $x = 150\,\text{mm}$ and $200\,\text{mm}$. A similar overprediction also appears in the profile of turbulence kinetic energy. In the case of $l = 7 \times 10^{-4}\,\text{m}$, the velocity

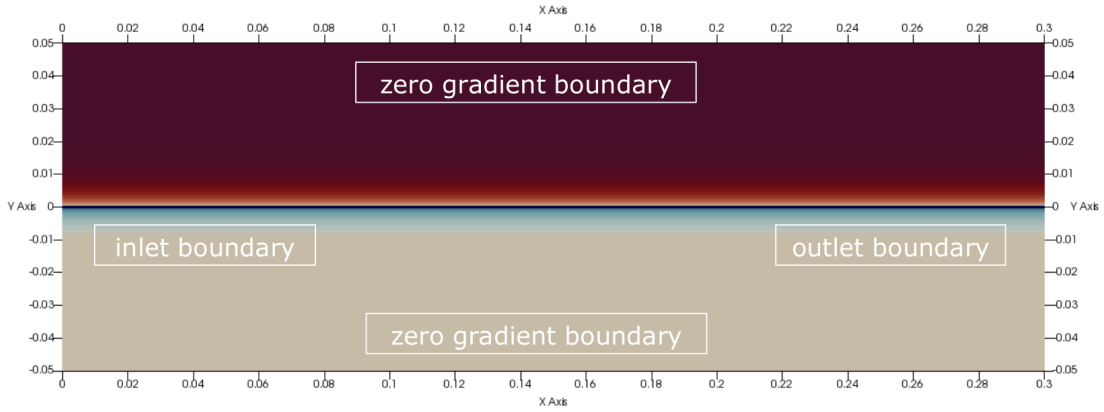

Figure 8.26: Initial and boundary conditions for two-dimensional computation of the plane mixing-layer

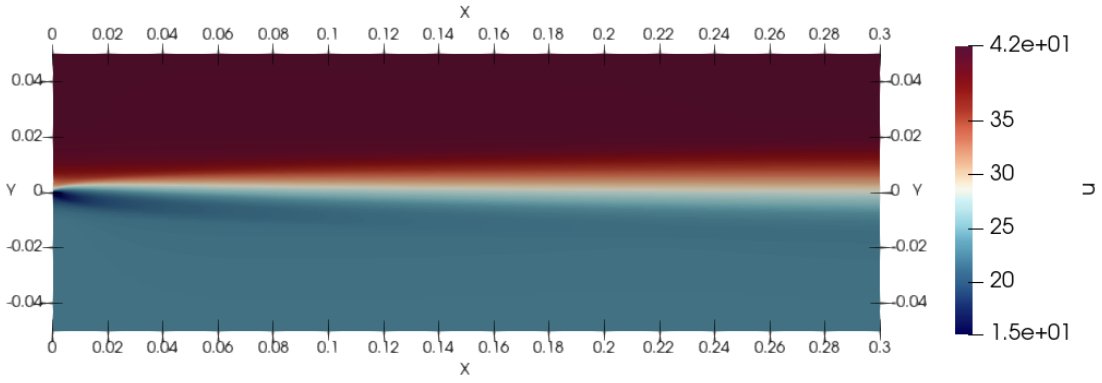

Figure 8.27: The contour profile of velocity, $\bar{u}_x$, at steady state using Reynolds-averaged ten-moment equations with p-system type hyperbolic-relaxation Prandtl's one-equation model for the plane mixing-layer

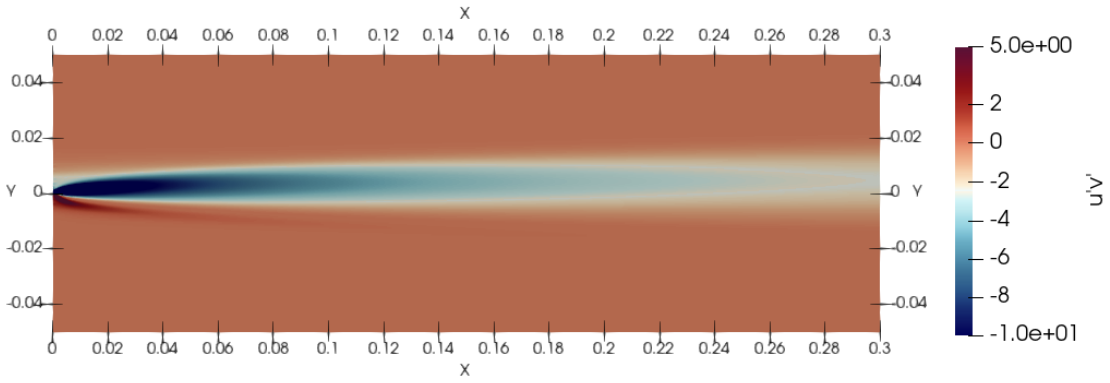

Figure 8.28: The contour profile of Reynolds-stress, $\overline{u'_x u'_y}$, at steady state using Reynolds-averaged ten-moment equations with p-system type hyperbolic-relaxation Prandtl's one-equation model for the plane mixing-layer

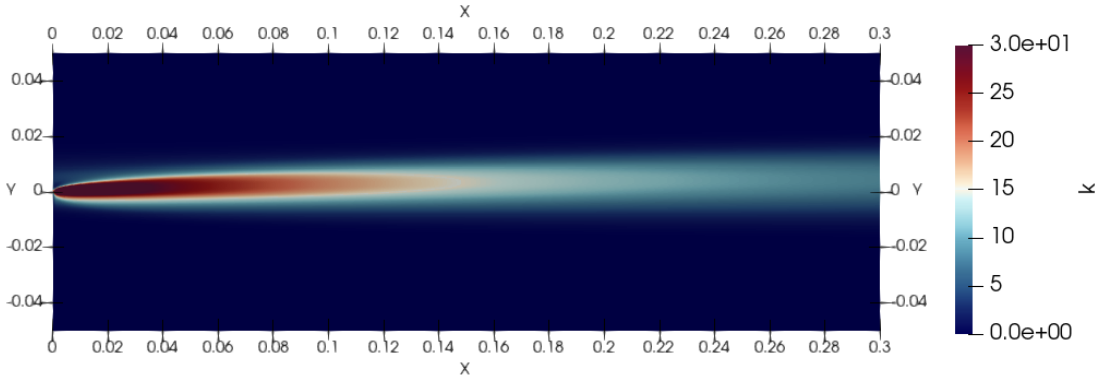

Figure 8.29: The contour profile of turbulence kinetic energy, k, at steady state using Reynolds-averaged ten-moment equations with p-system type hyperbolic-relaxation Prandtl's one-equation model for the plane mixing-layer

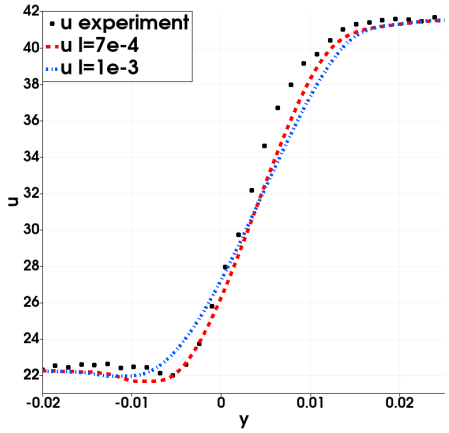

(a) $\bar{u}_x$ at $x = 150\,\mathrm{mm}$

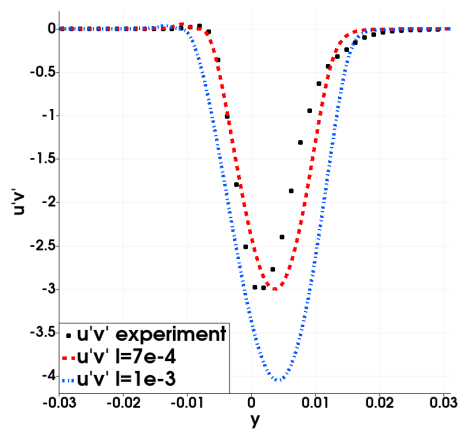

(b) $\overline{u'_x u'_y}$ at $x = 150\,\mathrm{mm}$

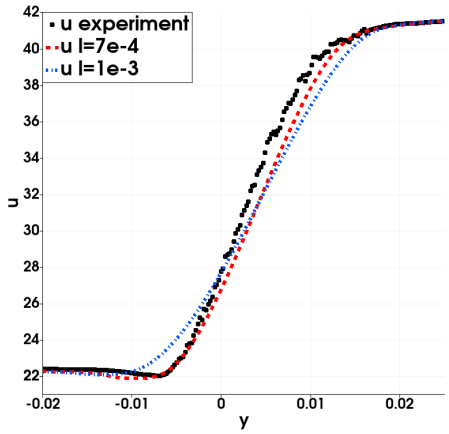

(c) $\bar{u}_x$ at $x = 200\,\mathrm{mm}$

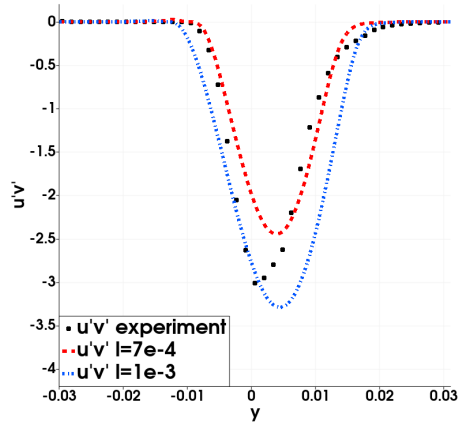

(d) $\overline{u'_x u'_y}$ at $x = 200\,\mathrm{mm}$

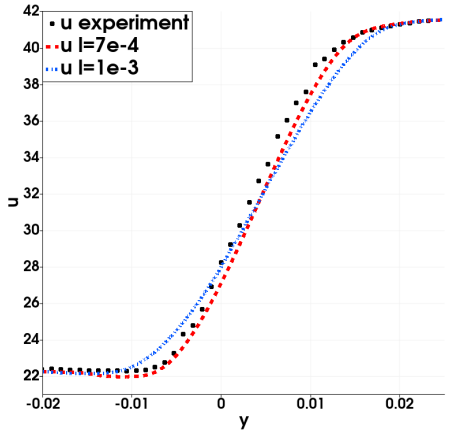

(e) $\bar{u}_x$ at $x = 250\,\mathrm{mm}$

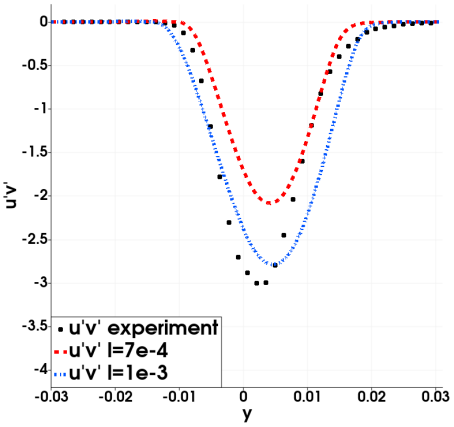

(f) $\overline{u'_x u'_y}$ at $x = 250\,\mathrm{mm}$

Figure 8.30: Experimental measurement and numerical solution profile of velocity and shear Reynolds-stress at $x = 150\,\mathrm{mm}$, $200\,\mathrm{mm}$ and $250\,\mathrm{mm}$ using Reynolds-averaged ten-moment equations with p-system type hyperbolic-relaxation Prandtl's one-equation model for the planar mixing-layer

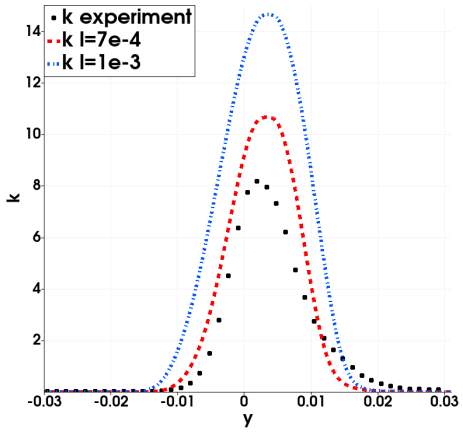

(a) k at $x = 150\,\mathrm{mm}$

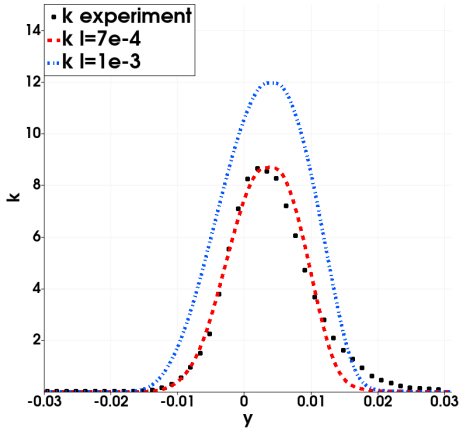

(b) k at $x = 200\,\mathrm{mm}$

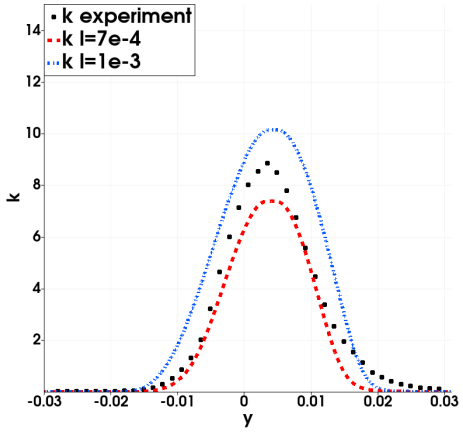

(c) k at $x = 250\,\mathrm{mm}$

Figure 8.31: Experimental measurement and numerical solution profile of turbulence kinetic energy at $x = 150\,\mathrm{mm}$, $200\,\mathrm{mm}$ and $250\,\mathrm{mm}$ using Reynolds-averaged ten-moment equations with p-system type hyperbolic-relaxation Prandtl's one-equation model for the planar mixing-layer

profile has better agreement with experimental measurements. The shear Reynolds-stress seems very close to the measurement at $x = 150\,\text{mm}$, however, it is underpredicted at the tail of the mixing-layer. These results are very similar to previously published solutions that are computed with the other RANS solvers, such as CFL3D and OVERFLOW, which are developed and validated by NASA Ames and Langley research centres [23]. The turbulent kinetic energy has a descending trend that is similar to the shear Reynolds-stress over the flowing direction of the mixing-layer, however, in general, the profiles with $l = 7 \times 10^{-4}\,\text{m}$ have better agreement with the experimental data.

According to the numerical approximations, it is clear that the free parameter, the turbulence length scale, has tremendous influence on the solution of full Reynolds-averaged ten-moment models. It is noticed that, in the original one-equation model, the production term, $\tau_{ij}\frac{\partial \bar{u}_i}{\partial x_j}$, the dissipation term, $C_D\frac{k^{3/2}}{l}$, and the diffusion term, $\frac{\partial}{\partial x_j}\left[(\nu + k^{1/2}l/\sigma_k)\frac{\partial k}{\partial x_j}\right]$ are all dependent on this turbulence length scale, l. The same influence is maintained in the equivalent hyperbolic-relaxation form. In addition, due to the appearance of the eddy viscosity, $\nu_T = k^{1/2}l$, in the source term of the Reynolds-averaged ten-moment equations, this length scale is not only the key parameter controlling the balance between each term in the turbulence model, but it also directly affects the viscous behaviour of the flow.

As discussed, the aim here is to validate the equivalence of the derived model, not to improve the existing one-equation model. Due to the simple modelling of the dissipation term, time varying dissipated information is not fully considered, which is a limitation of one-equation models in general, as compared to two-equations models. In two-equation models, an additional PDE corresponding to the dissipation rate or the specific dissipation rate is included, which provides a far superior treatment of the time evolution of the turbulence dissipation.

8.4.2 Numerical Approximations by the Cattaneo-Vernotte type Hyperbolic-Relaxation Two-Equation Models

The two-equation model is considered as "complete", since information of the fluid structure is no longer necessary for the model. In Prandtl's one-equation model, the production, dissipation and diffusion of the turbulence kinetic energy are dependent on the turbulence length scale, l. However, in two-equation models, these terms are related to a new variable, dissipation rate, ϵ, in the k-ϵ model or the specific dissipation rate, ω, in the k-ω model. The time evolution of these new variables is described by an additional PDE. However, as

introduced earlier, the initial or the boundary conditions of ϵ and ω are commonly proportional to the inverse of the turbulence length scale. Therefore, the selection of l still influences the computational solutions through specification of the boundary conditions. In this test, a constant value of $l = 3.5 \times 10^{-4}$ m is selected to determine the inlet boundary condition of ϵ and ω, which gives good results.

For the standard k-ϵ model, the boundary condition of the dissipation rate, ϵ, is defined by the function given in Eq. (8.7), where the closure coefficients are given by Eqs. (6.4). For the Wilcox k-ω model, the boundary condition of the specific dissipation rate, ω, is defined by the function given in Eq. (8.8), where the closure coefficients are given by Eqs. (6.17)

The profile of the horizontal velocity, $\bar{u}_x$, shear Reynolds-stress, $\overline{u'_x u'_y}$, and turbulence kinetic energy, k, over the cross stream-wise direction at the same location, $x = 150\,\text{mm}$, 200 mm and 250 mm are plotted in Figs. 8.32–8.33. The black circles denote the experimental measurements and the red dash line and blue dash dot line denote the numerical solutions of full Reynolds-averaged ten-moment equations with hyperbolic-relaxation version of standard k-ϵ and Wilcox k-ω model respectively.

As shown, both two-equation models are able to accurately reproduce the physical behaviour of the mixing-layer. Turbulence kinetic energy is generated at the location of the shear layer, which dissipates and diffuses to the free stream flows. In general, the difference between the solutions of the two-equation models is very small. Both models capture the velocity profile of the mixing-layer precisely. Unlike the solution of Prandtl's one-equation, they predict the stable growth of the shear Reynolds-stress and turbulence kinetic energy over the stream direction. However, their solutions overpredict the shear Reynolds-stress and turbulence kinetic energy at all sampled locations. This typical feature is inherited from the standard k-ϵ and Wilcox k-ω models. To improve the original models, some closure parameters are modified and some new terms are further introduced in their latter versions [50]. As mentioned, the aim here is to validate the equivalence of the derived models to their traditional form, therefore, recent improvements of these traditional models, which could be incorporated, are not discussed in this project.

8.5 Two-Dimensional Free-Jet

In this numerical experiment, the Reynolds-averaged ten-moment equations with derived hyperbolic-relaxation turbulence models are further validated by solving a two-dimensional

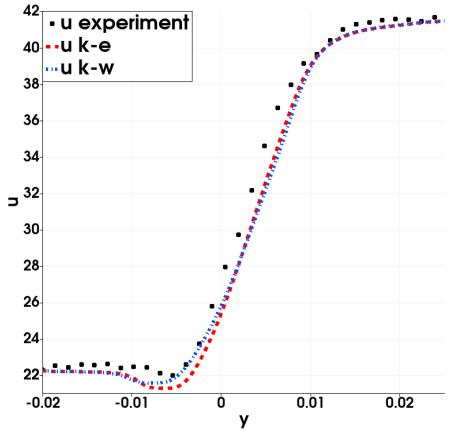

(a) $\bar{u}_x$ at $x = 150\,\mathrm{mm}$

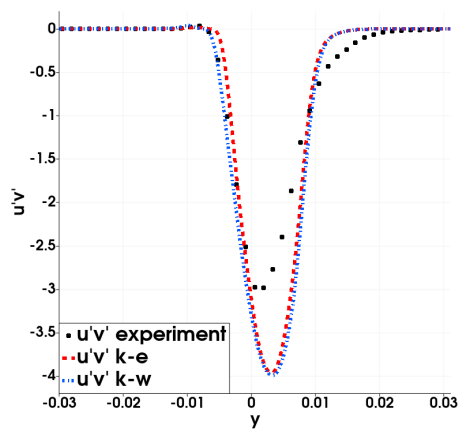

(b) $\overline{u'_x u'_y}$ at $x = 150\,\mathrm{mm}$

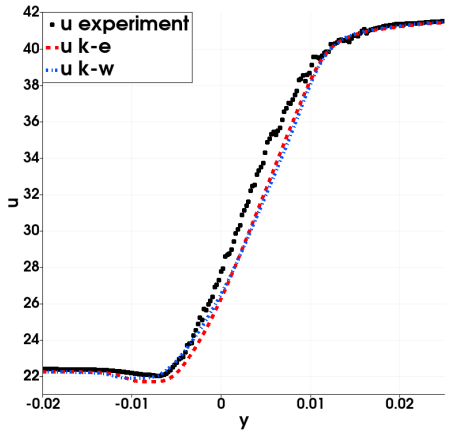

(c) $\bar{u}_x$ at $x = 200\,\mathrm{mm}$

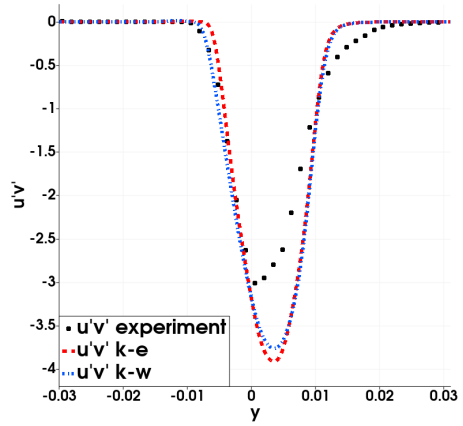

(d) $\overline{u'_x u'_y}$ at $x = 200\,\mathrm{mm}$

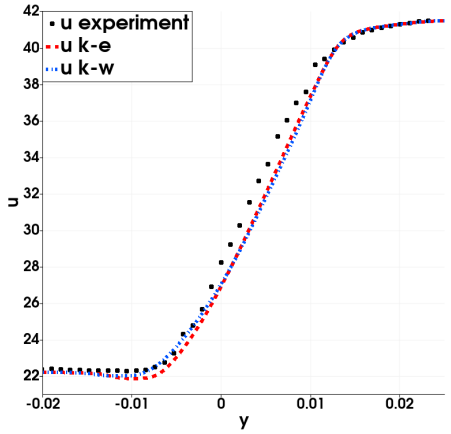

(e) $\bar{u}_x$ at $x = 250\,\mathrm{mm}$

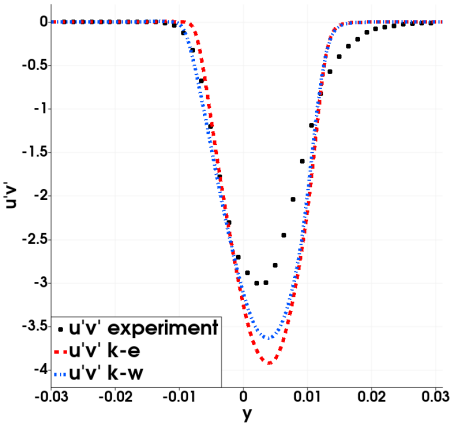

(f) $\overline{u'_x u'_y}$ at $x = 250\,\mathrm{mm}$

Figure 8.32: Experimental measurement and numerical solution profile of velocity and shear Reynolds-stress at $x = 150\,\mathrm{mm}$, $200\,\mathrm{mm}$ and $250\,\mathrm{mm}$ using Reynolds-averaged ten-moment equations with Cattaneo-Vernotte type hyperbolic-relaxation two-equation models for the planar mixing-layer

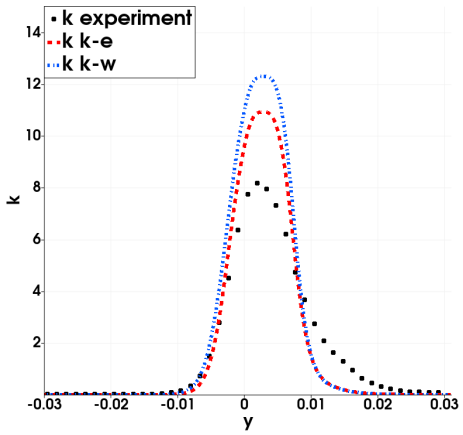

(a) k at $x = 150\,\mathrm{mm}$

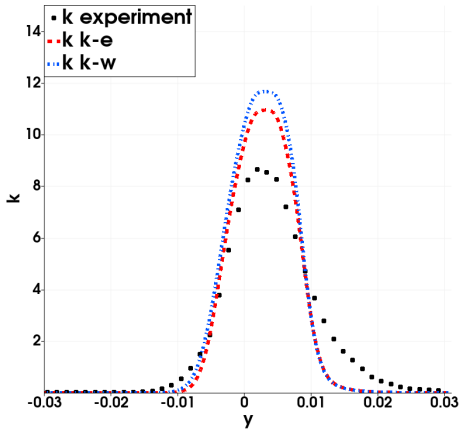

(b) k at $x = 200\,\mathrm{mm}$

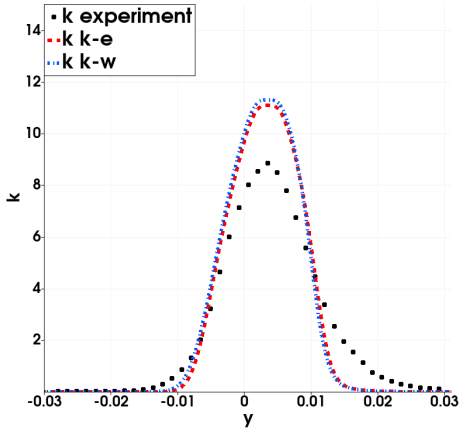

(c) k at $x = 250\,\mathrm{mm}$

Figure 8.33: Experimental measurement and numerical solution profile of turbulence kinetic energy at $x = 150\,\mathrm{mm}$, $200\,\mathrm{mm}$ and $250\,\mathrm{mm}$ using Reynolds-averaged ten-moment equations with Cattaneo-Vernotte type hyperbolic-relaxation two-equation models for the planar mixing-layer

planar free-jet problem. This is another canonical validation test for turbulence models. The numerical data is again compared against the experimental measurements at selected locations. The experiment was conducted by Terashima [46], which was originally designed to study the flow characteristics and vortex structure near the interface between turbulent/non-turbulent regions in a planar turbulent jet. This is done by investigating the velocity and pressure field using a combined probe which measures the simultaneous data. The data is considered as reliable based on the fact that it agrees with the measurement from a previous study by Sakai [40] for a different research purpose with the same experimental setup. Moreover, the measurements show good agreement with other numerical results from LES and DNS simulations.

The sketch of the experimental apparatus and the coordinate system of the two-dimensional planar free-jet is shown in the Fig. 8.34. A contraction nozzle, with inlet side length $s = 240\,\text{mm}$ and outlet height $n = 16\,\text{mm}$, is designed to generate the turbulent air flow, which further enters into a skimmer installed 1.0 mm downstream of the nozzle exit. The skimmer, with height $d = 12\,\text{mm}$ and width $l = 236\,\text{mm}$, is used to eliminate the boundary layer that developed along the inner surface of the nozzle. A turbulent free-jet with uniform velocity profile $U = 27.5\,\text{m/s}$ is obtained at the skimmer exit, and the Reynolds number is reported as $Re = 22,000$ in the original paper. Based on the Reynolds number, $Re = \rho U d/\mu$, the dynamic viscosity can then be determined, $\mu = 1.82 \times 10^{-5}\,\text{kg/ms}$. The sidewall is placed vertically in the test section to block the entrainment from the surroundings, which produces the two-dimensional flow field. The coordinate system is built with x as the stream-wise direction, y as the cross stream-wise direction and z as the spanwise direction.

A two-dimensional computational domain, within $x \in [0\ ,\ 0.6]\,\text{m}$ and $y \in [-0.2\ ,\ 0.2]\,\text{m}$, is designed in the test section as shown in the Fig. 8.35. The domain is decomposed by the graded structured grid as shown in the Fig. 8.36, where the coarse grid version is shown for illustration. A large number of mesh cells are placed at the nozzle exit to resolve the large gradients of flow properties. The growth rate of meshing in x and y direction is 1.01 and 1.005 respectively. Several grid resolutions, (400×600), (600×600) and (800×800), with the same mesh growth rate are tested for a convergence study. The solution differences among the selected grid resolutions are very small. Here, the solutions from the grid resolution, (600×600), are considered to be representative and are therefore further used for comparison.

To simulate the same physical environment in the numerical test, an impermeable wall

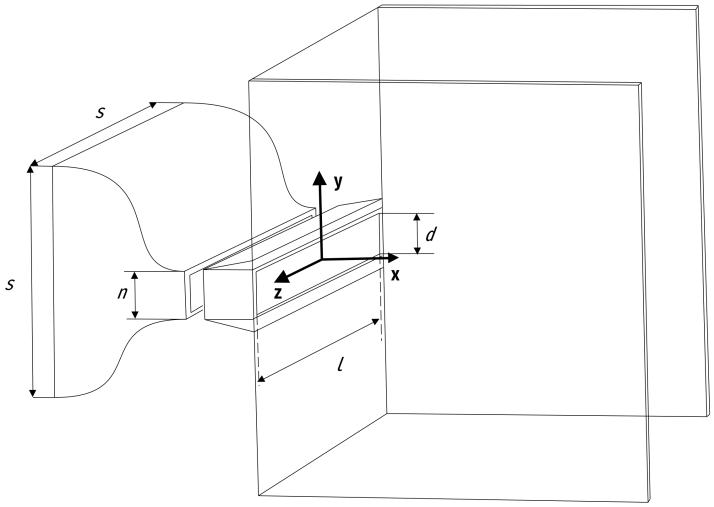

Figure 8.34: Experimental setup of two-dimensional free-jet

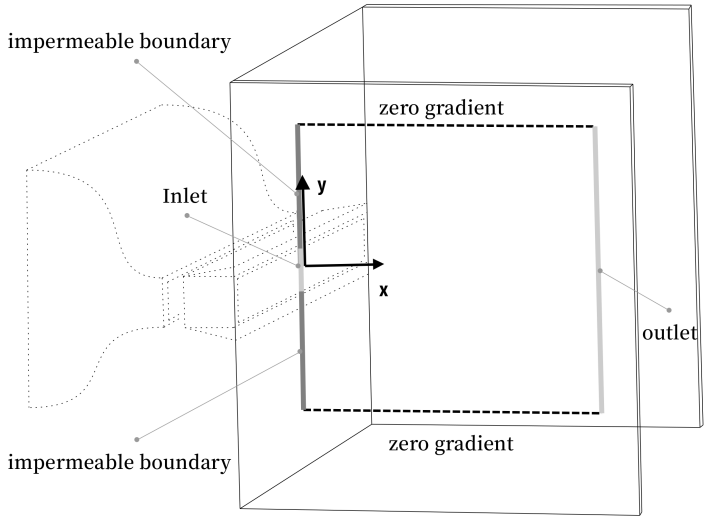

Figure 8.35: The computational domain and boundary conditions of two-dimensional free-jet

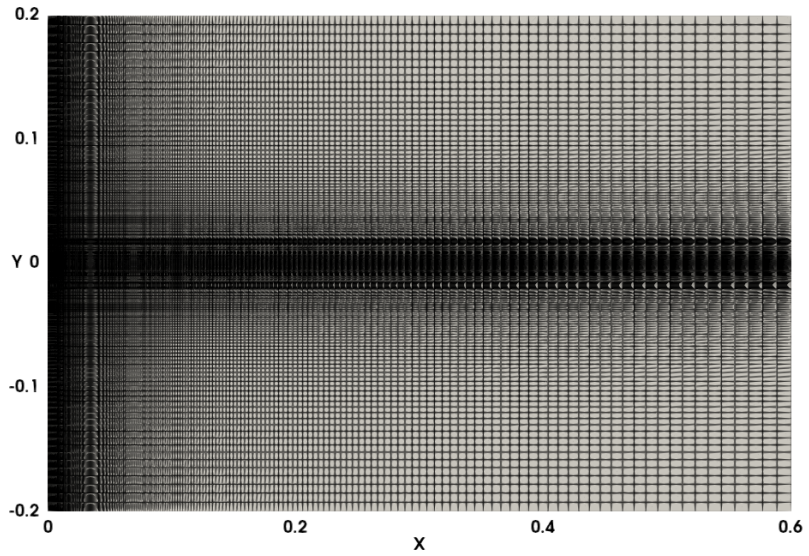

Figure 8.36: The computational grid for the two-dimensional free-jet computation

boundary condition is used to inhibit the entrainment above and below the flow inlet. An inlet and outlet boundary condition is used for flow entrance and exit. To maintain a stable solution, the variables $\overline{\Psi}_{xx}$ and $\overline{\Psi}_{zz}$ are specified as 101 325 Pa at the top and bottom boundaries, while the zero gradient boundary condition is applied to the rest of variables. The experiment was carried out under room temperature, $T = 293\,\mathrm{K}$, and pressure, $p = 101\,325\,\mathrm{Pa}$, according to inquiries made by the author, therefore, all flow properties for the initial and boundary setup are chosen under the same conditions. The same selection of relaxation time is used, including $\tau_k = 1 \times 10^{-4}\,\mathrm{s}$ for the p-system type hyperbolic-relaxation Prandtl's one-equation model and $\tau_k = \tau_\epsilon = \tau_\omega = 1 \times 10^{-3}\,\mathrm{s}$ for the Cattaneo-Vernotte type hyperbolic-relaxation two-equation models. The data over the cross stream-wise direction at location $x/d = 20$, 30 and 40 are sampled and compared against the measurements. One notes that the measured data reported in the original paper is non-dimensionalized by the corresponding center values, but is dimensionalized back in this test for further comparison.

8.5.1 Numerical Approximations by the P-System type Hyperbolic-Relaxation Prandtl's One-Equation Model and the Cattaneo-Vernotte type Hyperbolic-Relaxation Two-Equation Models

As discussed in the mixing-layer problem, for the one-equation model, the length scale, l, must specified within the whole computational domain. It plays an important role on the generation, dissipation and diffusion of turbulence kinetic energy, which also affects the momentum diffusion. For the two-equation models, the length scale is used to determine the dissipation, ϵ, or the specific dissipation, ω, at the boundaries. In this test, the values $2 \times 10^{-3}\,\mathrm{m}$ and $1 \times 10^{-3}\,\mathrm{m}$ are selected for the one- and two-equation model respectively, which give good results.

The streamlines of the two-dimensional computation, using the Reynolds-averaged ten-moment equations with hyperbolic-relaxation Prandtl's one equation model, at the steady state are shown in the Fig. 8.37. Due to the similarity, the streamlines plots of the two-equation models are not presented. They clearly illustrate the far field flows enter from the top and bottom boundaries and further entrain with the free-jet emitted from the nozzle. The cell-wise solution data over the cross-streamwise direction at location $x = 0.24\,\mathrm{m}$, $0.36\,\mathrm{m}$ and $0.48\,\mathrm{m}$ are sampled and compared against measurements in Fig. 8.38. The one-equation model provides good approximations in the velocity field, however it fails to capture the magnitude of shear Reynolds-stress at all selected locations. As checked by the author, the underprediction of the shear Reynolds-stress in this simulation is independent of the value of length scale. In general, the two-equation models provide far better agreement with the experimental data in either velocity or shear Reynolds-stress at all sampled locations. They successfully predict the momentum dissipation and the trend of diffusion. In comparison with the k-ω model, the k-ϵ model gives better results in the shear Reynolds-stress at the edges of free-jet. As shown, at location $x = 0.48\,\mathrm{m}$, the numerical approximation of the k-ϵ model almost perfectly matches the measurements.

8.6 Axisymmetric Free-Jet

In this section, the axisymmetric version of the Reynolds-averaged ten-moment equations coupled with derived hyperbolic-relaxation turbulence models, introduced in the Chap-

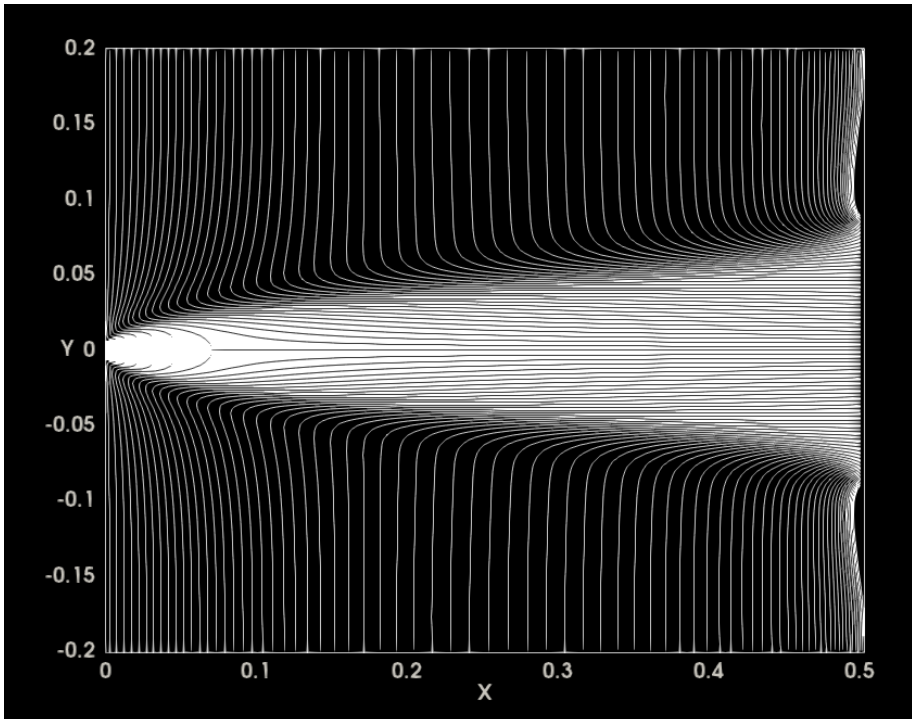

Figure 8.37: The streamlines of the two-dimensional planar free-jet computation using Reynolds-averaged ten-moment equations with p-system type hyperbolic-relaxation Prandtl's one-equation model

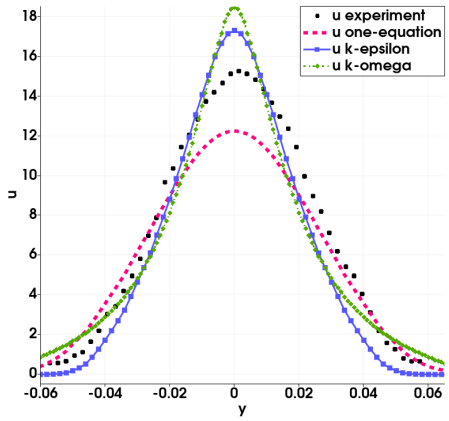

(a) $\bar{u}_x$ at $x = 240\,\mathrm{mm}$

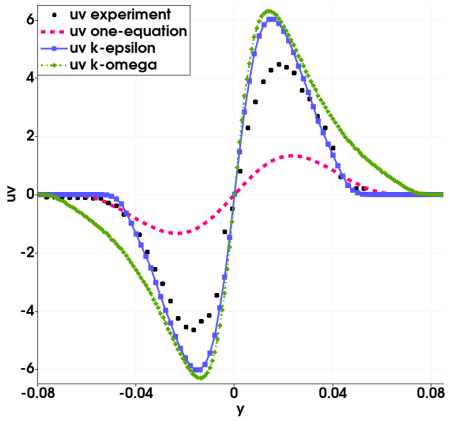

(b) $\overline{u'_x u'_y}$ at $x = 240\,\mathrm{mm}$

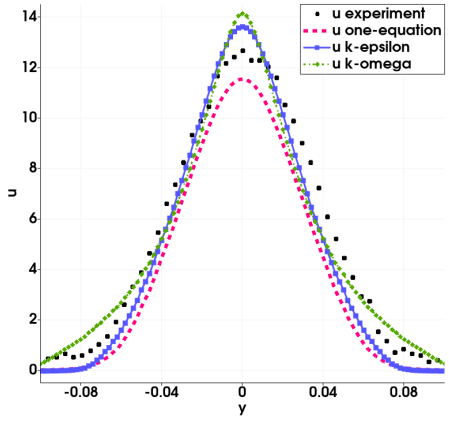

(c) $\bar{u}_x$ at $x = 360\,\mathrm{mm}$

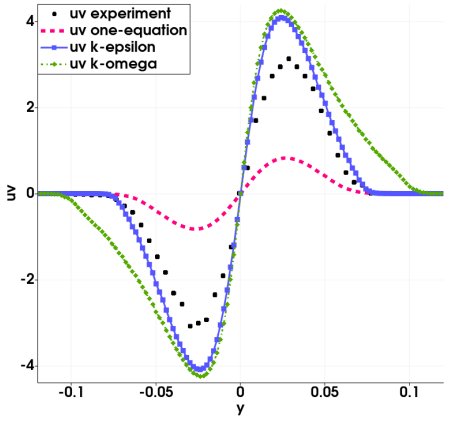

(d) $\overline{u'_x u'_y}$ at $x = 360\,\mathrm{mm}$

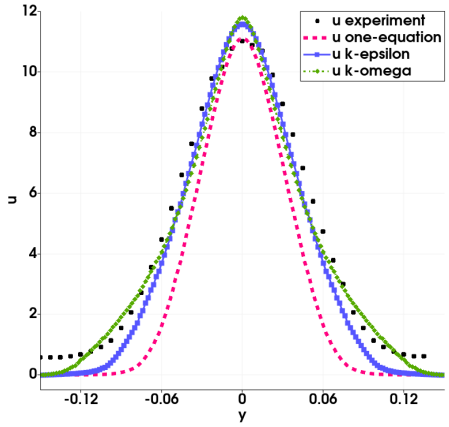

(e) $\bar{u}_x$ at $x = 480\,\mathrm{mm}$

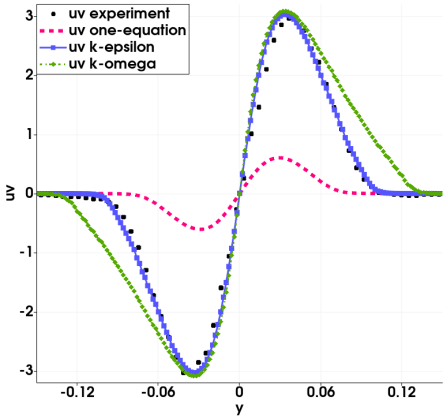

(f) $\overline{u'_x u'_y}$ at $x = 480\,\mathrm{mm}$

Figure 8.38: Experimental measurement and numerical solution profile of velocity and shear Reynolds-stress at $x = 240\,\mathrm{mm}$, $360\,\mathrm{mm}$ and $480\,\mathrm{mm}$ using Reynolds-averaged ten-moment equations with hyperbolic-relaxation one- and two-equation models for the planar free-jet

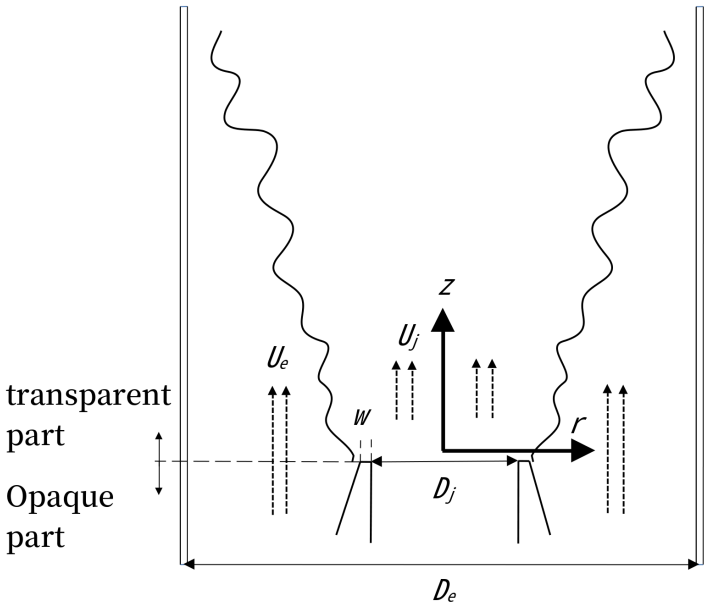

Figure 8.39: Experimental setup of axisymmetric free-jet

ter 7, are applied to solve a circular free-jet problem. The numerical solutions are again sampled and compared against the experimental measurements at different locations. The experiment was originally designed to investigate the development of turbulent axisymmetric jets in the near-field region, close to the nozzle exit. It was conducted by Amielh [3] in 1996 and collected by the European Research Community on Flow, Turbulence and Combustion (ERCOFTAC) in their "Classic Collection Database". In this study, this classic experimental data is used for the validation of the turbulence models.

The experimental set-up is shown in the Fig. 8.39. A nozzle with diameter $D_j = 26\,\text{mm}$ and edge thickness $w = 0.8\,\text{mm}$ is placed at the center of a circular duct with diameter $D_e = 285\,\text{mm}$. The fully developed, turbulent, axisymmetric air jet is emitted vertically from the nozzle into a low speed coflowing air stream provided by the external duct. The velocities of the jet and coflowing air are $U_j = 12\,\text{m/s}$ and $U_e = 1\,\text{m/s}$ respectively. The external circular duct is built high enough, the height of transparent part is 12 m, to allow measurements up to 40 times the jet diameter, D_j.

The computational domain and boundary conditions set-up are shown in the Fig. 8.40. A rectangle area, enclosed by the dashed and solid lines, is selected as the computational domain, which starting from the end of nozzle exit. Within this domain, half of the free-jet, within a two-dimensional cross sectional area, can be simulated. Due to the axisymmetric

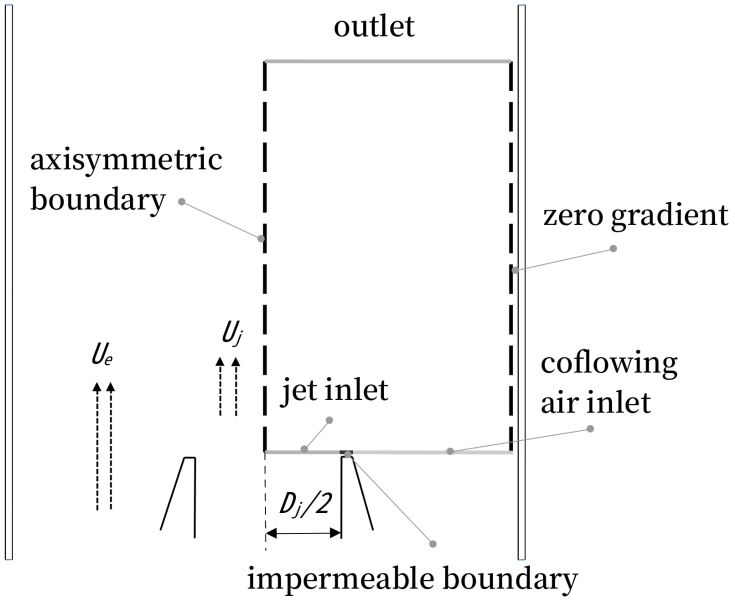

Figure 8.40: The computational domain and boundary conditions of axisymmetric free-jet

geometry, the results from this region are valid at any angular positions. To simulate the free-jet within this computational domain, the appropriate boundary conditions must be selected at each boundary surface. The jet and coflowing air inlet boundary conditions are specified at the bottom surface: they are separated by the impermeable boundary condition due to the presence of the nozzle edge. The axisymmetric and zero-gradient boundary conditions are specified at the left and right surfaces respectively, and the top surface is treated as an outlet boundary, where the zero-gradient boundary condition is used for all conserved variables.

A graded mesh is again used for the computations. Cells are concentrated at the left bottom corner to resolve the large gradient of the flow properties in the near region of the nozzle exit. The growth rates of meshing in the r and z directions are 1.01 and 1.005 respectively. A coarse version of the computational region with mesh grid is shown in the Fig. 8.41 for illustration. A similar mesh convergence study is done using the grid resolutions (200×300), (400×600) and (600×800). Based on the comparison between the solutions at the steady state, the solutions of the grid resolution (400×600) are chosen to represent the numerical solutions of the derived models.

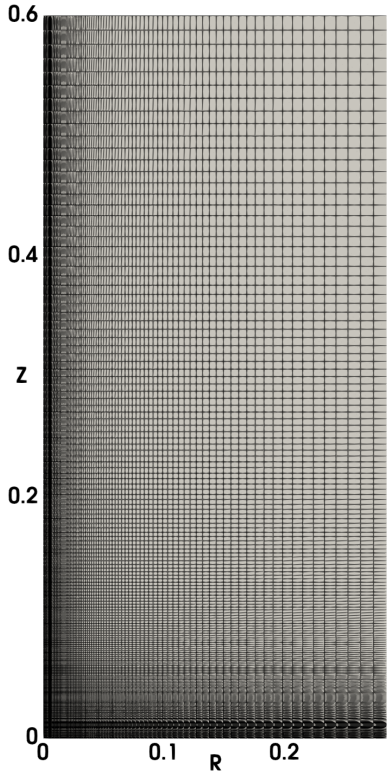

Figure 8.41: The computational grid for the axisymmetric free-jet computation

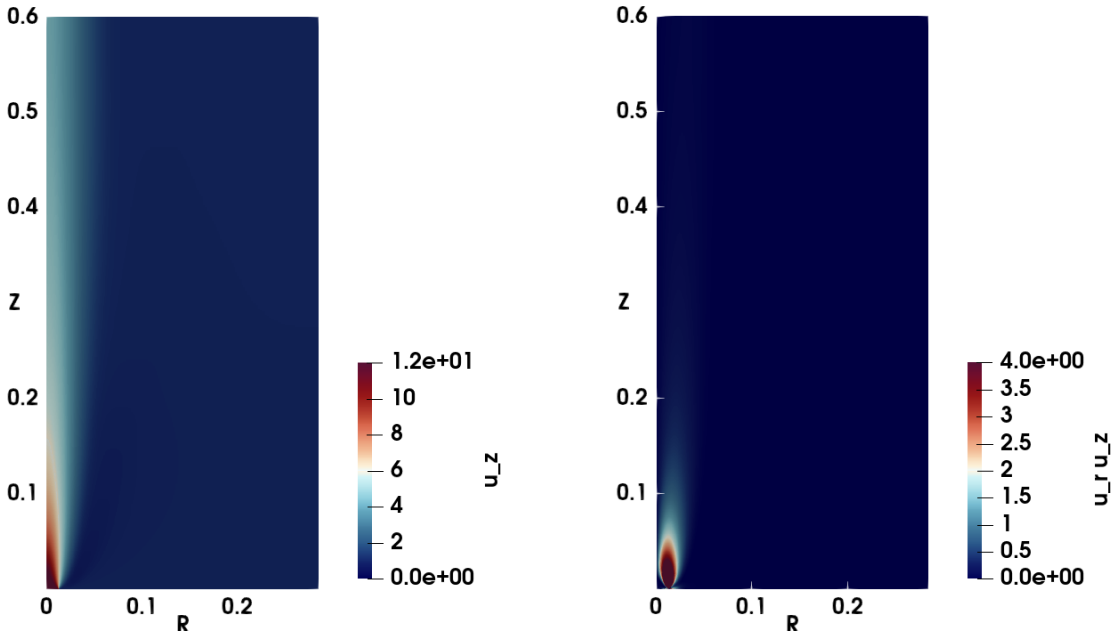

(a) velocity $\bar{u}_z$ (b) shear Reynolds-stress $\overline{u'_r u'_z}$

Figure 8.42: The contour profiles of the axisymmetric free-jet computation at steady state using the Reynolds-averaged ten-moment equations with p-system type hyperbolic-relaxation Prandtl's one-equation model

8.6.1 Numerical Approximations by the P-System type Hyperbolic-Relaxation Prandtl's One-Equation Model and the Cattaneo-Vernotte type Hyperbolic-Relaxation Two-Equation Models

In this test, the same length scale values that were used in the two-dimensional planar free-jet, are chosen for the one- and two-equation turbulence models. The contour plots of the velocity, u_z, and shear Reynolds-stress, $\overline{u'_r u'_z}$, of the computation, using Reynolds-averaged ten-moment equations with p-system type hyperbolic-relaxation Prandtl's one-equation model, at steady state are shown in the Figs. 8.42. Due to the similarity, the contour plots of two-equation models are not presented. As shown, half of the free-jet, within a two-dimensinal cross sectional area, is presented on the left side of the computational domain.

The numerical solutions at locations $z = 65\,\text{mm}$, $195\,\text{mm}$ and $260\,\text{mm}$ are sampled and compared with the experimental data, which are shown in the Fig. 8.43. The profile

of velocity, u_z, and shear Reynolds-stress, $\overline{u_r' u_z'}$, are again of interest at each selected location. The black dots indicate the experimental measurements. The red dashed line, blue solid line with square and green dashed line with diamond indicate the numerical solutions of hyperbolic-relaxation Prandtl's one-equation model, standard k-ϵ model and Wilcox k-ω model respectively. In general, all derived models approximate the dissipation and diffusion of the momentum within the domain where the free-jet and coflowing flow entrained. The Prandtl's one-equation model overpredicts the momentum diffusion and shear Reynolds-stress component at the selected location that close to the nozzle exit but it gives good approximations at the rest of the sampled locations. The two-equation models only successfully capture the velocity profile near the nozzle exit. They overpredict the velocity profile at the rest of selected locations. Moreover, they also overpredict the shear Reynolds-stress at all sampled locations.

To conclude, the axisymmetric form of the Reynolds-averaged ten-moment equations coupled with hyperbolic-relaxation turbulence models reproduce the momentum diffusion between the circular turbulent jet and coflowing air. The trend of velocity and Reynolds-stress over the streamwise direction is predicted, however, the results from the two-equation models are not ideal due to the overprediction.

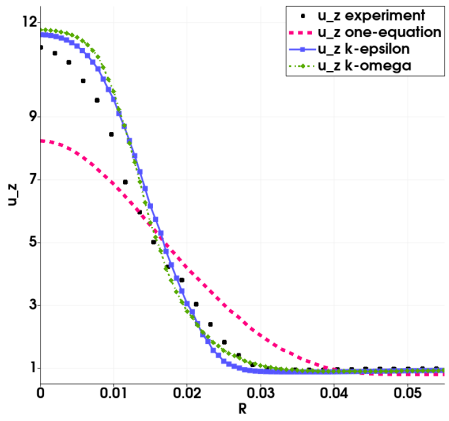

(a) $\bar{u}_z$ at $x = 65\,\text{mm}$

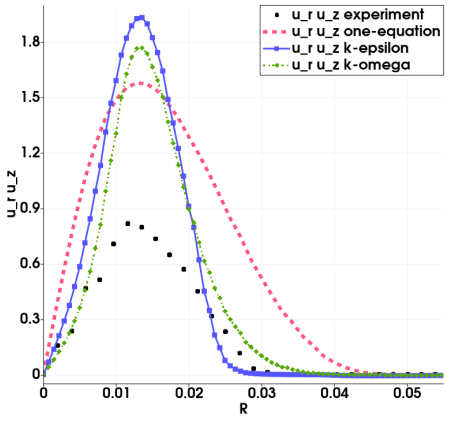

(b) $\overline{u_r' u_z'}$ at $x = 65\,\text{mm}$

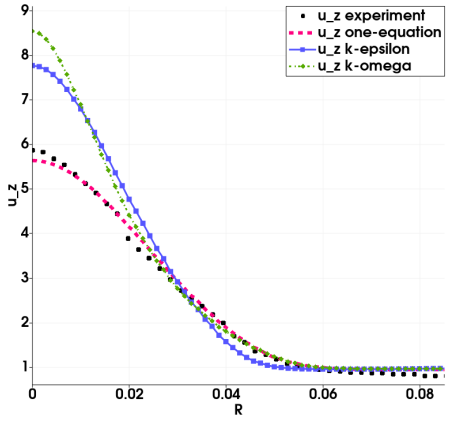

(c) $\bar{u}_z$ at $x = 195\,\text{mm}$

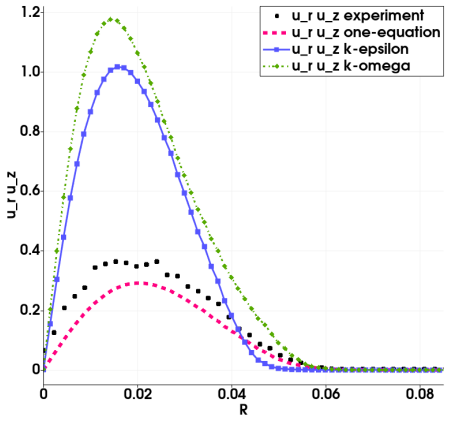

(d) $\overline{u_r' u_z'}$ at $x = 195\,\text{mm}$

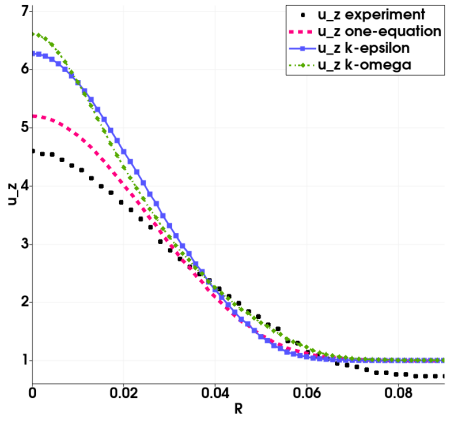

(e) $\bar{u}_z$ at $x = 260\,\text{mm}$

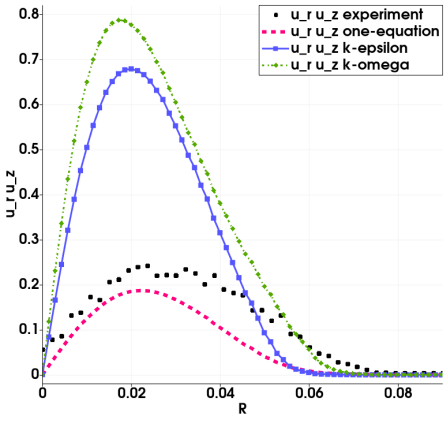

(f) $\overline{u_r' u_z'}$ at $x = 260\,\text{mm}$

Figure 8.43: Experimental measurement and numerical solution profile of velocity and shear Reynolds-stress at $x = 65\,\text{mm}$, $195\,\text{mm}$ and $260\,\text{mm}$ using Reynolds-averaged ten-moment equations with hyperbolic-relaxation one- and two-equation models for the axisymmetric free-jet

Chapter 9

Compressible Turbulence Modelling

In the traditional turbulence model, to take the effects of compressibility into account, the effect of density fluctuation, ρ', must be considered. In the Reynolds averaging procedure, this introduces more terms of fluctuating density correlation, which results in a more complicated form of the momentum equations in RANS. To address this issue, the density-weighted averaging procedure was suggested by Favre, which is commonly referred to as Favre-averaging [50]. It introduces the mass-averaged velocity, $\tilde{u}_i$, which, for time averaging, is defined as

$$\tilde{u}_i\left(x_i\right) = \frac{1}{\bar{\rho}} \lim_{T\to\infty} \frac{1}{T} \int_t^{t+T} \rho\left(x_i, t\right) u_i\left(x_i, t\right) \mathrm{d}t \,. \tag{9.1}$$

Based on this definition, the conventional Reynolds averaged momentum can be expressed as

$$\overline{\rho u_i} = \bar{\rho}\bar{u}_i + \overline{\rho' u_i'} = \bar{\rho}\tilde{u}_i \,, \tag{9.2}$$

which dramatically simplifies the mathematical expression without changing the physical meaning. One notes that a similar decomposition as for Reynolds averaging is also introduced for Favre averaging. The velocity can be split into mass-averaged part and fluctuating part, as

$$u_i = \tilde{u}_i + u_i'' \,. \tag{9.3}$$

Multiplying by the density and doing a time average forms the Favre average, which can be expressed as

$$\overline{\rho u_i} = \bar{\rho}\tilde{u}_i + \overline{\rho u_i''} \,. \tag{9.4}$$

As defined earlier by Eq. (9.2), the Favre average of the fluctuating velocity vanishes, $\overline{\rho u_i''} = 0$. However, based on the same equation, the conventional Reynolds-averaged

velocity fluctuation, $\overline{u_i''}$, is not zero, because

$$\overline{u_i''} = -\frac{\overline{\rho' u_i'}}{\bar{\rho}} \,. \tag{9.5}$$

Introducing this decomposition rule for the velocity while using the conventional decomposition rule for the other primitive variables of the ten-moment equations and time average the resulting equations, the Favre-averaged ten-moment model can be obtained

$$\frac{\partial \bar{\rho}}{\partial t} + \frac{\partial}{\partial x_k}\left(\bar{\rho}\tilde{u}_k\right) = 0 \,, \tag{9.6}$$

$$\frac{\partial}{\partial t}\left(\bar{\rho}\tilde{u}_i\right) + \frac{\partial}{\partial x_k}\left(\bar{\rho}\tilde{u}_i\tilde{u}_k + \overline{\rho u_i'' u_k''} + \overline{P}_{ik}\right) = 0 \,, \tag{9.7}$$

$$\begin{aligned}\frac{\partial}{\partial t}\left(\bar{\rho}\tilde{u}_i\tilde{u}_j + \overline{\rho u_i'' u_j''} + \overline{P}_{ij}\right) + \frac{\partial}{\partial x_k}\Big(&\bar{\rho}\tilde{u}_i\tilde{u}_j\tilde{u}_k + \overline{\rho u_j'' u_k''}\tilde{u}_i + \overline{\rho u_i'' u_k''}\tilde{u}_j + \overline{\rho u_i'' u_j''}\tilde{u}_k + \overline{\rho u_i'' u_j'' u_k''} \\ &+\tilde{u}_i\overline{P}_{jk} + \tilde{u}_j\overline{P}_{ik} + \tilde{u}_k\overline{P}_{ij} + \overline{u_i'' P_{jk}'} + \overline{u_j'' P_{ik}'} + \overline{u_k'' P_{ij}'} + \overline{u_i''}\,\overline{P}_{jk} + \overline{u_j''}\,\overline{P}_{ik} + \overline{u_k''}\,\overline{P}_{ij}\Big) \\ &= -\frac{3\overline{P}_{ij} - \overline{P}_{kk}\delta_{ij}}{3\tau_{\mathcal{G}}} \,.\end{aligned} \tag{9.8}$$

It has the same form as the Reynolds-averaged ten-moment equations, except for the additional unknowns, such as $\overline{u_i''}\,\overline{P}_{jk}$, due to the fact that $\overline{u_i''} \neq 0$. To completely close the system, a turbulence model that approximates the unknowns such as $\overline{\rho u_i'' u_j''}$, $\overline{\rho u_i'' u_j'' u_k''}$, $\overline{u_i'' P_{jk}'}$ and $\overline{u_i''}\,\overline{P}_{jk}$ is required.

As stated, to maintain the numerical advantages, the first-order hyperbolic turbulence model is preferred. The traditional turbulence models that supply the approximation of all above mentioned unknowns can be adjusted to the hyperbolic form using the same methods as previously introduced. For the turbulence models, such as the one-equation, two-equation and three-equation models, using the Boussinesq approximation,

$$\bar{\rho}\tau_{ij} = -\overline{\rho u_i'' u_j''} = 2\mu_T \overline{S}_{ij} - \frac{2}{3}\bar{\rho}k\delta_{ij} \,, \tag{9.9}$$

where

$$\overline{S}_{ij} = \frac{1}{2}\left(\frac{\partial \tilde{u}_i}{\partial x_j} + \frac{\partial \tilde{u}_j}{\partial x_i} - \frac{1}{3}\frac{\partial \tilde{u}_k}{\partial x_k}\delta_{ij}\right) \,, \tag{9.10}$$

the same trick, introducing a new tensor that represents the summation of averaged generalized pressure tensor and Reynolds-stress tensor, $\overline{\Psi}_{ij} = \overline{P}_{ij} + \overline{\rho u_i'' u_j''}$, can be used to avoid second-order derivatives in the momentum and energy equations of the time averaged ten-moment model. This tensor can be expressed as

$$\overline{\Psi}_{ij} = \frac{1}{3}\overline{P}_{kk}\delta_{ij} - 2\mu\overline{S}_{ij} + \frac{2}{3}\bar{\rho}k\delta_{ij} - 2\mu_T\overline{S}_{ij} \,. \tag{9.11}$$

According to the definition, the same equation, as introduced for the Reynolds-averaged ten-moment equations, can be used to extract the quantities of interest. For example, the averaged shear stress component, $\overline{P}_{ij}$ for $i \neq j$, can be obtained by

$$\overline{P}_{ij} = \frac{\mu}{\mu + \mu_T} \overline{\Psi}_{ij} \,, \tag{9.12}$$

the shear Reynolds-stress component, $\overline{\bar{\rho} u_i'' u_j''}$ for $i \neq j$, can be obtained by

$$\overline{\rho u_i'' u_j''} = \frac{\mu_T}{\mu + \mu_T} \overline{\Psi}_{ij} \,, \tag{9.13}$$

and the deviatoric stress tensor can be expressed as

$$\bar{t}_{ij} = \frac{1}{3} \overline{P}_{kk} \delta_{ij} - \overline{P}_{ij} = -\frac{\mu}{\mu + \mu_T} \left(\overline{\Psi}_{ij} - \frac{1}{3} \overline{\Psi}_{kk} \delta_{ij} \right) . \tag{9.14}$$

This trick avoids the presence of velocity gradient while simplifying the Favre-averaged ten-moment equations, as it does for the Reynolds-averaged ten-moment equations. Here, the approximation of the eddy viscosity is needed, whose formula is distinct among different turbulence models. However, to find out the appropriate model for $\overline{\rho u_i'' u_j'' u_k''}$, $\overline{u_i'' P_{jk}'}$ and $\overline{u_i''}\,\overline{P}_{jk}$ can be a challenge, as these terms are not negligible in the case of compressible flow.

There is another challenge caused by the production term of the compressible turbulence models. The general form of turbulence kinetic energy equation for compressible flow can be written as

$$\frac{\partial \bar{\rho} k}{\partial t} + \frac{\partial \bar{\rho} \tilde{u}_j k}{\partial x_j} = \bar{\rho} \tau_{ij} \frac{\partial \tilde{u}_i}{\partial x_j} - \epsilon + \frac{\partial}{\partial x_j} \left[(\mu + \mu_T) \frac{\partial k}{\partial x_j} \right] , \tag{9.15}$$

where the production term $\bar{\rho} \tau_{ij} \frac{\partial \tilde{u}_i}{\partial x_j}$ cannot be expressed algebraically by the averaged deviatoric stress tensor in the same way as was introduced for the incompressible case. This term, including the velocity gradient, still remains after the hyperbolization procedure. The resulting equations are consequently not in balance-law form, which can cause difficulties in numerics.

One notes that, to derive the p-system type hyperbolic-relaxation form for any compressible turbulence models is difficult. This is because the density introduces yet a new dependency, which causes a different asymptotic form than that discussed earlier. However, in general, the Cattaneo-Vernotte model remains applicable in such a situation, since the presence of density does not change that model's corresponding asymptotic form.

Chapter 10

Conclusion

To summarize, the scope of this project is to design appropriate turbulence models that allow the Gaussian ten-moment equations to be applied to turbulent flow problems for the first time. The Reynolds-averaging technique, which includes splitting the macroscopic flow variables into mean and fluctuating components and averaging the resulting governing equations, is applied to the ten-moment equations. Akin to RANS, new unknowns, including averaged fluctuating flow quantities and corresponding correlations are created in the Reynolds-averaged ten-moment equations. The flow turbulence behavior is assumed to be represented by these unclosed terms. To close the Reynolds-averaged ten-moment equations, turbulence models that approximate the new unknowns are required. Many existing RANS turbulence models could be adapted to close the Reynolds-averaged ten-moment equations, nevertheless, the second-order derivative in the traditional RANS models damage the first-order pure hyperbolic nature of the original system. Moreover, the formula of the traditional production terms breaks the balance-law form. This motivates the exploration of first-order hyperbolic turbulence models, so that the numerical advantages brought by the first-order model can be maintained. Based on the investigation of the existing RANS models, most of their equations take the form of convection-diffusion equations. This special type of equation is commonly used to predict the time evolution of Reynolds-stress or turbulence kinetic energy and dissipation rate or specific dissipation rate in the traditional models. Using relaxation methods, the traditional hyperbolic-parabolic type turbulence models can be transformed into the equivalent first-order hyperbolic-relaxation versions, which are well suited to the Reynolds-averaged ten-moment equations.

As a first exploration, Prandtl's one equation model is transformed into two equivalent hyperbolic-relaxation forms. The p-system type hyperbolic-relaxation version of Prandtl's

one-equation model is then coupled to the Reynolds-averaged ten-moment equations. To study the wave modes of the full model, the eigenstructure of the equations system is studied and all wave speeds corresponding to the fundamental solutions are found. Moreover, the solutions of this type of equations are dispersive, which means the wave speed and damping rate of different solution modes are dependent on the wave number or frequency. To verify the stability of the models, the dispersion relations are investigated. Furthermore, one- and two-dimensional numerical tests are designed to illustrate that the hyperbolic-relaxation versions provide the equivalent solution as the original equation. The Reynolds-averaged ten-moment equations coupled with the p-system type hyperbolic-relaxation Prandtl's one-equation model are then used to solve a canonical two-dimensional turbulent plane mixing-layer and free-jet problems. The numerical solutions are compared against the experimental measurements, which illustrate that the model is able to reproduce physical phenomenon of the flow stream mixing.

Akin to the one-equation model, the relaxation methods are further applied to the well-known two-equation models, the standard k-ϵ and Wilcox k-ω model. However, the diffusion coefficients in those models involve multiple variables. The creation of the equivalent p-system type hyperbolic-relaxation form is very difficult. The Cattaneo-Vernotte method is not affected by the complexity of the diffusion coefficients. Similarly, one- and two-dimensional numerical tests are designed for the two-equation models, which clearly illustrate the equivalence between the original models and the hyperbolic-relaxation forms. The Cattaneo-Vernotte type hyperbolic-relaxation two-equation models are then coupled with the Reynolds-averaged ten-moment equations and the dispersion property is then investigated. These models are further validated by solving the same mixing-layer and free-jet problems as mentioned previously.

Although the p-system and Cattaneo-Vernotte type hyperbolic-relaxation forms provide the same solutions as the original equation, these two types of equation systems exhibit different dispersive wave behaviours. The value of the relaxation time, which controls the acceptable equivalent performance are different as well. Based on the investigation, the Cattaneo-Vernotte form accepts larger values of the relaxation time, while providing the same level of equivalence. This reduces the stiffness introduced in the flux and source of the hyperbolic-relaxation equations. Moreover, the application of this approach is independent of the formula of the diffusion coefficient, which makes it superior in this study. Unfortunately, the resulting hyperbolic-relaxation forms generated by these two relaxation methods in the current work are not Galilean invariant, which motivates the author to

improve the models in future work.

In modern RANS models, many new terms, containing cross derivatives, are introduced to improve the approximation of the complex turbulence behaviour, such as flow separation. These terms can not be easily dealt with by the relaxation methods, which break the pure hyperbolic nature as well. They are usually treated as part of a source term in the traditional models. To take the effect of this type of term into account, the relaxation method would have to be improved or reconsidered.

To summarize, the study of the current project introduces the pure hyperbolic first-order turbulence models without losing the diffusive nature. It allows the Gaussian ten-moment equation to be applied to turbulent flow problems. It implies, for the first time, that the accurate modelling of complex turbulence behaviour by the first-order PDEs is possible.

References

[1] M. R. A. Abdelmalik and E. H. van Brummelen. Moment closure approximations of the Boltzmann equation based on φ-divergences. *Journal of Statistical Physics*, 164(1):77–104, 2016.

[2] G. D. Van Albada, B. Van Leer, and W. W. Roberts. A comparative study of computational methods in cosmic gas dynamics. *Upwind and High Resolution Schemes*, page 95–103, 1997.

[3] M. Amielh, T. Djeridane, F. Anselmet, and L. Fulachier. Velocity near-field of variable density turbulent jets. *International Journal of Heat and mass transfer*, 39(10):2149–2164, 1996.

[4] M. Arora. *Explicit Characteristic-based High-resolution Algorithms for Hyperbolic Conservation Laws with Stiff Source Terms*. PhD thesis, University of Michigan, 1996.

[5] T. J. Barth. On discontinuous Galerkin approximations of Boltzmann moment systems with Levermore closure. *Computer Methods in Applied Mechanics and Engineering*, 195:3311–3330, 2006.

[6] P. L. Bhatnagar, E. P. Gross, and M. Krook. A model for collision processes in gases. I. small amplitude processes in charged and neutral one-component systems. *Physical Review*, 94(3):511–525, Jan 1954.

[7] L. Boltzmann. Weitere Studien über das Wärmegleichgewicht unter Gasmolekülen. In *Kinetische Theorie II*, pages 115–225. Springer, 1970.

[8] F. Brini. Hyperbolicity region in extended thermodynamics with 14 moments. *Con-MechTherm*, 13:1–8, 2001.

[9] S. L. Brown. *Approximate Riemann Solvers for Moment Models of Dilute Gases*. PhD thesis, University of Michigan, 1996.

[10] S. L. Brown, P. L. Roe, and C. P. T. Groth. Numerical solution of a 10-moment model for nonequilibrium gasdynamics. Paper 95-1677, AIAA, June 1995.

[11] R.P. Canale and D. Steven C. Chapra. *Numerical Methods for Engineers*. McGraw-Hill Education, 2014.

[12] G. Y. Cao, H. M. Su, J. X. Xu, and K. Xu. Implicit high-order gas kinetic scheme for turbulence simulation. *Aerospace Science and Technology*, 92:958–971, 2019.

[13] C. Cattaneo. Sulla conduzione del calore. *Atti Del Semin. Matem. E Fis. Della Univ. Modena*, 3:83–101, 1948.

[14] C. Cattaneo. A form of heat-conduction equations which eliminates the paradox of instantaneous propagation. *Comptes Rendus de l'Académie des Sciences*, 247:431–433, 1955.

[15] G. Q. Chen, C. D. Levermore, and T. P. Liu. Hyperbolic conservation laws with stiff relaxation terms and entropy. *Communications on Pure and Applied Mathematics*, 47(6):787–830, 1994.

[16] G. Q. Chen and T. P. Liu. Zero relaxation and dissipation limits for hyperbolic conservation laws. *Communications on Pure and Applied Mathematics*, 46(5):755–781, 1993.

[17] J. Delville. Description of the data base: Plane turbulent mixing layer from C.E.A.T. Poitiers. Report, University of Poitiers, June 1995.

[18] W. Dreyer. Maximization of the entropy in non-equilibrium. *Journal of Physics A: Mathematical and General*, 20:6505–6517, 1987.

[19] T. I. Gombosi. *Gaskinetic Theory*. Cambridge University Press, 1994.

[20] H. Grad. On the kinetic theory of rarefied gases. *Communications on Pure and Applied Mathematics*, 2:331–407, 1949.

[21] A. Harten, P. D. Lax, and B. Van Leer. On upstream differencing and Godunov-type schemes for hyperbolic conservation laws. *Upwind and High Resolution Schemes*, pages 53–79, 1997.

[22] J. A. Hittinger. *Foundations for the Generalization of the Godunov Method to Hyperbolic Systems with Stiff Relaxation Source Terms*. PhD thesis, University of Michigan, 2000.

[23] D. C. Jespersen, T. H. Pulliam, and M. L. Childs. OVERFLOW turbulence modeling resource validation results. Report, NASA Ames Research Center.

[24] S. Jin. Runge-Kutta methods for hyperbolic conservation laws with stiff relaxation terms. *Journal of Computational Physics*, 122(1):51–67, 1995.

[25] W. P. Jones and B. E. Launder. The prediction of laminarization with a two-equation model of turbulence. *International Journal of Heat and Mass Transfer*, 15(2):301–314, 1972.

[26] G. M. Kremer. *An Introduction to the Boltzmann Equation and Transport Processes in Gases*. Springer-Verlag, 2010.

[27] B. E. Launder and B. I. Sharma. Application of the energy-dissipation model of turbulence to the calculation of flow near a spinning disc. *Letters in Heat and Mass Transfer*, 1(2):131–137, 1974.

[28] B. E. Launder and D. B. Spalding. *Mathematical models of turbulence*. Academic Press, 1972.

[29] C. D. Levermore. Moment closure hierarchies for kinetic theories. *Journal of Statistical Physics*, 83(5-6):1021–1065, 1996.

[30] C. D. Levermore and W. J. Morokoff. The Gaussian moment closure for gas dynamics. *SIAM Journal on Applied Mathematics*, 59(1):72–96, 1998.

[31] T. P. Liu. Hyperbolic conservation laws with relaxation. *Communications in Mathematical Physics*, 108(1):153–175, 1987.

[32] J. G. McDonald. *Extended Fluid-Dynamic Modelling for Numerical Solution of Micro-Scale Flows*. PhD thesis, University of Toronto, 2011.

[33] J. G. McDonald. Approximate maximum-entropy moment closures for gas dynamics. *AIP Conference Proceedings*, 1786(1):140001–1–140001–12, 2016.

[34] J. G. McDonald and C. P. T. Groth. Numerical modeling of micron-scale flows using the Gaussian moment closure. In *35th AIAA Fluid Dynamics Conference and Exhibit*, page 5035.

[35] J. G. McDonald, J. S. Sachdev, and C. P. T. Groth. Application of Gaussian moment closure to micro-scale flows with moving and embedded boundaries. *AIAA Journal*, 52:1839–1857, 2014.

[36] I. Müller. *Thermodynamics*. Pitman Publishing, Boston, 1985.

[37] I. Müller and T. Ruggeri. *Rational Extended Thermodynamics*. Springer-Verlag, New York, 1998.

[38] P. J. Olver. *Introduction to Partial Differential Equations*. Springer, 2014.

[39] P. G. Saffman and D. C. Wilcox. Turbulence-model predictions for turbulent boundary layers. *AIAA Journal*, 12(4):541–546, 1974.

[40] Y. Sakai, N. Tanaka, and T. Kushida. On the development of coherent structure in a plane jet (part 1, characteristics of two-point velocity correlation and analysis of eigenmodes by the kl expansion). *JSME International Journal Series B*, 49(1):115–124, 2006.

[41] W. S. Shen, C. J. Zhang, and J. Zhang. Relaxation method for unsteady convection–diffusion equations. *Computers and Mathematics with Applications*, 61(4):908–920, 2011.

[42] H. Struchtrup. *Macroscopic Transport Equations for Rarefied Gas Flows: Approximation Methods in Kinetic Theory*. Springer-Verlag Berlin and Heidelberg Co. KG, 2006.

[43] H. Struchtrup and M. Torrilhon. Regularization of Grad's 13 moment equations: Derivation and linear analysis. *PhysFluids*, 15(9):2668–2680, 2003.

[44] Y. Suzuki. *Discontinuous Galerkin Methods for Extended Hydrodynamics*. PhD thesis, University of Michigan, 2008.

[45] Y. Suzuki and B. van Leer. Application of the 10-moment model to MEMS flows. Paper 2005-1398, AIAA, January 2005.

[46] O. Terashima, Y. Sakai, K. Nagata, Y. Ito, K. Onishi, and Y. Shouji. Simultaneous measurement of velocity and pressure near the turbulent/non-turbulent interface of a planar turbulent jet. *Experimental Thermal and Fluid Science*, 75:137–146, 2016.

[47] M. Torrilhon. Modeling nonequilibrium gas flow based on moment equations. *Annual Review of Fluid Mechanics*, 48:429–458, 2016.

[48] P. Vernotte. Les paradoxes de la theorie continue de l'équation de la chaleur. *Comptes Rendus de l'Académie des Sciences*, 246:3154–3155, 1958.

[49] D. C. Wilcox. Reassessment of the scale-determining equation for advanced turbulence models. *AIAA Journal*, 26(11):1299–1310, 1988.

[50] D. C. Wilcox. *Turbulence modeling for CFD*. DCW Industries, 2010.

[51] D. C. Wilcox and I. E. Alber. A turbulence model for high speed flows. In *Proc. of the 1972 Heat Trans. & Fluid Mech. Inst.*, pages 231–252, Stanford, CA, 1972. Stanford Univ. Press.

[52] D. C. Wilcox and Morris W. Rubesin. *Progress in turbulence modeling for complex flow fields including effects of compressibility*. NASA, 1980.

[53] K. Xu. A gas-kinetic BGK scheme for the Navier–Stokes equations and its connection with artificial dissipation and Godunov method. *Journal of Computational Physics*, 171(1):289–335, 2001.

[54] K. Xu. *Direct modeling for computational fluid dynamics: construction and application of unified gas-kinetic schemes*, volume 4. World Scientific, 2014.